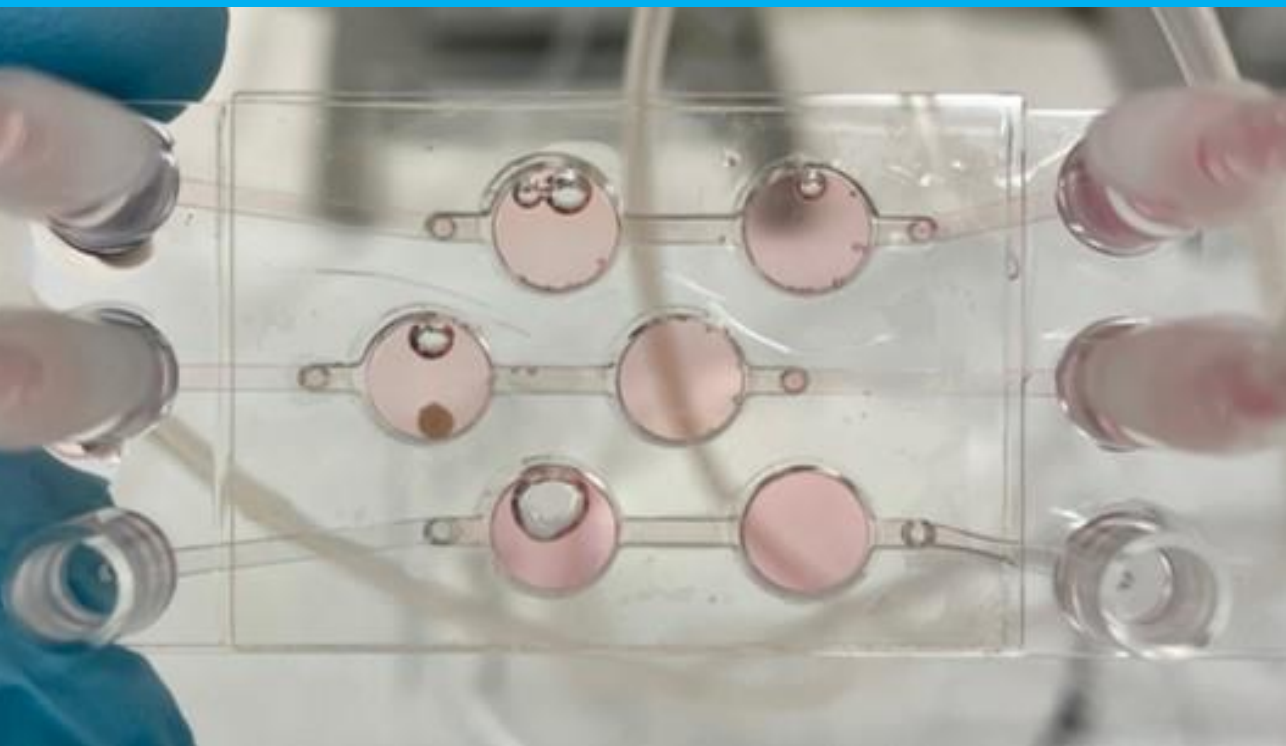


MSc thesis in BioMedical Engineering

Development of a microfluidic system for modelling the heart-kidney interaction *in vitro*

Design guidelines and proof-of-concept

Maricke Angenent



DEVELOPMENT OF A MICROFLUIDIC SYSTEM FOR MODELLING THE HEART-KIDNEY INTERACTION *in vitro*

DESIGN GUIDELINES AND PROOF-OF-CONCEPT

by

Maricke Lauren ANGENENT

A thesis submitted to the Delft University of Technology in partial fulfillment of the requirements for the degree

Master of Science in Biomedical Engineering

to be defended publicly on Wednesday September 28, 2022.

Student number: 4574516
Project duration: January 1, 2022 – September 28, 2022
Thesis committee: Prof. dr. ir. R. Dekker, TU Delft, supervisor
Prof. dr. P. M. Sarro, TU Delft
Dr. M. Mastrangeli, TU Delft
Dr. ir. B. van Meer, TU Delft

An electronic version of this thesis is available at <http://repository.tudelft.nl/>.



ABSTRACT

Cardiorenal Syndrome (CRS) is a multi-organ disease characterized by a reciprocal pathological interaction between the heart and kidneys during acute or chronic injury. Yet, a complete understanding of the underlying bi-directional pathophysiological mechanisms is lacking, hence obscuring effective diagnostic strategies, patient stratification and adequate administering of intervention therapies. Thus far, **CRS** has only been modelled in *in vivo* animal models, which are inherently limited in terms of experimental control and translatability of results to humans physiology. This underlines the need to develop more advanced *in vitro* models that accurately recapitulate the complex inter-organ cross talk responsible for the onset and progression of **CRS**. However, to date no such disease model system has been reported.

This project set out to design, develop and validate a microfluidic set-up, which would then enable the investigation of **CRS** in a three-dimensional environment. To that end, a theoretical framework covering all aspects related to **Multi-Organ-on-Chip (MOoC)** design was developed. This framework then formed the foundation for an extensive list of requirements to establish an ideal microfluidic set-up for a heart-kidney disease model. Various conceptual circuit designs were proposed and evaluated on the basis of the set requirements and their associated priority. Two systems were identified for further proof-of-principle studies: The IBIDI pump system and the Fluigent system.

By executing feasibility studies, simulating computational fluid dynamics, designing specific organoid inserts and eventually setting-up the proposed microfluidic circuits, a better understanding of the technological and biological challenges to be addressed was obtained. It was found that this project best be continued with a commercially available system that is highly versatile and allows for modular adaptations to render it fit-for-purpose. Overall, the Fluigent system is recommended, since it offers unparalleled experimental control and features a user-friendly plug-and-play set-up. The system can be automatized with open-source software and minimal adaptations render it feasible to realize recirculation as well as a single-pass unidirectional flow. Proof-of-principle experiments were promising, but more experimental iterations with a focus on in-depth biological tissue characterization are required to further evolve and fully validate the proposed cardiorenal model. Pressing issues entail establishing physiologically relevant scaling ratios, reducing required medium volume and identifying the exact disease models to incorporate once the physiological organoid system is functional.

PREFACE

This thesis marks the end of my time as a student at the Technical University of Delft. Starting out as a Nanobiology BSc student in 2016, I was helplessly unaware of the great time that lay before me and the many kind, passionate and above all supportive people I would meet. The years have flown by and now on the verge of obtaining my final Master of Science Degree in Biomedical Engineering, I am glad to say that I feel ready for the next adventures that are awaiting me.

From the very first start of my academics career, I have been much interested in topics and forthcoming challenges that are right at the cross section of multiple fields. Therefore it was with great pleasure to embark on this project that required nothing less than an interdisciplinary approach.

It is honest to say that the past couple of months have been an absolute roller-coaster and though I had no doubt about successfully completing my thesis sometime, I certainly felt far from confident plenty of times. However, I was not alone and therefore I would like to express my sincere gratitude to all the people that have helped me to find the right direction during this dynamic, difficult and sometimes uncertain period in my life.

I would like to start by thanking Prof. Ir. Ronald Dekker for his help and guidance during the final year of my masters. For it was not for his pro-active communication that I found both an internship and thesis position that fit perfectly with my interests. Besides, thank you for the project update discussions that we had that always showed me a completely other side of the story and prompted new perspectives on the performed experiments. I am thankful for the charismatic and enthusiastic attitude that you brought to the table and that you showed me the importance of enjoying the work you are doing rather than worrying about the outcomes.

Furthermore, I want to thank the members of the Department of Anatomy and Embryology at the LUMC for giving me the opportunity to join the research group and always being open to help out whenever questions arose. I also appreciate the openness with which I was received in the group and the interest that was taken in the executed work. In particular, I want to thank Dr. Ir. Berend J. van Meer. You gave me the freedom and guidance to come up with feasible experiments, contributed important technological considerations during the project and who always asked the right critical questions.

Most importantly, I want to express my gratitude to Beatrice. Working together day-to-day has been a great pleasure. The countless times that we were both lost in questions but continued nevertheless, the brainstorming sessions, periods of excitement but also disappointment and the overall progress that we have made the past months really is unforgettable. I am thankful to have been your student.

Lastly, a special thanks goes to dr. Bjorn de Wagenaar, who kindly made time teach me how to design CAD-files and who helped to produce 3D-printed prototypes that were used during this studies.

My time as a student has been remarkable and it is save to say that in terms of experiences, attitudes, opinions, worldviews and so many more personal aspects I have greatly changed and grown. Many thanks to all the other people not mentioned here that have enriched all the experiences along the journey.

*Maricke Lauren Angenent
Delft, January 2013*

CONTENTS

Abstract	i
Preface	ii
List of Tables	vii
List of Figures	viii
Acronyms	xi
1 Introduction	1
1.1 Cardiorenal syndrome	1
1.2 Current cardiorenal syndrome disease models	2
1.2.1 CRS disease models	2
1.2.2 Pathophysiological mechanisms in cardiorenal syndrome	4
1.3 Microphysiological systems	4
1.4 Problem statement and societal relevance	5
1.5 Research objective	6
1.6 Thesis structure	7
2 Theoretical Framework	8
2.1 Cell sourcing and culture method	8
2.2 Microfluidic platform architecture	9
2.2.1 Cellular environment	10
2.3 Material	11
2.4 Organ model scaling	11
2.4.1 Direct scaling	11
2.4.2 Allometric scaling	12
2.4.3 Functional scaling	13
2.4.4 Residence-time based scaling	14
2.5 Coupling of organ models	15
2.6 Fluid circulation	16
2.7 Flow rates	17
2.8 Blood surrogate media	21
2.8.1 Media formulation	21
2.8.2 Media volume	22
2.9 MOoC read-outs	23
2.10 State-of-the-art MOoCs	24
3 Microfluidic Model Design Requirements	25
3.1 Cell sources and culture method	25

3.2	Microfluidic platform configuration	26
3.3	Cellular environment	26
3.4	Material	26
3.5	Organ model scaling	27
3.6	Coupling of organ models	27
3.7	Fluid circulation	28
3.8	Flow rates	28
3.9	Common media	29
3.10	Analysis	29
4	Conceptual Design	31
4.1	Choice of microfluidic chip	31
4.1.1	IBIDI chip limitations	32
4.2	Microfluidic system set-up	33
4.2.1	IBIDI pump system	33
4.2.2	Fluigent system	34
4.3	System design limitations	36
4.3.1	Limitations of the IBIDI pump set-up	36
4.3.2	Limitations of the Fluigent set-up	38
4.4	Mesh design	39
4.4.1	Mesh purpose	39
4.4.2	Mesh requirements	39
4.4.3	Mesh conceptual prototypes	41
5	Feasibility Studies	44
5.1	Biological and functional assays	44
5.1.1	Medium	44
5.1.2	Tissue viability and integrity in static chip environment	46
5.1.3	Tissue localization in chip	47
5.1.4	Mesh prototyping	49
5.1.5	Mesh functional testing	51
5.2	Theoretical proof-of principle studies	54
5.2.1	Computational simulations of flow dynamics	54
5.2.2	Scaling the cardiorenal system	57
5.2.3	Chapter summary	60
6	Evaluation of the Design	62
6.1	System set-up	62
6.1.1	IBIDI set-up performance	63
6.1.2	Fluigent set-up performance	64
6.1.3	System related conclusions	65
6.2	Tissue characterization	65
6.2.1	Kidney Organoids	65
6.2.2	Cardiac Microtissues	66
6.2.3	MUSCLEMOTION analysis CMTs	67
6.3	Results computational simulations	68
6.3.1	Velocity profiles	68

6.3.2	Results particle trace	70
6.3.3	<i>In vitro</i> flow profile validation	72
7	Discussion	74
7.1	Experimental system evaluation	74
7.1.1	Microfluidic chip selection.	75
7.1.2	Pressure pump systems	75
7.1.3	Biological evaluation.	76
7.2	Meshes	77
7.3	Computational fluid dynamics simulation	78
7.4	Future work.	79
8	Conclusion	81
A	Design requirements	90
B	Choice of microfluidic system	93
C	Schematic overview KO-mesh designs	95

LIST OF TABLES

1.1	Classification of clinical types of CRS. Adapted from [13].	3
2.1	Different organ scaling methods and their applications. Adapted from [30]	15
2.2	Advantages and disadvantages of fluid circulation methods to choose in MOoC design	18
4.1	Summarized grading of the extent to which each considered microfluidic system complies with the set design requirements.	33
4.2	Tubing parameters for the IBIDI recirculation set-up and the Fluigent single-pass set up.	34
5.1	Aspect ratios tested in the design for KO meshes to achieve required permeability. Various pore diameters versus pore depths have been tested. The table reports the printing success.	50
5.2	Parameters of the organoid models to be embedded in the system.	57
5.3	Physical parameters used to determine first ball-park estimation of relevant scaling ratios for cardiorenal MOoC-system. Values based on 70 kg reference human [72]	58
5.4	Overview volumetric data of <i>in vivo</i> tissues compared to on-chip tissue and medium volumes [72].	59
6.1	Overview of advantages and disadvantages of evaluated microfluidic systems based on experimental observations.	65
A.1	Design requirements for a cardiorenal MOoC set-up, organized in accordance with the theoretical framework.	90
B.1	Design requirements evaluated for various commercially available systems to aid in decision making during the conceptual phase.	93

LIST OF FIGURES

1.1	Schematic overview of the main mechanisms involved in CRS. The cardiorenal connectors RAAS/SNS activation, oxidative stress and inflammation are involved in cross-talk between the organs and cause concomitant organ dysfunction and disease progression. Dysfunction of the heart results in hemodynamic changes which induces renal dysfunction. CRS has adverse cardiac, kidney and systemic consequences. Figure created with BioRender.com	5
4.1	The microfluidic chip of choice for this project is commercially available and features two interconnected organ chambers. Adapted from http://www.ibidi.com	32
4.2	Basic set-up of complete IBIDI system with a single fluidic unit to perfuse one channel. Image taken from [60]	35
4.3	Schematic overview Fluigent set-up: microfluidic single-pass unidirectional circulation to perfuse a single channel. Adapted from www.fluigent.com	36
4.4	Schematic overview Fluigent set-up: Recirculation over a single-channel facilitated by L-SWITCH component. Adapted from www.fluigent.com	37
4.5	Schematic overview Fluigent set-up: Recirculation over a single channel facilitated by two 2-SWITCHES. The second position of the valves is shown in the upper right corner. Adapted from www.fluigent.com	38
4.6	A-C: Conceptual design for the CMTs mesh that features a honeycomb-shaped well array to trap the CMTs and the exploded view of its on-chip placement. D: One of the conceptual designs for the KO mesh.	42
5.1	Light microscopy images of kidney organoids (500k cells) differentiated in APEL (A-C) vs BPEL (D-F) from day 7 onwards show clear differences in developed intact renal structures.	45
5.2	Immunofluorescence stainings of KOs to evaluate the effect of switching KOs from APEL to BPEL medium after maturation. A1-A3: Static control in APEL. B1-B3 Static control in BPEL.	45
5.3	Immunofluorescence stainings of KOs to evaluate tissue viability and integrity in static chip environment compared to control conditions. A1-A4: Static control in BPEL. B1-B4 72h static chip. C1-C4 72h static chip co-culture BPEL.	47
5.4	Immunofluorescence stainings of CMTs to evaluate tissue viability and integrity in static chip environment compared to control conditions. A1-A3 Static control BPEL (25div). B1-B3 72h static chip BPEL (14div). C1-C3 72h static chip co-culture BPEL (25div).	48

5.5	Representative results of MUSCLEMOTION analysis performed on 25 div CMTs subject to pacing at 1Hz.	48
5.6	Musclemotion results showed no significant differences in contraction duration, time to peak, relaxation time and contraction amplitude when cultured in static conditions or static on-chip conditions. Black dots represent obtained results for single microtissue.	49
5.7	First iteration of printed meshes for trapping CMTs fitted inside the Ibidi μ -slide	49
5.8	Results of 3D-printed KO meshes simulating pore-like membranes	51
5.9	Post-processing plasma-treatment of mesh improves the wettability of the material and results in better tissue-sedimentation into the honeycomb wells.	52
5.10	Representative pictures of KOs pipetted on top of mesh. Images taken at timepoint 0h.	53
5.11	The effect of tissue confinement and the potential cytotoxicity of the material on CMT beating patterns was analysed with the help of adjusted designs that fit a 24-well plate.	55
5.12	Schematic representation of the used geometry in the COMSOL Multiphysics simulations.	55
6.1	Evaluated microfluidic circuits for the purpose of this project.	63
6.2	Air bubbles were encountered upon assembly of the microfluidic chip. Air bubble localization does change over the time course of an experiment. The red arrows indicate the location of the microtissues.	64
6.3	Immunofluorescence stainings of KOs after 72h culture under flow compared to control conditions. A1-A4 Static control conditions. B1-B4 72h flow conditions KO only. C1-C4 72h flow conditions co-culture.	66
6.4	Immunofluorescence stainings of CMTs after 72h culture under flow compared to control conditions. A1-A4 Static control conditions (14div). B1-B4 72h flow conditions only CMTs (14div). C1-C4 72h flow conditions co-culture (14div).	67
6.5	Musclemotion results showed no significant differences in contraction duration, time to peak, relaxation time and contraction amplitude when cultured in static conditions or flow conditions for 72h. Black dots represent obtained results for single microtissue.	68
6.6	Simulation results for velocity magnitude in IBIDI μ -slide Perfusion exposed to various flow rates and with an inserted mesh. Computational Fluid Dynamic Simulations were performed using COMSOL Multiphysics.	69
6.7	Simulated shear stress profiles to determine the effect of flow rate and the insertion of a mesh on fluid dynamics.	71
6.8	Sideview of the results from simulated particle traces at a flow rate of 100 μ L/min. Figures represent the 15 second time point. The legends indicate the maximum and minimal particle velocities. (A) Spread of particles in an empty organ-chamber. (B) Spread of particles in chip with a honeycomb-array mesh inserted.	72

6.9	Snapshot of <i>in vitro</i> flow profile validation with Fluoro-Max dyed polystyrene microspheres at a flow rate of 100 $\mu\text{L}/\text{min}$	73
C.1	Schematic overview of tested KO-mesh designs with various pore diameters and inter pore spacing distances.	96

ACRONYMS

2D two-dimensional. 9

3D three-dimensional. 4, 6, 7, 9, 24–26, 40, 41, 55, 57

ALI Air Liquid Interface. 10

CKD Chronic Kidney Disease. 1, 2, 4, 6

CMTs cardiac microtissues. viii, ix, 25, 26, 39–42, 44, 46–49, 51–54, 57–61, 66, 67, 70, 72, 74, 77, 78

CRS Cardiorenal Syndrome. i, 2–6, 16, 25, 27, 74, 77, 80

ECM Extracellular Matrix. 4, 10, 26

FU Fluidic unit. 34, 35

GFR Glomerular Filtration Rate. 3

HF Heart Failure. 1, 4, 6

hiPSC human induced pluripotent stem cell. 3, 6, 9, 25, 77

KOs kidney organoids. viii, ix, 25, 26, 41, 42, 44–47, 50, 52, 53, 60, 61, 65, 66, 75–78

MOoC Multi-Organ-on-Chip. i, iv, vii, 5–17, 19, 21–25, 27, 28, 30, 31, 33, 38, 46, 47, 58–62, 65, 74, 77, 79–81, 90

MPS Microphysiological System. 4, 5, 8, 24

OoC Organ-on-a-Chip. 4, 5, 10, 11, 13, 15, 16, 23, 24, 27, 31, 57, 60, 74, 75, 77

PDMS polydimethylsiloxane. 11

RAAS Renin-Angiotensin-Aldosterone System. 4

RTBS residence-time based scaling. 14

SNS Sympathetic Nervous System. 4

WRF Worsening Renal Function. 2

1

INTRODUCTION

In healthy individuals, the heart and kidneys synergistically interact to maintain key physiological functions, such as sustaining hemodynamic homeostasis and upholding constant organ perfusion. More specifically, the cross-talk between the two organs is essential to control blood pressure, renal sodium and water excretion, arterial perfusion, oxygenation and extracellular fluid balance including the intravascular volume [1]. The heart-kidney interdependency is complex and tightly controlled by a broad array of regulatory mechanisms. In medical contexts cardiac and renal dysfunction often coexist and significantly increase mortality and morbidity among patients [2]. In fact, in the setting of **Heart Failure (HF)**, 20-30% of patients admitted for acute decompensated HF present a severe decline in renal function and more than 60% has at least some symptoms of mild renal dysfunction [3]. Moreover, up to 40-60% of patients who suffer from chronic HF also have **Chronic Kidney Disease (CKD)** [4]–[6]. Among end-stage and advanced stage CKD patients, cardiovascular illnesses are the predominant cause of death accounting for as much as 40-50% of all deaths [7], [8]. Besides, nearly 75% of end-stage renal disease patients have left ventricular hypertrophy [3], [9]. From this data, it is clear that heart and kidney dysfunction are not isolated events, but rather overlap and reciprocally influence each other. Therefore, it is relevant to not only consider individual organ pathologies, but also to analyse and unravel the systemic multifactorial pathophysiology. Thus far this remains to be an unresolved clinical challenge.

1.1. CARDIORENAL SYNDROME

The relationship between the heart and kidneys has first been described as early as 1836, when significant cardiac structural changes in a patient with advanced renal failure was reported [10], [11]. Since then the overlap between cardiac and renal disease has surged interest and efforts have been made to identify the precise connections between the dysfunctional heart and kidneys. The cardiorenal link encompasses bidirectional hemodynamic cross-talk between the heart and kidneys, alterations in neurohormonal path-

ways and the release of molecular signatures that characterize the clinical presentations of **Cardiorenal Syndrome (CRS)** [10].

CRS is categorized in two main groups depending on the primary site (or *primum movens*) of organ failure responsible for disease progression, onset and systemic disease [3]. These two groups, cardiorenal or renocardiac, are further arranged into five subgroups according to the clinical manifestations as outlined in Table 1.1 [4]. Type 1 **CRS** is defined as acute cardiorenal syndrome and is characterized by an acute worsening of heart function that gives rise to immediate kidney injury or dysfunction. The resulting **Worsening Renal Function (WRF)** complicates heart failure and/or acute coronary syndrome and contributes to prolonged hospitalizations and higher rates of morbidity and mortality among patients. Type 2 **CRS**, chronic cardiorenal syndrome, involves chronic heart failure that induces **CKD** or dysfunction. In type 3 **CRS**, acute renocardiac syndrome, the kidney is the primary precipitant organ and acute kidney injury causes acute cardiac failure. In type 4 **CRS**, chronic renocardiac syndrome, chronic kidney disease results in heart dysfunction. To account for the multiplicity of diseases that may culminate in **CRS**, especially when the initial insult is difficult to identify due to the interaction of several complex pathways, a fifth **CRS** category includes all the secondary clinical **CRS** presentations [10]. In **CRS** type 5, acute or chronic systemic disorders result in simultaneous adverse cardiovascular events and renal dysfunction. Examples of responsible systemic diseases include sepsis, diabetes mellitus, cirrhosis or vasculitis [2], [12]. An important note with regard to this classification system is that once a patient has been diagnosed with a specific subtype of **CRS**, the disease may evolve into another type of **CRS** over the course of disease progression [3].

The outlined five subgroups help to identify distinctive biomarkers, facilitate differential diagnosis and point to more relevant prognostic factors, hopefully to finally aid in deciding on the most appropriate therapy. Consequently, research has been aimed at identifying the particular mechanistic pathways and biomarkers that are dysregulated in and representative of each of the clinical types of **CRS**.


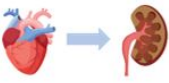



1.2. CURRENT CARDIORENAL SYNDROME DISEASE MODELS

A major challenge in **CRS** investigation is the establishment of models which mimic the exact pathophysiology of the syndrome [14]. Ideally, such a model should facilitate the analysis of cross-organ communication as well as include a systemic dimension. Yet, most *in vitro* models of renal or heart failure are reductive, single-organ systems, thus preventing the study of underlying mechanisms involved in concomitant organ dysfunction.

1.2.1. CRS DISEASE MODELS

Historically, animal models have been used in the identification of molecules that play a role in cardiac and renal injury. The majority of these preclinical studies has been performed in either rats or mice. An extensive overview of *in vivo* models that recapitulate heart-kidney interactions and capture some the **CRS** hallmarks has been provided by Gabbini et al. [13]. In short, animal models have been used to primarily understand uni-

Table 1.1: Classification of clinical types of CRS. Adapted from [13].

Type		Cardiorenal Syndrome	Description	Primary events
I		Acute Cardiorenal Syndrome	Acute impairment of cardiac function leading to acute kidney injury (AKI)	<ul style="list-style-type: none"> Acute decompensated heart failure Cardiogenic shock Acute coronary syndrome
II		Chronic Cardiorenal Syndrome	Chronic abnormalities in cardiac function result in progressive chronic kidney disease (CKD)	<ul style="list-style-type: none"> Chronic heart failure Left ventricular remodelling Cardiomyopathy
III		Acute Renocardiac Syndrome	Acute worsening of kidney function causes acute cardiac failure	<ul style="list-style-type: none"> Acute kidney ischemia Glomerulonephritis
IV		Chronic Renocardiac Syndrome	Chronic kidney disease contributes to progressive cardiac dysfunction	<ul style="list-style-type: none"> Chronic glomerular disease Chronic kidney disease
V		Secondary Cardiorenal Syndrome	Systemic conditions result in both cardiac and renal dysfunction	<ul style="list-style-type: none"> Systemic diseases (e.g. diabetes mellitus; sepsis; amyloidosis)

directional effects of cardiac impairment on renal function or vice versa. With respect to this research project, it is relevant only to consider the read-outs that have been used in such models to quantify organ function and their respective impairments. The main reported read-outs to evaluate renal function in this context are **Glomerular Filtration Rate (GFR)**, serum creatinine levels, morphology of glomeruli and tubules, renal fibrosis, rate of apoptosis and renal inflammation levels. Alternatively, alterations to the heart have been quantified in terms of cardiac hypertrophy, cardiac contractility, myocyte apoptosis, myocardial energy metabolism and heart remodelling. Even though ideal *in vivo* models would combine elements of chronic cardiac and renal dysfunction in a single organism to mimic the complex bidirectional nature of **CRS**, no such models have been reported yet [15], [16]. Nevertheless, the read-outs reported above provide a useful starting point to consider when designing novel disease models.

Despite the valuable information obtained from animal models, the predictive value and translatability to human patients remains inherently limited [13]. An alternative to animal models, are (human) *in vitro* models. Various *in vitro* models have been reported to recapitulate some of the specific hallmarks associated with **CRS** as summarized by Gabbin et al. [13]. The main advantage of those *in vitro* models is the possibility to use human cell sources and higher experimental controllability. Especially with the advance of **human induced pluripotent stem cell (hiPSC)** technology, it is becoming feasible to develop patient-specific disease models. This paves the way towards identifying the predominant pathophysiology in individual **CRS** patients, identifying characteristic biomarkers and developing novel therapeutic interventions.

1.2.2. PATHOPHYSIOLOGICAL MECHANISMS IN CARDIORENAL SYNDROME

CRS is a multifaceted syndrome and disease progression is mediated by various key contributors. Pathophysiological mechanisms that govern **CRS** onset and progression can be subdivided into hemodynamic mechanisms and non-hemodynamic mechanisms, also called cardiorenal connectors. Hemodynamic mechanisms refer to the interaction between cardiovascular functionality and renal output, such as blood pressure, extracellular volumes, renal function, cardiac output and cardiac contractility [17]. On the other hand, cardiorenal connectors primarily include dysregulation of neurohormonal systems (**RAAS** and **SNS**), tissue inflammation, atherosclerotic degeneration and metabolic dysregulation [4]. In addition, tissue fibrosis has been labelled as a key driver in the pathophysiology of **CRS** as it is a common, systemic, consequence of inflammation and oxidative stress. Since fibrosis is already used as a marker of both severe **HF** and **CKD** it is proposed as a starting point to generate representative disease models for both the heart and kidney [12], [18].

Although some potential disease driving pathways along the cardiorenal axis have been proposed, a complete understanding of the underlying mechanisms of **CRS** is still missing. This is mostly due to significant limitations in existing disease models of **CRS** as outlined in 1.2.1. A basic understanding of the mechanistic disease pathology is required to start thinking about simplified minimally viable *in vitro* disease models that still capture nearly the complete syndrome. Figure 1.1 presents an overview of main mechanisms that contribute to **CRS**, which for the purpose of this project mainly serves as a simplified introduction to the biological aspect of the disease.

1.3. MICROPHYSIOLOGICAL SYSTEMS

Current disease models are commonly limited in terms of their biological complexity and they often inaccurately mimic human nature. As a response to this limitation, a trend has emerged towards the use of a **Microphysiological System (MPS)** as novel *in vitro* disease model to obtain higher degrees of relevancy and to incorporate a systemic dimension into the model. Ideally, such a model system allows us to probe single mechanistic relationships at the time in the context of complex multi-organ crosstalk. Collaborations among biology and engineering related fields have led to a tremendous leap forward with regard to the applicability of **MPSs** [19]. A **MPS**, among which **Organ-on-a-Chip (OoC)** models can be classified, is a miniature replication of a micro-millimeter sized human tissue construct fabricated *in vitro* to mimic organ function on the smallest scale [20]. Whereas conventional cell-based models lack part of the important physiological *in vivo* processes such as flow, shear stress and tissue-tissue interaction, **MPSs** offer independent control over a wide range of such study parameters [21]. The microfluidic design provides a novel strategy to mimic the native cellular microenvironment and tissue function by individual spatiotemporal control over biomechanical, biochemical and cellular parameters in accordance with the outstanding research question. Single organ **MPS**-devices aim to replicate specific biological features of an organ or tissue within a suitable microenvironment that includes optimized media formulations, tissue perfusion and **three-dimensional (3D)** bio-engineered substrates that function as **Extracellular Matrix (ECM)** structures.

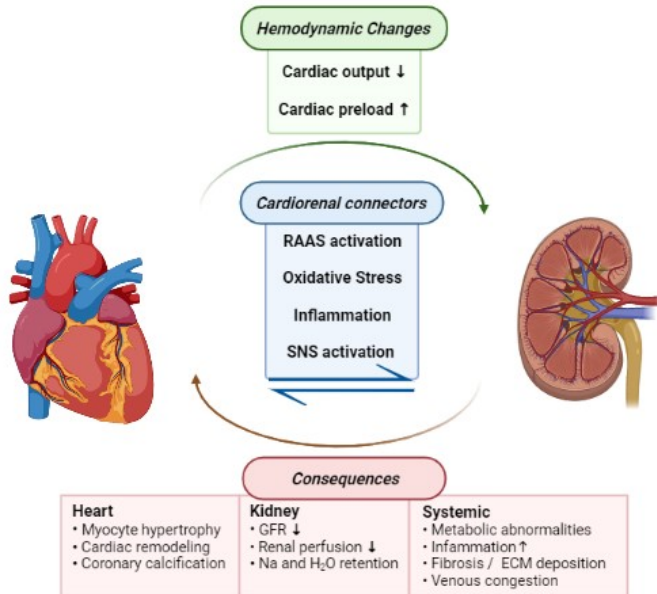


Figure 1.1: Schematic overview of the main mechanisms involved in CRS. The cardiorenal connectors RAAS/SNS activation, oxidative stress and inflammation are involved in cross-talk between the organs and cause concomitant organ dysfunction and disease progression. Dysfunction of the heart results in hemodynamic changes which induces renal dysfunction. CRS has adverse cardiac, kidney and systemic consequences. Figure created with BioRender.com

Contrary to single **OoC** platforms, the recent emergence of multi-MPSs or **Multi-Organ-on-Chip (MOoC)** platforms marks a novel breakthrough to provide clarity in systemic diseases such as **CRS**. In **MOoCs**, multiple organ models are fluidically or functionally interconnected to create a dynamic exchange of secreted factors, thus facilitating the study of more complex cross-organ interactions. The **MOoC** field is on its way to transform *in vitro* disease studies and numerous system designs have already been reported for various organ combinations. Nevertheless, to achieve the full potential of **MOoC** devices, there are still many questions to be answered and considerations to be made when designing a novel **MOoC**, as will be elaborated on in Chapter 2.

1.4. PROBLEM STATEMENT AND SOCIETAL RELEVANCE

In the context of **CRS**, a major limitation in our understanding of the disease is the lack of consistent data on temporal and causal relationships between changes in cardiac function and the development of renal dysfunction, and vice versa [14]. Thus far several potential pathways have been suggested that are involved in the regulation of the cardio-renal axis, which in case of disruption might contribute to the development of **CRS**. However, the lack of specific biomarkers complicates early detection, classification and treatment of the syndrome. The current treatment approaches are commonly frag-

mented and single-organ centred, whereas a multidisciplinary approach would greatly improve the effectiveness, quality of care and timely manner of CRS treatment administration [2]. On top of that, widespread prevalence and incidence data show an increase in confirmed CRS cases. On one hand, this observed increase can be attributed to a growing occurrence of acute and chronic cardiovascular disease, including acute decompensated HF, arterial hypertension and valvular heart disease. On the other hand, the incidence of CKD is becoming more common due to an aging population. Aging is associated with a chronic inflammatory state and cardiac secondary effects such as volume and pressure overload and secondary hyperparathyroidism, which contributes to calcific heart disease. Taken together, limited treatment availability and expected increases in prevalence, underline the importance of continuing and advancing cardiorenal research, both in a clinical setting based on patient analysis and in research setting to acquire a more comprehensive understanding of the bidirectional molecular mechanisms that are at the ground of this disease.

In particular, novel *in vitro* disease models are required to study the complex heart-kidney interaction encountered in CRS in a human environment. There is a need to bridge the gap between 3D hiPSC-models and more controllable disease modelling strategies. The challenge here is to design a system that is compatible with conventional established cell-biology methods, and yet allows the systemic coupling of multiple organ models to elucidate their interactions over time. CRS presents an excellent example for the need to develop more accurate models to study organ-organ interaction and one which could benefit greatly from a tailored MOoC platform.

1.5. RESEARCH OBJECTIVE

To date MOoC models that combine the heart and kidneys have not been reported yet, leaving many challenges to be addressed. Therefore, the overall aim of this project is:

To develop a microfluidic system which can be used to study the heart and kidney interaction in vitro.

Such a system would be a great stepping stone towards *in vitro* disease modelling of CRS in a controllable three-dimensional environment. Ultimately, paving the way towards novel strategies to elucidate the complex causative pathological pathways and to then aid in the discovery of therapeutic targets to alleviate the syndrome. Since this master thesis project was started during the initiation of the overall project, the main focus has been on first of all identifying the microfluidic system requirements, building the conceptual design and perform subsequent feasibility studies. The scope of this project mainly covered the technological aspect of optimizing a set-up comprised of commercially available components, rather than the biological and cellular optimization studies.

The proposed specific goals were:

- Design and set up a 'cardio-renal unit' consisting of preferably commercially available components (e.g. chips, pumps, tubing) according to the requirements provided by the supervisors;

- Test the system using cardiac- or kidney-only organoids developed to investigate whether organ-specific secreted factors are detected and their levels.
- Test the system using a cardiac and kidney organoid co-culture to study the organ-organ interaction with a high level of control: unidirectional flow might be used to investigate how the kidney affects the heart or vice versa, while recirculating flow might be used to investigate the long-term reciprocal interaction.

During the execution of this project the goals were slightly adjusted to be in line with the performed experiments and the problems encountered. As such, microfluidic flow simulations were generated, 3D-printed geometrical meshes were designed for organoid trapping and preliminary system test runs were executed.

1.6. THESIS STRUCTURE

This project covers the early stages towards the development of a novel microfluidic system to capture heart-kidney organ interaction, including conceptualization of the design and embodiment of first proof-of-concept set-ups. Chapter 2 concerns itself with an exploratory review and the resulting theoretical framework that was established to guide microfluidic platform design. This chapter is mainly written to serve as an introduction to the MOoC field and become acquainted with the range of aspects related to MOoC that require consideration during the design phase of an experiment. Based on the presented theoretical framework, the list of design requirements is presented in Chapter 3. Chapter 4 then describes the conceptual system designs that were developed. Subsequently, feasibility studies and computational fluid dynamics (CFD) simulations are presented in Chapter 5 that will aid the realization of the design. Next, in Chapter 6 the conceptual designs are experimentally evaluated and the simulated results are presented. Finally Chapter 7 and 8 discuss and conclude the findings of the experimental evaluation, respectively.

2

THEORETICAL FRAMEWORK

Guiding principles, considerations and proven strategies from literature have been reviewed and summarized to constitute a theoretical framework to guide decision making during the experimental design phase. The design considerations are presented here in accordance with the order in which each aspect presents itself when setting up a novel MOoC experiment.

2.1. CELL SOURCING AND CULTURE METHOD

The first design criteria to consider when designing a novel platform is the type of cell source or tissue construct that should be incorporated into the MPS. Multiple types of cells from various sources may be included. Generally, cell sources can be classified depending on where they were retrieved: commercially available cell lines, primary cells obtained from human donors, *ex vivo* tissue biopsies and stem cell sources [22].

Commercially available, immortalized cell lines have the advantage of exhibiting indefinite growth, their culture protocols are well-established and cellular responses are reproducible and predictable, providing experimental robustness. Yet, these advantages come at the cost of over time accumulation of karyotypic abnormalities. As a result, the physiological relevancy is lowered as culture periods are commonly extended [21]. Although limited in lifespan, primary cells isolated directly from human tissue better approximate the *in vivo* situation as they retain native functional and metabolic properties. Primary cells capture the genetic and functional mature phenotype of human tissues and are useful in modelling disease pathologies when obtained from donor patients [22]. Common issues encountered with primary cells are related to their limited availability, ethical concerns, batch variations and the requirement of specialized culture conditions [21]. The necessity of specialized culture conditions is especially limiting with respect to the use of primary cells in integrated multi-organ systems, as the common medium requirement (2.8) is likely to be sub-optimal to maintain proper cell viability [22]. Another common cell source that includes pre-existing, well-differentiated

cells for organ-on-chip approaches are *ex vivo* tissue biopsies. The advantage of tissue biopsies is that they entail natural extracellular matrices and tissue structures and are therefore capable of accurately recapitulating biological information also in a diseased context. Nevertheless, due to ethical and practical issues the availability of *ex vivo* tissue for experimental purposes is limited [23]. Stem cell-derived sources may address some of the above mentioned challenges. The motivation behind the use of stem cell sources in MOoC models, is their ability to be differentiated into specialized cells of various lineages and be assembled in multiple-cell type structures that resemble the *in vivo* counterparts of interest [23]. Stem cell sources include embryonic stem cells (ESCs) and adult stem cells (ASCs), but they do come with ethical concerns. Instead, the use of **human induced pluripotent stem cell (hiPSC)**s in disease models has emerged as a strategy to generate disease-specific cell lines that can be differentiated into a multitude of cell types with a similar genetic make-up. The effective use of hiPSCs depends on robust and well-defined differentiation protocols, but will ultimately contribute to patient-specific models to aid in the development of personalized therapeutic strategies. A drawback of using hiPSCs in disease models is the functional immature phenotype that is often achieved *in vitro*. Furthermore, tissue preparation time is another hurdle to be overcome, as differentiation times of hiPSCs can be long and more expensive resources are required compared to the use of conventional cell lines. Embedding hiPSCs derived tissues into MOoC would require the optimization of differentiation and maturation protocols.

Another consideration related to the cellular aspect of disease models is the type of cell culture method that is used. Traditionally, there are multiple techniques to grow and culture cells *in vitro*. Among those are **two-dimensional (2D)** cellular monolayers and **3D** cell cultures, such as spheroids and organoids. In MOoC platforms, monolayers or 3D tissue constructs may be grown directly on the chip by cell seeding and subsequent maturation in the respective chambers. The benefit of this approach is minimal disturbance of the tissue constructs and the confounding influence of growth under dynamic rather than static conditions can be avoided. Externally developed and matured cell constructs can also be transferred to the MOoC device at the initiation of an experiment. In this case the microfluidic platform must feature an accessible open MOoC organ chamber design.

During the early design phase of a novel MOoC platform, it is essential to critically consider the cell types and tissue constructs to be included to accurately represent the envisioned disease model. Then, chambers in the chip must be developed to cater to the specific needs of each individual cell population in terms of required size and culture method, to ensure prolonged cellular viability over the course of experiments.

2.2. MICROFLUIDIC PLATFORM ARCHITECTURE

From a platform point of view, it is essential to determine the most optimal chip configuration to provide an appropriate *in vitro* culture environment in line with the desired outcomes [24]. Typically, microfluidic devices feature microfluidic channels which both allow continuous perfusion of the organ chambers and facilitate control over biomechanical forces if flow parameters are altered. Parameters such as medium reservoir

volumes, organ chamber size, corners, inflow/outflow geometry, channel dimension and spatial organisation of channels are all affecting the final flow rate and thus will inevitably affect the device performance [22].

Chip designs are commonly organ-oriented with various geometrical features that support the main organ functions of the cultured tissue types. To guide chip architecture, a distinction can be made between whether a parenchymal tissue or physiological barrier structure is to be modelled, as both tissue types require different methods of perfusion and cell embedding [24]. The first class, parenchymal tissues, is typically modelled by seeding cells directly on chip in monolayers, embedding cells into natural or synthetic hydrogels or seeding them onto specifically designed scaffolds that feature an optimal matrix composition and have desirable electromechanical properties [25]. The second class, including barrier tissue chips such as the skin, lung, liver and intestines, is particularly suited to advance our understanding of selective transport and to identify factors involved in maintaining barrier integrity [24]. Typically, physiological barriers are modelled in compartmentalized devices, in which cell culture chambers and microfluidic channels are separated by a porous membrane that features a predefined porosity. Nutrient and drug transport across the barrier tissues is facilitated by independent fluid flows in different compartments. The porous membrane can be engineered in terms of structural, mechanical, chemical and even optical properties to achieve the required properties. In the context of modelling cellular barriers between external and internal environments, [Air Liquid Interface \(ALI\)](#) conditions are frequently established. In these models, one cellular compartment is continuously exposed to air to stimulate particular differentiation patterns.

In [MOoCs](#), the microfluidic architecture is ideally modular and can be configured in a way that the types and the order of the tissues can be adapted to fit with the biological questions posed. Either single-[OoCs](#) must be engineered to feature reversible interconnections such that the linking order and timing can be controlled or alternatively multi-organ platforms may be designed with single-organ hosting chambers. These individual chambers may then be directly linked via microfluidic channels on-chip.

2.2.1. CELLULAR ENVIRONMENT

An additional challenge is to ensure optimal conditions for each included organ-model. Not only the correct architecture of the microfluidic chip in itself is important, but the effect of the microenvironment and the composition of the scaffold or [ECM](#) should be considered. The tissue environment must replicate the local *in vivo* environment as closely as possible and should be engineered to stimulate adequate cell growth, support specific tissue characteristics and be bio-compatible with the proposed experiments. Systematic studies on the effect of cell-microenvironmental cues induced by microfluidic materials are recommended and must address the influence of biomaterial properties such as surface roughness, stiffness, wettability and topography [26]. The influence of the cellular micro-environment may manifest itself biologically in terms of cell adhesion, proliferation, differentiation and secreted products. Ultimately, the required cellular environment depends on what type of functional tissue is to be incorporated and is further defined by the context of use.

2.3. MATERIAL

Material selection is key to achieve an efficient and fit-for-purpose microfluidic system. The material of choice must be bio-compatible with all included cell types and must be. Important considerations include cost, re-usability, transparency, sterility, hydrophobicity and gas-permeability [20]. A range of materials have been used to engineer OoC platforms, but the majority are fabricated with polydimethylsiloxane (PDMS) as it has a number of useful characteristics such as ease of processing, affordability, fast prototyping, optical transparency and bio-compatibility. In addition, the stretching properties of PDMS facilitates recapitulation of stretch-related mechanical processes, such as breathing for lung-tissue or beating for the heart. However, PDMS-based chips are also prone to absorb small hydrophobic molecules which raises critical concerns with respect to the use of PDMS devices in drug or secretome studies [27]. To some extent, this issue can be addressed by accounting for the passive drug absorption by the PDMS material in physiological based pharmacokinetic models [28] or applying inert (lipid based) coatings [29]. Besides the material for the chip itself, other materials are commonly used during either the fabrication process of devices or to include additional features, resulting in multi-material chips.

2.4. ORGAN MODEL SCALING

MOoCs find their main application in replicating key aspects of the human system on the microscale. Achieving a systemic on-chip miniaturized dimension that accurately recapitulates *in vivo* metabolism and biomolecule exchange requires a well-defined strategy for organ scaling. The so-called scaling factor is a major design criteria, as it defines the boundaries of the dimensions of the microfluidic devices in terms of interconnected organ chamber sizes, microfluidic channel volumes and determines the amount of required cellular material. Theoretically, any cell or tissue that can be cultured *ex vivo* can be integrated in microfluidic platforms, but when cross-organ interaction studies are concerned, specific attention should be paid to their proportional scaling with the other organs of interest. In order to obtain an adequate *in vivo-in vitro* translation, scaling can be prioritized according to cell number, cell mass or cell-to-media volume. Another consideration is the role of and the adequate distribution of media and diffusion of oxygen through all tissue constructs [19]. Various scaling approaches to emulate *in vivo* organ proportions and functional organ relationships have been proposed, yet no consensus has been reached on the optimal scaling rules for microsystems [24]. Here direct scaling, allometric scaling, functional scaling and time-residence based scaling methods are shortly explained.

2.4.1. DIRECT SCALING

Direct scaling is the most straightforward method to scale down organs and thus far remains the gold standard in reported MOoCs. It implies that organs of interest are proportionally scaled down based on easily accessible anatomical data, such as total biomass, tissue volume or metabolic activity [30]. For example, one can simply decide on a suitable scaling factor compatible with the dimensions of the microfluidic device and subsequently divide the size of each target organ by this miniaturization factor [30]. Reported

scaling factors include 30,000 [31], 73,000 [32], 100,000 [33], but may range up to 400,000 [32]. Nevertheless, factors above 100,000 are likely to result in systems that are too small for operation [20].

Instead of basing the scaling factor on total organ size, cell number may be taken as the point of reference. In tissues, cell number is an important determinant of physiological functioning and is often taken as a key parameter to characterize drug filtration or absorption rates [34]. Therefore, the seeded cell number in each cell culture compartment is significantly important in an experimental set-up to simulate inter-tissue crosstalk [34]. To determine the required number of cells in a system, a straight forward, linear mass ratio can be computed, independent of organ function. As an example, this direct scaling approach for cell numbers was applied to determine the ratio 'r' between the number of endothelial cells and hepatocyte cells to be seeded in a two-organ model to simulate hepatic-vascular interaction. Here, fractions of the specific organs of interest with respect to total body weight are considered, as the underlying assumption is that cell mass does not vary with cell size nor weight [30]. Vascular endothelial tissue makes up 6.28% of total body weight, whereas hepatocytes present 60% of liver mass which then presents 2.6% of body mass. Using these numbers to calculate the ratio between the mass of endothelial cells and hepatocytes M_{endo}, M_{hep} according to Equation 2.1, results in a correlation that should be maintained in the designed *in vitro* experiment. In this example, this implies that the number of endothelial cells must be 4 times greater than the number of hepatocytes in order to maintain a physiological relevant interaction [34]. This method is relatively simple as merely knowledge of the respective masses of the tissue of interest is required, yet it oversimplifies the complex functional relationship between tissues.

$$r = \frac{M_{endo}}{M_{hep}} = \frac{6.28}{0.6 \times 2.6} \approx 4 \quad (2.1)$$

Thus, whereas direct scaling provides a tool to gain an initial idea about the organ sizes to embed in integrated MOoCs, it is limited with respect to physiological relevance as it is known that various organs scale differently depending on function and complexity. As a result, using a single scaling factor for multiple organs is likely to result in distortion of the relationship between organs and complicates *in vivo-in vitro* translation [30].

2.4.2. ALLOMETRIC SCALING

Allometric scaling captures the relationship between body mass and physiological parameters [34], [35]. Physiologically, organ size does not scale isometrically with organ mass (as assumed in direct scaling), but instead obeys various different allometric power laws related to metabolic activity, blood circulation times and level of innervation [35]. To conserve the same relationships between different tissues in a downscaled *in vitro* environment, allometry can be used to evaluate and quantify the relationship between different tissue types of interest. Governing laws dictate that physiological parameters are correlated with the total mass of an organism through various physical metrics [36]. The standard allometric equation includes an observable physiological parameter 'Y'

that correlates with system mass 'M' according to a simple power law shown in Equation 2.2 [34], [37].

$$Y = a \times M^b \quad (2.2)$$

Here, 'a' is a proportionality constant and the exponent 'b' depends on the biological quantity of interest. As an illustrative example, the nonlinear relationship between organs size and total body mass, which depends on coefficients related to the target species, is given by Equation 2.3.

$$M_{organ} = a \times M_{body}^b \quad [\text{kg}] \quad (2.3)$$

Using Equation 2.3 in combination with available datasets and established values for the coefficients 'a' and 'b', provides a tool to relate each individual OoC unit represented by M_{organ} to the total mass of the integrated system, M_{body} [35], [36].

Experimental designs that aim to recapitulate metabolic interactions between organs rather than organ mass relations, may instead benefit from adhering to allometric scaling laws that correlate metabolic rates. Matching the cellular basic metabolic rate (BMR) on the microfluidic chip to the BMR of cells in the body is an especially relevant scaling method to facilitate the study of metabolic diseases in multi-organ models [38]. It has been proposed that metabolic rates follow an allometric power law with coefficient $b = 3/4$, as nutrients are supplied to tissues via a fractal distribution network [39]. In this case the scaling relation becomes as shown in Equation 2.4.

$$\text{Metabolicrate} = a \times M^{3/4} \quad [\text{s}^{-1}] \quad (2.4)$$

Besides organ mass and metabolic rates, many other biological variables obey allometric scaling laws and may be used instead to derive the appropriate scaling factor in integrated MOoCs depending on the research aim [37]. Among those are pulmonary and vascular networks $b = 3/4$, blood volume $b = 1$, blood circulation times $b = 1/4$ and cellular metabolism $b = -1/4$ [38]–[40].

Though allometric scaling is a straightforward scaling method, it is limited especially on the milli- and micrometer scale, as adhering to the coefficients reported in literature results in respective organ sizes larger than the total feasible microfluidic system size. It has been speculated that allometric relationships based on mass parameters break down at the microscale, and hence not optimal in the design of MOoCs [35], [36].

2.4.3. FUNCTIONAL SCALING

To overcome the limitations of direct and allometric scaling, functional scaling has been proposed [35]. Functional scaling ensures the recapitulation of specific organ functions of interest on the microscale, rather than preserving relative masses and flow rates. In functional scaling, the most relevant organ functions to be included are identified, such

as pumped volume, beating frequency, filtration rate or absorption rate. The most important organ function may be a volume-mediated process or a surface-mediated process, which requires 2D or 3D scaling respectively. After specifying the functional parameter for each organ and deciding whether this is a volume-related or surface-related process, the MOoC can be scaled accordingly. The system can be subsequently validated by checking that each simulated organ meets the specific required functional activity. This may necessitate iterative optimization of the scaled tissues as *in vitro* tissue functionality is hard to theoretically predict due to confounding system factors. Whereas functional scaling is a valid alternative to allometric scaling, it is hard to capture the multifunctional nature of some organs and the question of how to define the major function of an organ in a multifactorial disease context still needs to be addressed [30].

2.4.4. RESIDENCE-TIME BASED SCALING

Finally, scaling can be based on known reaction kinetics in an approach termed **residence-time based scaling (RTBS)** [30]. This type of scaling matches the fluid residence time for each included organ and is derived from two physiologically relevant constraints:

- The ratio of organ chamber sizes and liquid residence times for each compartment must mimic physiological *in vivo* values.
- The volume to cell-ratio should be close to the physiological values found in humans

These requirements ensure that chemical cues secreted by cells in the MOoC system are not diluted beyond concentrations where they are no longer detectable. Commonly, RTBS is combined with pharmacokinetic simulations to validate whether the system is actually physiologically relevant [30]. Downsides to using RTBS as a scaling method are that it relies on the assumption that each organ module has a certain level of intrinsic activity and it does not account for the limited mass transfer between organ chambers due to the physical constrictions of MOoC platform design.

Overall, not many reported MOoCs with rational scaling and design principles exist, which makes it hard to make comparisons among systems. An overview of the various scaling methods and their limitations is presented in Table 2.1.

Table 2.1: Different organ scaling methods and their applications. Adapted from [30]

Methods	Direct scaling	Allometric Scaling	Functional Scaling	Residence Time-based Scaling
<i>Scaling principle</i>	Organs of interest are directly scaled according to defined scaling factor	Scaling of organs is based on allometric power laws that correlate parameter of interest to total mass	Scaling is based on identified main organ function	Scaling is based on blood residence time in each organ.
<i>Advantage</i>	<ul style="list-style-type: none"> • Intuitive • Easy to apply 	<ul style="list-style-type: none"> • Rich literature on anatomical parameters • Relatively straightforward 	<ul style="list-style-type: none"> • Preserve physiological organ function on microscale • Recapitulates most relevant organ functions in MOoC design • Easy and robust if functional data is available • Differential scaling of organs in MOoC depending on purpose 	<ul style="list-style-type: none"> • Captures reaction kinetics and dynamics between organs of interest • Prevents dilution of (secreted) biochemical cues
<i>Disadvantage</i>	<ul style="list-style-type: none"> • Results in distortion of appropriate relationship between organs • Over-simplifications same scaling factor is applied to each tissue type 	<ul style="list-style-type: none"> • Allometric scaling laws break down at microscale • Results depend on diffusive limit and mass transport 	<ul style="list-style-type: none"> • Organ function of interest may be hard to quantify <i>in vitro</i> • Hard to recapitulate more than one organ function accurately • Complex system designs require many different parameters and optimization requires computational approaches 	<ul style="list-style-type: none"> • Only successful if activity and capacity of organ modules are comparable to <i>in vivo</i> counterparts • Requires consideration of mass transfer between tissues • Mostly applicable for pharmacokinetic studies • Often requires computational simulations

2.5. COUPLING OF ORGAN MODELS

In order to create integrated MOoC set-ups, individual OoC models must be linked to facilitate the envisioned interaction. Coupling of individual organ models depends on both the microfluidic chip design and the specific purpose of the study. From a design perspective, MOoC systems can be created by functional coupling of organ models, physical or 'fluidic' direct coupling of stand-alone OoC models or alternatively by combining multiple organ models directly on a single chip.

The simplest coupling solution is to link single-organ systems functionally. In this type of set-up, medium is transferred sequentially between various organ chambers to study the effect of the secretome of one tissue type on another [27]. Functional coupling of individual organ modules can help to acquire information about media compatibility, allows to determine optimal scaling parameters and removes the challenge of varying flow rates between organ chambers. Thus, as an important preliminary step towards developing more complex MOoCs, functional coupling can be implemented to evaluate

the performance of single organ modules and further optimize individual organ chamber conditions [27]. Once each individual organ model has been characterized, a more complex type of coupling may be attempted.

Direct, physical coupling of single OoCs can be achieved through a capillary tubing system that links the media outflow of one organ to the inflow of the next organ [41]. Along the implemented tubing network, flow sensors, valves or other microfluidic components may be included to achieve the circuit of interest. Alternatively, capillary tubing systems may be indirectly connected via a central microfluidic mother board [24]. This additional component in the microfluidic set-up contains all microfluidic connection points which enables increased control over the particular flow to each connected organ-model. A central mother board facilitates automatized switching between differential microfluidic routes and facilitates easy integration of additional sensor components or other units to aid direct, real-time read-outs. Moreover, the 'plug-and-play' approach results in highly modular platform configurations allowing for the maturation and optimization of single organ models prior to system integration. Another advantage is the relative ease with which other serially connected tissue types may be added to the system or the ability to replace individual organ models in case of unforeseen dysfunction.

Lastly, MOoCs can be realized by combining organ models onto a single platform [42]. Recent research efforts have been focused on engineering user-friendly chip designs that directly integrate the organ models of interest by means of microfluidic channels. The main advantage of this approach is that the dead volume and required medium is minimized. Ideally, such in-house produced chips are compatible with commercially available tubing and perfusion systems and may exhibit culture chambers specifically designed to meet the tissue culture demands.

2.6. FLUID CIRCULATION

Control over the fluid dynamics is essential in MOoC models in order to mimic the *in vitro* blood flow across organs. MOoCs can be distinguished from each other based on the required method of fluid circulation and how this circulation is actually achieved in the system, an overview is provided in Table 2.2. Medium supply in MOoCs can either be static, unidirectional, bidirectional or involve recirculation of the medium. Single-pass or unidirectional perfusion is mainly applied to study the influence of one organ on other organs. Moreover, unidirectional flow is preferred in models that incorporate tissue types that are exposed to high mechanical shear stresses *in vivo* such as endothelial cells, as these stresses form important physical cues for the tissue maturation and integrity [20]. Bidirectional flow and recirculation of media are used to emulate reciprocal organ-organ interactions and are thus interesting to use in the context of studying systemic diseases, such as CRS.

In general, fluid circulation can either be passive or actively controlled by pumping mechanisms [20]. Passive control of fluid circulation depends on gravity-driven flow. During the experimental phase, gravity-driven platforms are commonly placed on a rocker platform. The angle of the rocker platform can be changed periodically to, for exam-

ple, introduce a bidirectional flow. The main advantage of systems that rely on gravity-driven flow is that the need for external fluid loops is eliminated, thus reducing the overall required liquid volume to operate the system. As such, it is easier to achieve near-physiologically blood surrogate volumes and generate detectable metabolite concentrations. In addition, pumpless systems potentially offer higher throughput, lower system costs and are less prone to introduce errors such as air bubbles and unwanted leakage of medium [43].

The main hurdle related to gravity-driven systems is to design platforms in which full medium recirculation is achieved, avoiding unintentionally retained medium that is then mixed with fresh medium in the respective organ chambers. In MOoC systems, incomplete medium circulation gives rise to problems related to reduced oxygenation and inadequate nutrient supply to organ chambers, which is especially problematic when relatively large tissue constructs like organoids are embedded [44]. On top of that, quantification and downstream analysis of the cellular secretome and parametric control over exact concentration profiles is not as straight forward to perform [43].





Yet, the circulation in the majority of reported MOoC systems is controlled by an active pumping system. Such a pumping system can be externally incorporated in the complete microfluidic set-up, or alternatively may be integrated in the chip design in the form of a micropump. External pumping systems can be subdivided into syringe pumps [44]–[46], peristaltic pumps [47]–[50] or pressure-based pumps. Lately, syringe pumps and peristaltic pumps are increasingly replaced by pressure controllers, which rely on the pressurization of media reservoirs in order to perfuse multi-organ set-ups. External pressure controllers are gaining popularity due to their high responsiveness and the generation of stable, pulseless flows in connected systems. Therefore, they are suitable to perform highly controlled experiments in which accurate flow rates and shear stresses on the cell constructs are a key research parameter. In addition, with an external pressure controller, the experimental set-up is modular and can be adapted to either provide single-pass flow or unidirectional recirculation.

To overcome the requirement of troublesome off-chip connections with external pumping systems and to further reduce the circulating volume, on-board micropumps have been developed: peristaltic micro-pumps [51], [52], pneumatic micro-pumps [53], [54] and kinetic (stirrer-based) pumps [55] as summarized in Table 2.2. Whereas micropumps are paving the way towards ever smaller microfluidic systems, caution should be taken with respect to the complex external wiring and tubing that is often still required and complicates the overall set-up.

2.7. FLOW RATES

Flow rates in MOoCs should be optimized to ensure fluid residence times in organ chambers that resemble *in vivo* organ perfusion times and to ensure that secreted factors can accumulate to levels above a given threshold concentration to be both measurable and exert an effect on the next organ model. Ideally, flow rates can be controlled and adjusted per individual organ chamber, as each tissue type has a unique metabolic profile and thus specified blood-perfusion demands. Namely, the on-chip flow rate affects

Table 2.2: Advantages and disadvantages of fluid circulation methods to choose in MOoC design

Type	Passive control	Active pumping systems					
	Gravity-driven system	Externally connected system			Internal on-board system		
		Syringe pump	Peristaltic pump	Pressure controller	Peristaltic micro-pump	Pneumatic pressure-based pump	Kinetic pump
							
Description	Flow is induced by hydrostatic pressure difference of fluid levels in connected reservoirs	Motor-controlled moving of a piston injects desired medium volumes in system	Based on compression and relaxation of flexible tubing	Pressurizes a medium reservoir from which fluid is pushed into the multi-MPS	Pressure is applied to a set of flexible membranes that generate pulsatile flow	Air pressure directly applied to on-chip organ chambers induces flow based on differences in liquid levels	Motor controlled integrated-stirrer bar induces kinetic flow
Advantages	<ul style="list-style-type: none"> - Easy set-up - No additional pump is required thus limiting confounding variables - Entire system is contained on single-chip without external fluidic loops (compact design) 	<ul style="list-style-type: none"> - Allows injection of very small medium volumes at the time - Flow rate is controlled independently of fluidic resistance in system 	<ul style="list-style-type: none"> - Convenient to use - Infinite fluid dispersion - Compatible with large volumes - Re-injection of same sample 	<ul style="list-style-type: none"> - Developed specifically for microfluidics - Fast response time - Able to handle large fluid volumes - Pulseless and stable flow - Can be used with a flow sensor for direct feedback (flow and pressure control) 	<ul style="list-style-type: none"> - Minimizes require dead volume - Integrated design results in compact system - Offers flexibility in chip design 	<ul style="list-style-type: none"> - Single pressure source for multiple circuits due to easy branching - Higher throughput - Fewer tubing required 	<ul style="list-style-type: none"> - No tubing require - Simple structure and set-up - High throughput
Disadvantages	<ul style="list-style-type: none"> - Flow rate inherently depends on channel geometries and tilt angle - Possible retainment of medium in tissue chambers 	<ul style="list-style-type: none"> - Volume is limited to size of syringe - Recirculation is impossible - Pressure may reach high values - Flow oscillations due to motor steps - Slow response time 	<ul style="list-style-type: none"> - Pulse in the flow rate - Flow accuracy decreases over time - Low precision - Tube aging influences performance - Large dead volumes 	<ul style="list-style-type: none"> - Higher costs - High pressures exceeding ~ 8 bar difficult to achieve - Possible back-flow of medium - Large dead volumes 	<ul style="list-style-type: none"> - Requires expert fabrication - Must be connected to external pressure controller 	<ul style="list-style-type: none"> - Pressure applied directly to organ chambers may interfere with tissue culture 	<ul style="list-style-type: none"> - Limited pumping efficiency - Shear stress on cells not recapitulated - Currently only in 24-well format

shear stress experienced by tissue constructs, influences cell polarity and determines the concentration gradient of oxygen and nutrient availability to a large extent [44].

The desired experimental flow rate depends on the main research objective that is to be answered. If shear stress on tissue constructs is relevant and the range of permitted

shear stress is defined within the study parameters, the desired flow rate may be calculated with Equation 2.5. This equations describes the shear stress due to laminar flow and holds for Newtonian fluids under steady condition in rectangular microchannels. Here ' τ ' is the shear stress of interest, ' w ' is the channel width, ' h ' is the channel height and ' η ' is the dynamic viscosity of the medium.

$$Q_{desired} = \frac{\tau w h^2}{6\eta} \quad [\text{m}^3\text{s}^{-1}] \quad (2.5)$$

If shear stress is not the main determinant, another key starting point is to consider the fluid residence times within each organ compartment of the designed system. Ideally, *in vivo* tissue perfusion rates are mimicked in the microfluidic set-up to in accordance with the respective organ chamber volumes and cell seeding densities. To follow this reasoning, *in vivo* blood residence times ' τ_{phys} ' must first be calculated using the ratio of blood flow through each organ per time unit ' Q_{vivo} ' and the corresponding organ volume ' V_{organ} ', as shown in Equation 2.6 [32].

$$\tau_{phys} = \frac{V_{organ}}{Q_{vivo}} \quad [\text{s}] \quad (2.6)$$

From the *in vivo* physiological fluid residence times ' τ_{phys} ' and the on-chip organ chamber volume ' V_{chip} ', the required *in vitro* flow rate ' $Q_{desired}$ ' can be calculated with Equation 2.7.

$$Q_{desired} = \frac{V_{chip}}{\tau_{phys}} \quad [\text{m}^3\text{s}^{-1}] \quad (2.7)$$

The required organ residence time can thus be achieved by varying organ chamber size or alternatively by directly altering the respective flow rate if active control mechanisms are implemented. In MOoC systems, the medium flow rate can be optimized and controlled for each individual set-up in a system-dependent manner depending on whether the flow circulation is achieved passively or actively.

First of all, flow-profiles in passive, gravity-based systems can be optimized by designing MOoC systems with specific channel and chamber geometries. The flow in gravity-regulated systems mainly depends on balancing the pressure drop across the system. It can be varied by adjusting the hydraulic resistances of the channels or tubing in accordance with the research aim. The hydrostatic pressure drop ' ΔP ' across a given organ chamber depends on the height difference between the inlet and outlet at a given platform tilt angle ' h ', the gravity constant ' g ' and the density of the cell culture medium ' ρ ', as shown in Equation 2.8. Furthermore, since the hydraulic resistance of any microfluidic segment ' $R_{segment}$ ' depends on the proportion between the corresponding pressure gradient imposed on both ends ' ΔP ' and the desired flow rate through the segment ' $Q_{desired}$ ', the hydraulic resistance of a microfluidic segment follows from Equation 2.9

[43]. Rewriting Equation 2.8 and Equation 2.9 results in an expression for the desired flow rate that depends on the hydraulic channel resistance and the pressure difference determined by the platform tilt angle, as shown in Equation 2.10.

$$\Delta P = \rho gh \quad [\text{Nm}^{-2}] \quad (2.8)$$

$$R_{segment} = \frac{\Delta P}{Q_{desired}} \quad [\text{Nsm}^{-5}] \quad (2.9)$$

$$Q_{desired} = \frac{\Delta P}{R_{segment}} = \frac{\rho gh}{R_{segment}} \quad [\text{m}^3 \text{s}^{-1}] \quad (2.10)$$

The channel sizes must be designed such that they provide a hydraulic resistance that indeed limits medium flow to the desired range. In general, the fluidic resistance of a segment ' $R_{segment}$ ' consists of the sum of hydraulic resistances in each fluidic branch: the resistance of the channels that lead up to and away from the cell culture chamber and the resistance of the organ chamber itself as shown in Equation 2.11.

$$R_{segment} = R_{channel_{in}} + R_{chamber} + R_{channel_{out}} \quad [\text{Nsm}^{-5}] \quad (2.11)$$

To achieve the required flow rate, the corresponding required height, width and length of the microfluidic channels can be calculated in order to achieve customized hydraulic resistances. In case of rectangular microfluidic channels with a low aspect ratio ($w > h$), the channel resistance ' $R_{channel}$ ' can be approximated by Equation 2.12 [43]. In Equation 2.12, ' η ' is the dynamic viscosity of the culture medium, ' L ' is the length of the channel, ' h ' is the height of the channel and ' w ' the width of the channel.

$$R_{channel} = \frac{12\eta L}{1 - 0.63 \frac{h}{w}} \cdot \frac{1}{h^3 w} \quad [\text{Nsm}^{-5}] \quad (2.12)$$

Thus, if the desired on-chip flow rate and organ chamber residence times are known, corresponding channel dimensions can be calculated with help of the above outlined calculation scheme. This provides a useful guideline in chip design. Vice versa, if chip dimensions are known (for example from commercially available products) the formulas may instead be used to calculate the theoretical flow rates or chamber residence times.

On the other hand, when instead of gravity, active pumping systems are equipped to generate flow in microfluidic set-ups, another approach should be taken as optimizing chip geometries alone is no longer enough. Syringe pumps or peristaltic pumps control fluid flow volumetrically by using a mechanical movement to alter a contained volume. In the case of syringe pumps, different flow rates can primarily be achieved by modifying the syringe volume and customizing the system-infusion rate. Peristaltic pumps are known to have limited capacity to generate perfectly controlled flow rates. Here, the generated flow rate is primarily dependent on the peristaltic pump head structure, which includes

rollers and tubing of particular dimensions, and the driving speed of the pump. To adjust the generated flow rate, it is recommended to either change the tubing dimensions as microfluidic resistance decreases with tubing diameter according to Equation 2.13, or to change the driving speed.

$$R \propto \frac{1}{d^4} \quad [\text{Nsm}^{-5}] \quad (2.13)$$

Lastly, when pressure controllers are chosen to drive flow, they are pre-programmed to exert a certain pressure on a contained medium column or reservoir that has a fluid outlet that links to the microfluidic set-up. Fluids move due to the pressure difference that arises between the reservoir inlet and outlet. Similar to gravity-driven flow, the flow rate depends on exact channel geometry. However, some pressure controllers have been equipped with company software that enables the user to directly approximate flow rates, especially if a complete company specific set-up is used, including microfluidic chip. To improve the precision and responsiveness of the actual achieved flow rate, external peristaltic pumps and pressure-driven pumps can be connected to a flow sensor that is integrated into the microfluidic set-up. This sensor provides the pumping system with direct feedback about the flow rate at defined points along the circuit and can thus be used to alter the pressure to achieve the requested flow value.

On a final note, flow rates are always affected by the total area and smoothness of the implemented substrates and the microfluidic channels, thus underlining the importance of considering material choice early on in the design phase. Furthermore, computational models and/or fluid simulation software, can be used to make theoretical estimations of fluid flow profiles and provide a guide to setting flow-related parameters. Subsequently, experimentally obtained results about generated flow can then be compared to the computationally derived flow rates as a means of validating novel microfluidic systems.

2.8. BLOOD SURROGATE MEDIA

2.8.1. MEDIA FORMULATION

Each tissue type embedded in a MOoC must be provided with a nutrient and growth factor supply that fulfils the specific tissue requirements. Therefore, MOoC culture conditions and the maintenance medium must adhere to a wide range of requirements, in part due to varying metabolic activities of the different tissue types [20]. This problem is further complicated when sensitive cell types are to be included in the system [24]. A universal medium, or 'blood surrogate', must feed all organ compartments in order to support growth, long term viability and facilitate functional integrity of every individual tissue type. The systemically shared medium interconnects the organ modules and thus mediates continuous organ cross talk by transporting nutrients, growth factors, cytokines, hormones, cell metabolites, drugs and other cellular components [30].

Typically, culture media contain various levels of animal-derived serum factors and are tissue type specific, which once used in MOoC set-ups may result in unwanted and unpredictable confounding effects on the differential tissues. To overcome this, a serum-free common medium that minimally influences tissue function, yet contains all the required nutritional components and growth factors for each individual organ would be

ideal. To date, such a standardized universal medium has not been reported, but various complementary strategies have been proposed to tackle the issue.

Firstly, a common medium formulation has been prepared by mixing already existing cell-type specific media of the target organs in equal ratios. In this way the common medium contains essential growth factors to meet the demands of all included organs at least to some extent [30], [56]. However, as the complexity of a MOoC rises and more than two organ models are integrated, the success rate of a mixed medium solution decreases as tissues will inevitably suffer from suboptimal medium conditions [22].

Another strategy is to start from a chosen formulation of minimal medium and subsequently add the required growth factors, hormones, fatty acids and lipids, vitamins and trace elements as demanded by the cultured tissues [24], [57]. The base medium can be chosen in line with the research purposes and may be the medium of the most demanding cell line in the system, as is often the case when liver cell cultures are involved due to their high metabolic rate [20], [33]. With respect to supplementing a base medium as functional blood surrogate, caution should be taken that none of the supplements are detrimental for any of the other organs. Therefore, it is good practice to execute isolated medium compatibility experiments prior for all tissue types prior to performing any chip-based experiments, and adjust the medium formulation according to the observed cellular results.

2.8.2. MEDIA VOLUME

Besides the media formulation, the total volume of the common circulating medium should be given consideration. This volume should ideally be scaled relative to the incorporated organ volumes. Especially when the end-goal is to capture organ-crosstalk, regulating the medium volume in the overall system is of utmost importance as it directly influences the concentrations of drug metabolites and tissue secreted factors in the microfluidic set-up [20]. Keeping the internal volumes minimal ensures that secreted factors are not diluted below the detection limit and that they reach concentrations high enough to exert an effect in the organ of interest. On the other hand, the available volume must be large enough to also maintain the on-chip cell cultures with adequate nutrition and provide a constant supply of fresh oxygen.

The total medium volume consists of all the circulating fluid that resides in the medium reservoirs, passes through the microfluidic channels and tubing and the interstitial volume of medium that is present in the organ chambers [20]. Regulating the medium volume is most straight forward in the direct scaling approach, as the established scaling factor can be applied again. In this case, the physiologically relevant blood surrogate volume for a particular device can be calculated by dividing the average volume of blood present in the human body by the same scaling factor as was used to compute the functional tissue volumes that were embedded in the system [32].

Ideally, multi-organ platforms are operated with minimized medium volumes to achieve a volume-to-cell ratio that matches human physiological values. Not only does this reduce the required resources, but it also helps to induce accurate organ interaction and facilitates medium read-outs. It is good practice to consider the required perfusion vol-

ume early-on in the design process.

2.9. MOOC READ-OUTS

The operation of MOOCs entails significant effort and often requires long experimental timelines. Therefore it is essential to optimise assaying techniques to extract maximal biological information over the time course of a single experiment [26]. Monitoring and analysis of MOOCs can be achieved by means of *in situ* monitoring, online analysis and downstream offline analysis [24].

Most current monitoring and analyses approaches still rely on offline analysis at the end of experiments. Offline measurements can be performed either on retrieved intact and dissociated tissue constructs from the microfluidic set-up or alternatively may be executed on effluent medium samples taken at distinct time points. Analysis is based on conventional biological assays, including multiplex assays, spectroscopy, sequencing and flow cytometry [19]. Typically, life-death staining and structural morphology are taken as a study end-point to characterize tissue integrity. To ensure representative results, limit biases and prevent disruption of the spatial organization of cells in tissues, chip design must allow for easy removal of tissue constructs and dismantling of the device from the set-up post-experimentally.

Ideally, novel platform designs are amendable to higher-throughput analytical systems that allow for continuous real-time information acquisition. Therefore, *in situ* monitoring is performed in the device itself and thus provides a way to track experimentally induced tissue changes over the time-course of an experiment. Such near-real time assessments of tissue state and functionality include continuous measurements of pH, oxygen levels, contraction force and beating frequency, barrier function quantification by means of trans-epithelial electrical resistance measurements, and direct cell tracking and labelling. Characterization of tissue types is commonly done through microscopy, though imaging in this case is limited by the three-dimensional, multi-material nature of the incorporated constructs, which complicates image acquisition. More recently, *in situ* monitoring has been advanced by incorporating specifically designed biosensors in MOOC platforms that allow direct online analysis. Such online functional readouts are likely to increase experimental consistency and will aid in capturing complex dynamic interactions. Automated optical and biochemical sensing modules may provide sensing data on: pH, O_2 , temperature, glucose and lactate levels, protein biomarkers and organoid morphology [48]. Integrated sensors provide direct insights into response related fluctuations in OOCs, otherwise missed by conventional periodic measurements.

Despite the advantages of integrated biosensors, they also generate vast amounts of information-rich data and thus require subsequent data-interpretation steps. Synergistic engineering in this respect, converging the fields of data analysis and cellular biology, will further advance the integration of artificial intelligence and machine-learning approaches in MOOC experimental pipelines.

Ultimately, *in vitro-in vivo* extrapolation is essential for the interpretation of results. This requires consideration of the measurement timescale versus physiological timescales,

spatial resolution in the miniaturized system and whether the read-outs are quantitative or qualitative in nature [26]. Ideally, real-time *in situ* measurements and post-experimental offline analysis are combined to provide insights into the functioning of the coupled organ systems, their metabolic profiles, systemic inflammation levels and demonstrate drug efficacy and toxicity. With respect to multi-organ systems, read-outs should capture both organ-specific functioning that can be compared to control experiments as well as include read-outs related to the systemic dimension to illuminate organ interactions.

2.10. STATE-OF-THE-ART MOOCs

The last years have seen a tremendous leap forward in terms of microfluidic fabrication technologies and microfluidic OoC approaches. As a result, increasingly complex multi-MPS designs are surfacing as the next big step towards realizing a complete *in vitro* human model system. Existing MOoC platforms generally recapitulate specific organ-organ interactions to provide unique insights into inter-cellular cross-talk on the microscale. Yet, most reported platforms are still limited in their physiological relevance or inaccurately mimic the native human environment. In order to further advance the potential of MOoC platforms, it is beneficial to acquire a broad overview of the existing platforms, their particular applications and design trade-offs that were made. Recently reported MOoC systems have been reviewed and categorized according to the described design criteria in this chapter. The systemic literature review written prior to this thesis included MOoCs that comprised at least two-organ-models, were operated with an active medium pumping system and incorporated experimentally derived 3D cellular constructs. The complete literature review is included in the Supplementary Materials.

3

MICROFLUIDIC MODEL DESIGN REQUIREMENTS

The theoretical framework of relevant design criteria for novel MOoCs as developed in Chapter 2, was used to establish a list of requirements for the design of an ideal MOoC system for the recapitulation of CRS *in vitro*. These requirements are further stratified into must-have requirements (Demands) and nice-to-haves (Wishes) to subsequently aid in prioritizing trade-offs during the actual design conceptualization phase. A complete overview of the requirements is provided in Appendix A Table A.1.

3.1. CELL SOURCES AND CULTURE METHOD

- **Cell culture conditions** Chip maintenance must be possible in an 37°C and 5% CO₂ environment for an extended period of time to ensure tissue viability and optimal culture conditions. Ideally, the humidity of the environment can be controlled and maintained high to prevent medium evaporation and drying out of the channels. (DEMAND)
- **3D hiPSC tissue constructs** The microfluidic chip must be bio-compatible with recently developed cardiac microtissues (CMTs) and kidney organoids (KOs), which are cultured in accordance with the established protocols [58], [59]. These 3D tissue constructs derived from hiPSCs that require up to three weeks pre-culture before they are mature enough to be transferred to the system. The use of established protocols reduces the need for extensive organoid characterization as this has already been performed before. (DEMAND/WISH)

3.2. MICROFLUIDIC PLATFORM CONFIGURATION

- **Separate culture chambers** The system must render at least two organ chambers to confine the respective tissues and allow the study of reciprocal crosstalk in the absence of direct cellular contact. These microfluidic chambers may either be hosted on a single platform or be fluidically coupled to facilitate the prolonged co-culture in a single circulatory system. (DEMAND)
- **Open-culture system** It is desired that externally cultured and matured tissue constructs can be transferred onto the chip device prior to starting the experiment. Therefore, the on-chip chambers must be open at the initiation of an experiment and it must be possible to tightly seal the chip prior to the introduction of flow. (DEMAND)
- **Double-chamber chip** Two-microfluidic chambers integrated on a single microfluidic chip such that it can host both organ models. This presents the advantage of reducing the required death tubing volume and thus contributes to lowering the internal system volume. (WISH)

3.3. CELLULAR ENVIRONMENT

- **Scaffold-free** No scaffold or additional ECM reconstituent is used in the disease model to maintain the tissue constructs. Any scaffold material may interfere with the secreted products of the CMTs and KOs, thereby limiting observable cross-organ effects, which is the aim of this project. Preferable, only tissue-constructs are loaded in the tissue chambers. (DEMAND)
- **Culture inserts** It is valuable to consider the integration of existing tissue culture inserts into the chip environment. Culture inserts are already extensively used in tissue culture applications and can be used to pre-culture tissue specimens under defined conditions and in accordance with established protocols. Subsequently, the insert can be inserted in the chip, thus omitting the need of manual tissue transfer and preventing tissue disturbance. (WISH)

3.4. MATERIAL

- **Bio-compatible** Microfluidic devices must ensure biocompatibility with the tissue constructs. It is essential that 3D tissue structures do not dissociate nor lose their shape as this will contribute to loss of function. In addition surface properties must prevent fibroblasts from proliferating and migrating outwards of the tissue constructs. To further ensure tissue viability, it is vital that no residual toxic particles are released from progressive wear-down of the tubing or the device itself. Surface passivation steps may be incorporated in the protocol to further ensure bio-inertness of the material. (DEMAND)
- **Non-absorbing material** In order to achieve organ cross talk, molecular and cellular secreted factors should remain in the circulating medium to exert an effect on the downstream tissue construct. The chip material should not absorb any biomolecules such that the expected limited availability and concentration is not

reduced even further. Alternatively, a mitigation strategy may be used to passivate the surface, such as the application of a coating (DEMAND)

- **Air-permeable coverslip** The culture chambers must be closed by an air-permeable lid or coverslip to ensure adequate oxygenation over pro-longed culture periods. (DEMAND)
- **Sterility** Performing cellular experiments in OoC devices requires sterility to avoid microbial contamination. With respect to MOoC experiments, all the various microfluidic components must be sterilized prior to use and a methodology must be defined to maintain the sterile environment throughout the entire experiment. The appropriate sterilization method must be chosen for each component as either structural damage or alterations to the material properties must be avoided. (DEMAND)
- **Re-usable chips** Microfluidic chips are generally expensive devices. Since many proof-of-concept experiments are expected to be performed to validate both the microfluidic set-up and to optimize on-chip culture conditions, it is desirable that microfluidic chips can be used multiple times without the need for cumbersome cleaning protocols or altering material properties. (WISH)
- **Re-usable tubing** Perfusion sets and other connecting components can be cleaned and re-used for subsequent experiment without progressive wearing down of the material as this is hard to control in experimental settings. (WISH)

3.5. ORGAN MODEL SCALING

- **Scalable tissues** When a systemic disease such as CRS is concerned, functional scaling may prove to be physiologically more relevant than direct scaling if the main interest is to study the reciprocal interaction of tissues. Nevertheless, functional scaling is not straight forward to quantify and implement, therefore the method of direct scaling suffices during the initial phases of this project. This will be further described in section 5.2.2. (DEMAND)
- **Chamber size** Since relatively large organoids are to be used it is essential to ensure that the chip chamber sizes are big enough to fit the complete tissue construct. Yet, caution should be taken to keep the internal volumes as low as possible to maintain a near-physiological volume-to-cell ratio. (DEMAND/WISH)

3.6. COUPLING OF ORGAN MODELS

- **Single-pass system** Medium from one organ can be circulated to the subsequent organ with single pass through both organ chambers (series-connection). (DEMAND)
- **Modularity** The system should be modular in nature. This means that the used components are compatible with products from various companies to extend the possible circuits at later stages of the project. Ideally, the microfluidic set-up can gradually be extended to incorporate more sensors and chips with variable lay-

outs, while offering the possibility to run on tailored made protocols. This can be interpreted as a plug-and-play approach and is particularly useful in the step wise development of an increasingly complex system as every intermediate set-up can be validated during the process before proceeding. (WISH)

3.7. FLUID CIRCULATION

- **Automated flow control** The circulation, be that unidirectional or recirculation, must be computer controlled to omit human interference with the system. Automation of the flow ensures high control over parameters, facilitates repeatability of experiments and ensures constant conditions during the complete experiment. (DEMAND)
- **Types of flow** Flow has been shown to increase the maturation of tissue constructs and provides a way for prolonged, automated culture of tissue constructs in highly-controlled environments and is therefore a desirable attribute to MOoC culture systems. Unidirectional flow in the context of organoid co-culture facilitates the study of the effect of one organ's secretome on the other, whereas bidirectional flow may be used to study their reciprocal interaction. A unique property of recirculation of medium is that it contributes to the gradual accumulation of secreted cellular factors in the system, which may prove challenging in a unidirectional system. The designed set-up must be adjustable to constitute all three types of flow: unidirectional, bidirectional and recirculation. (DEMAND)
- **Pressure pump operated** Pressure pumps are reliable sources to generate non-pulsatile, continuous flow in microfluidic systems while providing an easy interface to control or adapt the settings of an experiment. (WISH)
- **Multiple chips in parallel** To increase experimental throughput and test various conditions simultaneously, the control unit must be able to perfuse a multitude of chips at the same time. This implies that the pressure controller must have multiple output ports. Typically a biological experiment requires three technical repeats and includes a control experiment versus a testing condition. Therefore, in order to test all conditions in parallel during a single experiment, a minimum of six microfluidic chips must be connected. To account for experimental error during the process, ideally two additional chips can be included. (WISH)

3.8. FLOW RATES

- **Refreshment of medium to support cell-culture** The flow in this project mainly functions to ensure continuous medium renewal in the on-chip culture chambers. Due to the use of organoids rather than cellular monolayers, shear stresses induced by the flow are less of a concern and flow rates may be varied in accordance with the calculated refreshment rate or desired experiment run time. (DEMAND)
- **Flow rate control per organ chamber** *In vivo* organs are exposed to different flow rates depending on their bodily location and function. In additional, the total blood residence time varies per organ. To account for this variability, microflu-

idic platforms can be designed to render individual control over the flow rate per organ chamber. (WISH)

3.9. COMMON MEDIA

- **Common media formulation** The system must be run with a single medium through a shared perfusion line to feed all organ models. The common medium must be kept as simple as possible with the least number of additional growth factors to prevent unwanted interference with any of the organoids. (DEMAND)
- **Low internal volume** The volumes used in the final set-up must be kept minimal to achieve physiologically relevant volume-to-cell ratios in the system, as will be explained further in section 5.2.2. Besides, the use of low volumes prevent dilution of secreted factors beyond detection limits and ensures that they can exert a possible effect on the co-cultured tissues. Yet, caution must be taken in that the supplied medium does fulfill the cellular nutrient and oxygen requirements. (DEMAND)

3.10. ANALYSIS

- **Material retrieval** It is desirable that the cellular material is accessible for post-experimental analysis and can thus be retrieved from the chip environment with minimal disturbances to the structure. Theoretically this implies that it must be possible to re-open the chip at the experimental endpoint. (DEMAND)
- **Sampling** A straightforward and effective sampling method must be achievable with the system. The main targets for detection are secreted factors commonly present in very low concentrations in the medium. Offline sample analysis mainly comprises high-performance liquid chromatography, mass spectrometry or commercially available assay kits for the selected biomarker. Each of these tests requires a minimal sampled volume which should be taken from the circulation during the experiment or collected at the end-point. For example, for the detection of proteins using an Enzyme-Linked Immunosorbent Assay (ELISA), typically between 50 and 100 μL of sample is required. When recirculation is implemented the sampled volume must be replaced by fresh medium to allow the continuation of the experiment. (DEMAND)
- **Live imaging** Live imaging during flow experiments is required to monitor tissue integrity and detect morphological changes early on during an experiment. (DEMAND)
- **Chamber access** Organ chambers are accessible at any desired time point during a flow experiment. In this case, medium samples may be taken from the respective chambers and used for offline analysis to monitor changes in the cellular microenvironment. Moreover, accessible chambers allow precise tissue perturbation at distinct time points by administering particular drugs directly to the organoids, rather than perfusing them throughout the entire system. (WISH)

- **Real time monitoring of flow** To maintain precise control over the parametric flow in the microfluidic system, the control unit must be able to export data files that contain the various flow-related parameters over time. This data may be used to compare the chip conditions across experiments and to rule out any confounding factors induced by altered flow rates. (WISH)
- **Integrated sensors** To control experimental conditions additional automated sensors can be incorporated in the design that provide real-time, continuous, *in situ* data on microenvironment conditions and tissue quality. Sensors that measure pH, O_2 , glucose concentrations or beating frequency directly can optimize the performance of MOoC platforms. (WISH)

4

CONCEPTUAL DESIGN

Based on the design criteria for a novel MOoC microfluidic set-up to capture cardiorenal crosstalk, two conceptual set-ups were proposed to perform feasibility studies with.

4.1. CHOICE OF MICROFLUIDIC CHIP

A prime starting point to developing any microfluidic set-up, is to decide on the microfluidic chip to be used throughout the experiments. The main design limitation with respect to this decision is that the chosen chip must be commercially available. The advantage of off-the-shelf chips is that they are under strict quality control, thus making them ideal to standardize experimental protocols. Since the project is aimed at establishing a MOoC system, it was essential that at least two types of tissues could be fluidically connected, while staying physically compartmentalized. Furthermore, fully developed organoids are to be transferred onto the chip once they have reached the required level of maturity. As such, the need for the chip to provide suitable pre-culture conditions for either type of tissues is omitted and the chip should solely offer a way to facilitate communication between culture chambers. Therefore, the preferred chip architecture consists of two on-chip interconnected chambers, as this greatly reduces the tubing complexity and further limits the inevitable dead-volume compared to the option of connecting two single-OoC. A thorough market search was performed to identify commercially available OoC devices that fit the requirements.

The IBIDI μ -slide III 3D perfusion was found to feature a suitable architecture in line with the above mentioned criteria and was thus chosen to perform proof-of-principle studies with. This microfluidic device is unique in its relatively straight-forward design and promised to serve adequately for the envisioned experiments. The on-chip microfluidic volume is 130 μ L per channel. Each reservoir additionally contains 60 μ L. That means that the total on-chip volume equals 250 μ L per channel. The chip and its exposed view are shown in Figure 4.1.

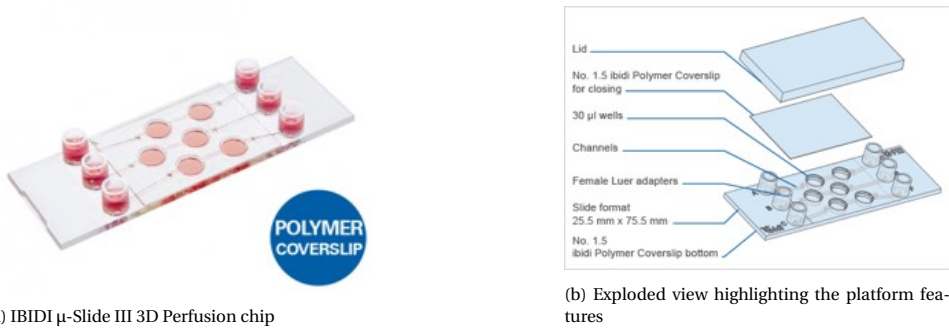


Figure 4.1: The microfluidic chip of choice for this project is commercially available and features two interconnected organ chambers. Adapted from <http://www.ibidi.com>.

4.1.1.1. IBIDI CHIP LIMITATIONS

Commercially available microfluidic chips are typically designed as generic as possible and therefore often fail to comply with all requirements. Therefore, it was inevitable to make some well-considered trade-offs related to the microfluidic chip of choice. The following limitations must be taken into account when interpreting the obtained results from feasibility studies and during subsequent design of follow-up experiments.

First of all, if the intended use of the IBIDI μ -slide is with either spheroids or organoids, as is the case in our experiments, the provided protocol prescribes to sandwich the 3D tissue constructs within gel matrices. We hypothesized that the chip could also be used without the additional scaffold material, by simply allowing the tissue to sediment to the bottom of the respective organ chambers. Whether this is indeed possible and in order to evaluate whether tissue integrity is maintained and tissue wash-out is prevented, feasibility studies have to be performed within the chip, see Chapter 5.

Secondly, in spite of the fact that the slide is designed to be compatible with high resolution light microscopy, this is only true for inverted microscopy techniques. Whereas this is not a problem as long as only tissue constructs are embedded in the chamber, it becomes challenging to actually image the tissue upon inclusion of fit-for-purpose components such as cell-culture inserts that elevate position of the tissue constructs.

Another consideration to keep in mind is the material properties of the chip. This platform can currently be ordered either **Uncoated**, making it hydrophobic, or with an **ibi-Treat Surface coating** which is an hydrophilic surface modification and supports cell-adhesion. Critically, none of those coatings prevents protein absorption by the chip, which is a high-priority requirement when biological assays are to be performed. To solve this problem, the chip may be treated with a surface passivisation coating which disables any type of protein binding. This would be ideal for our envisioned organoid applications, as it simultaneously ensures that the embedded tissue does not adhere to the surface. So far, no biological assays to quantify tissue adherence or protein absorbance by the chip material have been performed and thus further experimentation is required.

4.2. MICROFLUIDIC SYSTEM SET-UP

A hallmark of microfluidic experiments is the continuous and automatic perfusion of medium through the chosen chip devices. In order to achieve this perfusion, the pumping system must be chosen carefully depending on the research questions to be answered. This thesis focused on the development of a proof-of-principle microfluidic set-up and therefore emphasis has been placed on testing an initial set-up that complies with as many as possible requirements, yet is kept as simplistic as possible and is able to be developed with available products. Three established microfluidic systems were found to be suitable and were considered in more depth for the purpose of this research. The three systems were evaluated on the basis of the design requirements outlined in Chapter 4. For each of the design requirements a score was allocated based on available information, user-reviews and personal experience. A complete overview of the extent to which each microfluidic system conforms to the individual requirements is provided in Appendix B. The summarized results are presented in Table 4.1.

Table 4.1: Summarized grading of the extent to which each considered microfluidic system complies with the set design requirements.

	TissUse HUMIMIC Starter	IBIDI Perfusion system	Fluigent FlowEZ TM
✓	25	17	18
?	-	4	8
X	6	10	5

✓ = Fulfilled requirement; ? = Partly fulfilled requirement; X = Failed to meet requirement

The final system design decision was made on ground of the presented grading scheme, while taking into consideration the expected ease-of-use and the required costs for the actual realization of the complete system. As becomes evident the TissUse HUMIMIC Starter package, specifically designed for MOoC applications, has the highest overall score if judged purely based on the perfusion system itself. However, the TissUse HUMIMIC Starter package is not compatible with the previously selected microfluidic chip and should be operated with the TissUse microfluidic chips instead, which all together has a very high associated cost. Upon giving the requirements of costs and availability heavier weights during the design decision process, the TissUse HUMIMIC Starter package was found not to be feasible.

On the other hand, the IBIDI and Fluigent systems are readily available in the lab, therefore it was decided to run proof-of-principle experiments with both set-ups. During this project various dynamic assays with embedded tissue constructs and perfusion of culture medium have been performed, as will be commented upon in Chapter 6.

4.2.1. IBIDI PUMP SYSTEM

The first conceptual set-up to be tested was created with the IBIDI pump system, as this set-up promised to be advantageous in terms of ease of use. The IBIDI pump system allows for the application of continuous, unidirectional recirculatory flow. The IBIDI

Table 4.2: Tubing parameters for the IBIDI recirculation set-up and the Fluigent single-pass set up.

Type of tubing	ID Tubing	Tube Length	Total Working Volume	Dead Volume Tubing	Reservoir Size
Perfusion Set BLACK	0.5 mm	50 cm	2.6 mL	0.1 mL	2mL
Custom tubing Fluigent	0.794 mm	95 cm	4.47 mL	0.15 mL	Depends on set up

pump system is recommended to be used in conjunction with IBIDI channel slides, among which is the IBIDI μ -slide III 3D Perfusion, and runs on provided PumpControl software only. Chips produced by another company may be used given that they feature Leur-lock connections on the inlet and outlet. In that case, the performance of calibration experiments to determine the achieved flow rates is essential prior to starting any experiment.

The complete set-up comprises a pump system, required number of Fluidic unit (FU)s, perfusion set of choice (the tubing) and the microfluidic chip. The basic set-up is shown in Figure 4.2 [60]. Since our chosen microfluidic chip features three individual channels on a single chip (Figure 4.1), three FUs were connected to the pump such that all three microfluidic lanes could be perfused simultaneous. This enabled the testing of multiple experimental conditions at the same time. Various perfusion sets are available, each suitable for a particular range of flow rates. Here, the BLACK perfusion set was used (see specifications in Table 4.2), which allows to generate flow rates in the range of 0.08 mL/L to 1.10 mL/L. To keep the required volume as low as possible, the smallest type of compatible reservoirs were used with a total volume of 2 mL, each of which is to be operated with 1.25 mL per reservoir during the experiments. The set-up was used to run experiments up to 72h. The results are described in Section 6.1.1.

WORKING PRINCIPLE AND SETTINGS

The IBIDI pump is able to generate constant flow of medium by supplying the reservoirs of the FU with a constant air pressure (mbar) that is automatically set by the software based on the required flow rate. In the experiments presented here, the flow rate was set to 100 μ L/min. To ensure unidirectional flow over the chip and to prevent the reservoirs from falling dry, two valves that are integrated in the FU are continuously switched between two possible states, as described in more detail in the Instruction Manual [60]. The valve switching time was set to 60 seconds. Furthermore, the system was run with a positive air pressure such that the channel is perfused from left to right and the medium viscosity was set to 0.0072 [Pa · s].

4.2.2. FLUIGENT SYSTEM

Besides the IBIDI system, another conceptual set-up has been proposed created with the Fluigent system. In this microfluidic set-up, pressure-based flow control is realized by the Fluigent Flow EZTM control unit. The main advantage of this system is related to the high-level of modularity that can be achieved, thus rendering the system suitable for fit-for-purpose adaptation in line with the research question. Moreover, the circuit includes a flow sensor to ensure direct and real-time control over the actual flow rates, which is an important advantage. The Fluigent LineUPTM series can either be used with

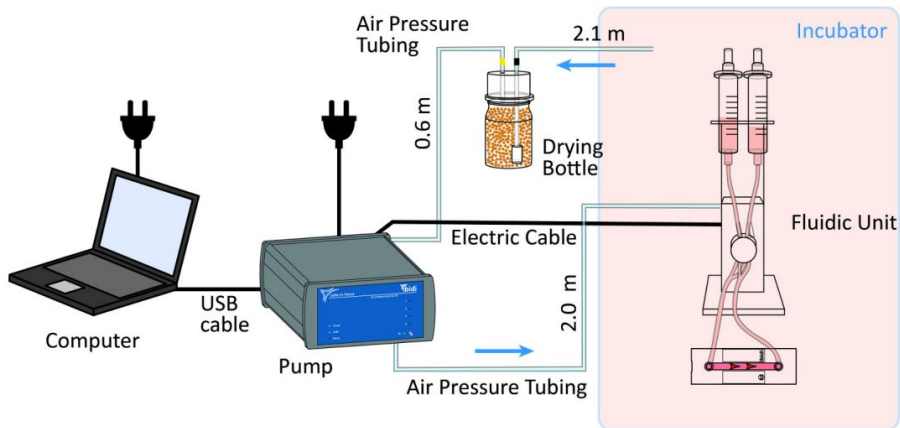


Figure 4.2: Basic set-up of complete IBIDI system with a single fluidic unit to perfuse one channel. Image taken from [60]

or without a computer due to the presence of a local control dial and is straightforward to extend to include multiple pressure controllers for multiple parallel experiments.

SINGLE-PASS CIRCUIT

The first proposed set-up is suitable to generate single-pass unidirectional flow in the microfluidic system. This circuit is particularly relevant to study the isolated effect of one organ-model on the subsequent other organ-model, without the reciprocal interaction. The schematic circuit is shown in Figure 4.3. The proposed set-up comprises a FLOW EZTM pressure controller (range = 0-345 mbar) that is connected to the power supply and pressure supply. Furthermore, since the ideal set-up is able to allow for microfluidic experiments to last up to 72h, 15 mL reservoirs are chosen. Nevertheless, the circuit may be realized with 2 mL or 50 mL medium reservoirs instead. The flow rate is constantly measured and controlled by means of an integrated flow unit (ideally range $S = 0 - 7 \mu\text{L}/\text{min}$) and medium is recollected after it has passed both organ chambers. To match the required volume of the IBIDI system, the flow rate is ideally set to $1 \mu\text{L}/\text{min}$ such that one 72h experiment requires 4.32 mL of medium. The tubing required to connect all the microfluidic components can be cut manually with desired lengths. The compatible tubing has an OD of $1/16''$ and ID of $1/32''$, which results in a total dead volume of $150 \mu\text{L}$ if a length of 95 cm is assumed.

RECIRCULATION CIRCUIT

Besides single-pass perfusion, it is possible to create recirculatory flow with relatively few adaptations to the overall circuit. To achieve this, two conceptual circulation schemes are proposed as shown in Figure 4.4 and 4.5. The most elegant option is to include the Fluigent 'L-SWITCH^{TN}', a 6 port/2-positions bidirectional microfluidic valve comparable to the valves that are already embedded in the IBIDI FU. Whereas the circuit becomes notably more complex if more than one channel is to be perfused, for the proof-of prin-

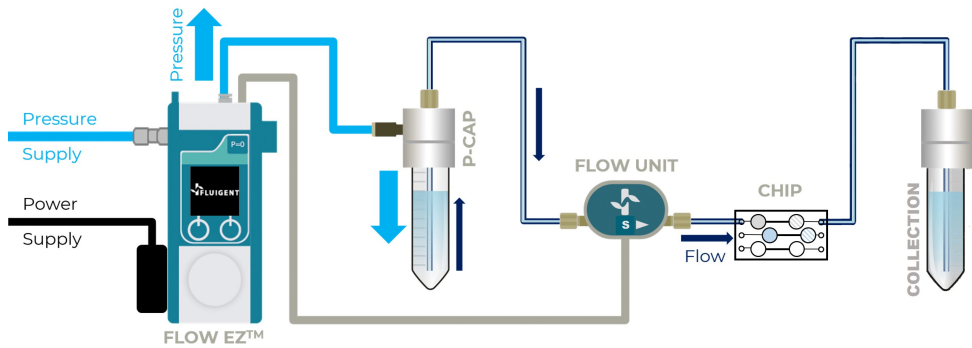


Figure 4.3: Schematic overview Fluigent set-up: microfluidic single-pass unidirectional circulation to perfuse a single channel. Adapted from www.fluigent.com

principle the presented scheme suffices. To realize this circuit, two Flow EZs are connected to two reservoirs, which contain equilibrated volumes of medium. The reservoirs are pressurized depending on the valve positions and media continuously flows into the microfluidic device, while the Flow Sensor monitors and controls the flow rate in real-time. In addition to the single-pass circuit (Figure 4.3), the Fluigent LineUPTM SWITCH EZ must be connected to provide control over the microfluidic valves. Moreover, the LINK EZ is required to establish a connection with the PC and facilitate an online interface for continuous monitoring. Ideally, the microfluidic circulation is controlled by creating an automated protocol in OxyGEN, the software provided by Fluigent, including valve actuation timing and the specified flow rate. In this case, since medium is recirculating, 2 mL reservoirs may be used to minimize the total working volume.

Alternatively, a conceptual design for recirculation was developed based on two 2-SWITCHTM valves, which are 3 port/2-way bidirectional microfluidic valves (see Figure 4.5). Since these components are already available in the lab, this designed scheme is economically more favourable especially if the purpose is to validate the feasibility of the Fluigent system for recirculation. Ideally, this set-up is created with the intuitive SWITCH EZ to control the valve positions, however this component can be substituted by the SWITCH-BOARD. The presented circuit is suitable to perfuse a single channel. The circulation control and valve switching times can be automatized with the available OxyGEN software. With this software, a time-based protocol should be created that can be run for at least 72h. Figure 4.5 shows the two possible configurations of the valves, which make it possible to recirculate medium while keeping the flow over the chip unidirectional.

4.3. SYSTEM DESIGN LIMITATIONS

4.3.1. LIMITATIONS OF THE IBIDI PUMP SET-UP

An inherent limitation of the fact that the IBIDI pump system runs on the PumpControl software is that it provides automatic calculations of pressure, flow rate and shear stress once the perfusion set, the type of slide and the viscosity of the medium are set. Whereas

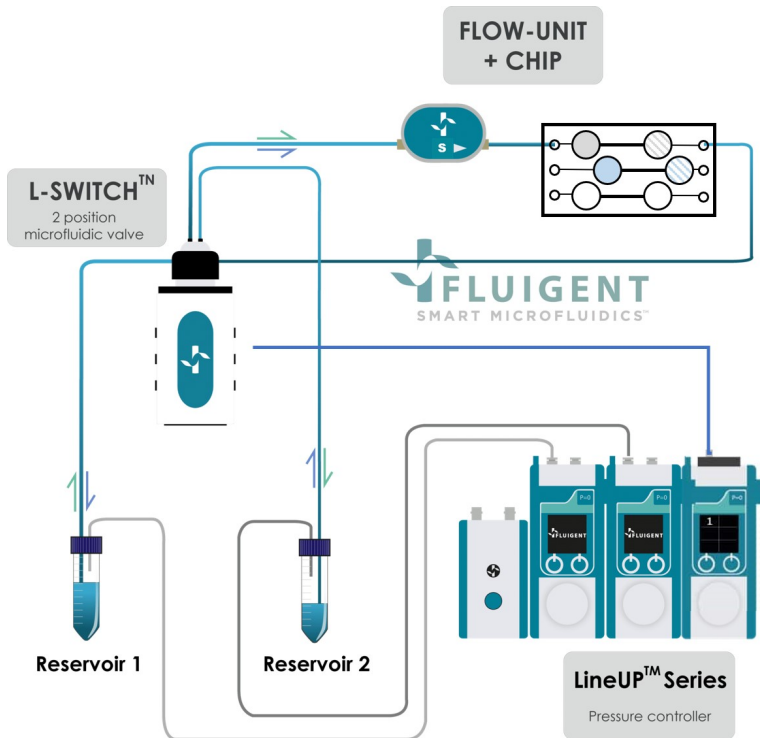


Figure 4.4: Schematic overview Fluigent set-up: Recirculation over a single-channel facilitated by L-SWITCH component. Adapted from www.fluigent.com

these calculations can be validated to some extent by performing pre-experiment calibration measurements, there is no guarantee that the parameters do not change over the time-course of an experiment. For example, flow rates might be affected by the appearance of bubbles in the tubing or inside the organ-chambers which is not accounted for by the PumpControl unit, due to the lack of real-time feedback loops based on measured data. Furthermore, as material properties of the tubing might change slightly upon reuse of the material, the calibration measurements should in fact be performed prior to initiating any experiment, which is in practice is not always done. As a result, the reproducibility of experiments is altered and the actual flow rate is hard to monitor. Besides, the current PumpControl software does not include the option to choose the IBIDI μ -slide III 3D Perfusion, but rather must be run with all the parameters set for another slide, the IBIDI μ -slide I Leuer 3D which features a different geometry. Ideally, future releases of the software will include the slide chosen for this project as it would make experiments more accurate.

On another note, the minimal flow rate that can be achieved while using the BLACK Perfusion Set in the set-up, is 0.08 mL/L. Although, this flow rate is acceptable in the case of microfluidic recirculation, it becomes problematic if a uni-directional single-pass system is to be realized. Theoretically, the IBIDI system can be programmed to facilitate

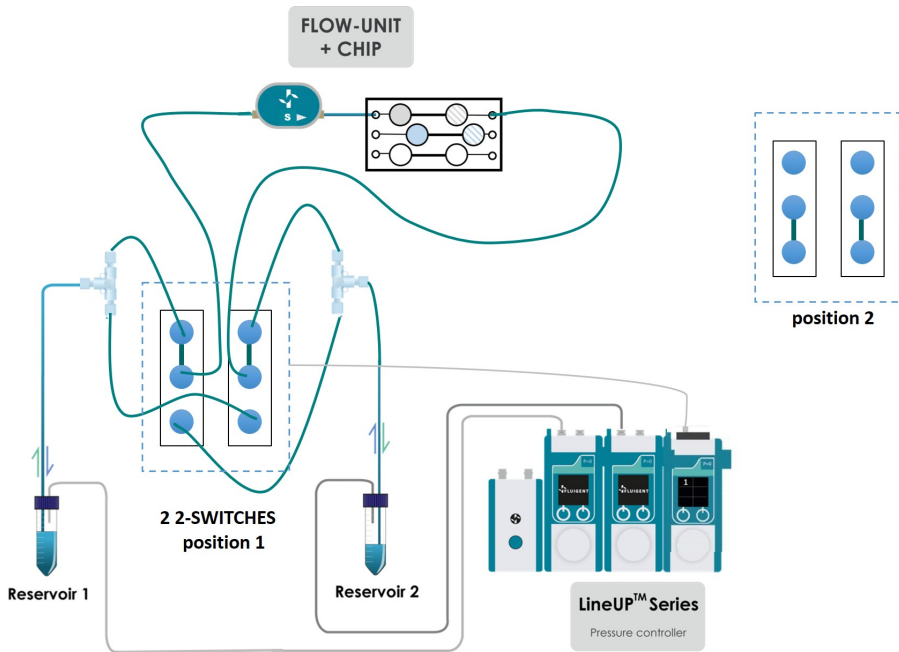


Figure 4.5: Schematic overview Fluigent set-up: Recirculation over a single channel facilitated by two 2-SWITCHES. The second position of the valves is shown in the upper right corner. Adapted from www.fluigent.com.

single-pass flow by programming the switching times of the integrated valves manually and ensuring that no valve switching happens during the experiment, thus collecting the medium on the other side of the channel. Nevertheless, this is not ideal as the largest compatible reservoirs can only contain 50 mL of medium. Considering the lower limit of flow, it implies that the maximal run time of any experiment would be a maximum of 625 min (10.4 h). In addition, secreted factors of interest would certainly be diluted beyond their detection limit, thus rendering the system inapplicable for this purpose. Besides, the recommended flow rate for the IBIDI μ -slide to ensure an optimal supply of oxygen and nutrients to the organ-chambers is actually in a higher range and reported to be 0.5 - 1 mL/min [61], which is relatively high if one is to achieve a physiologically relevant MOoC system.

This set-up is furthermore inherently limited by the on-chip volume and the total working volume required due to the tubing and the medium reservoirs. Feasibility studies with respect to the concentration of secreted factors of interest should be performed to evaluate whether the minimal volume is still within the acceptable range.

4.3.2. LIMITATIONS OF THE FLUIGENT SET-UP

The Fluigent system is optimized to be expandable, however this comes at the cost of additional connections in the circuit compared to the IBIDI system. Potentially, this could

lead to leakage problems if connections are not tight enough or worn out as well as increase the possibility of bubble formation and clogging in the tubing. In addition, the tubing has to be cut and connected manually, which renders it subject to human error during the set-up process. Whereas this feature does allow the user to choose the tubing length and thus makes the system adjustable to the available space, the tubing might be slightly different in each experiment. This affects the reproducibility of experiments.

Another expected pitfall related to this system is the requirement of sterility. To assemble the complete circuit under sterile conditions, the chip, tubing and all components should be connected and under the hood, however following assembly it is hard to transfer all the required components to the incubator without disrupting the tissue in the newly connected chip. Handling should be optimized to limit this problem.

Finally, although the L-SWITCH solution to create a recirculation circuit (Figure 4.4) is theoretically a relatively straight forward and easy to implement approach, according to Fluigent it is less reliable when used in combination with low flow-rates. This is because the L-SWITCH contains a small internal channel that is prone to get clogged, thus preventing continuous perfusion. Taking this factor into account, the conceptual set-up presented in Figure 4.5 is recommended for the purpose of this project.

4.4. MESH DESIGN

4.4.1. MESH PURPOSE

Preliminary experiments indicated that the relatively large tissue chambers and wide channels that are characteristic of the IBIDI μ -slide contribute to an instantaneous rise in pressure upon connecting the tubing to the chip inlet, thus inducing a very high flow. This unpredictable high flow rate at the start of each experiment was hypothesized to implicate the positional stability of the embedded CMTs, as they might easily flush from their respective chamber to the adjacent chamber. To ensure the confinement of CMTs to their respective chamber and to increase the experimental robustness, a mesh was proposed to tackle the problem. The envisioned main function of this mesh was to ensure that CMTs always maintain in their dedicated chamber during the experiment and do not enter the adjacent chamber where they could potentially interact and disturb the second embedded tissue type.

A secondary function of the proposed mesh is to guarantee that CMTs occupy a space throughout the complete chamber rather than accumulate together at the chamber outlet as a result of continuous exposure to the generated flow profile. Taken together, the designed mesh presents an elegant means to render a general, commercially available chip fit-for-purpose in our cardiorenal context.

4.4.2. MESH REQUIREMENTS

A list of requirements for the mesh was created in collaboration with Dr. Bjorn de Wagenaar (TU Delft) based on envisioned use of the meshes in the IBIDI μ -slide III 3D Perfusion to ensure CMTs confinement:

- **Organoid trapping** The mesh must be able to trap CMTs in a specific location and ensure they maintain in place even under harsh handling procedures and during

experimental flow-conditions.

- **Number of CMTs** The mesh fits at least 20 CMTs, which each is assumed to have an average diameter of 300 μm .
- **Easy fit** The mesh is easy to insert on and remove from the chip. Ideally this can be done in a straightforward manner with tweezers.
- **Tissue distribution** After CMTs deposition on top of the meshes, the tissues are distributed throughout the mesh by gravity alone. Gravity driven sedimentation does not require additional manual tissue manipulation nor spreading with a pipette tip to limit tissue disturbance.
- **Mesh height** The total height of the mesh is equal to the height of the chip chamber. Consequently, the air-tight seal between the coverslip and chip can be maintained while the coverslip simultaneously adds-value by pressing down on the mesh to prevent unwanted floating of the structure.
- **Sterilization** The mesh must be compatible with a sterilization method that does not adversely affect the material properties. This may be UV-exposure, autoclaving, plasma-treatment or a combination.
- **Bio-inert** The 3D printed material is bio-inert such that secreted factors are not trapped in the material. The hardness of the material is not a major concern, as the cardiac spheroids are already formed by the time they are placed onto the mesh. To further inhibit cell-surface interaction, surface passivisation treatments may be incorporated in the post-processing steps.
- **Bio-compatible** The material is bio-compatible for the CMTs and does not release toxic particles upon wear of the material due to constant exposure to fluid flow.
- **Hydrophilic surface** The material surface must be hydrophilic or be compatible with post-treatments to make it as such. Hydrophilicity is required to prevent bubble formation in the bottom of the mesh wells as these bubbles might interfere with adequate tissue perfusion during prolonged experiments.
- **Non-adherent, smooth surface** The material surface must not impose an effect on the embedded tissues and thus ideally is non-adherent and smooth. The smooth surface requirement is particularly important with an eye on the proliferative nature of fibroblasts, which are known to easily migrate out of pre-formed CMTs when encountered with rough surfaces. Optionally, post-processing steps may involve non-stick coatings.
- **Transparency** Ideally imaging can be done at various time points during the experiment without the need to sacrifice a chip to monitor tissue viability. This requires the mesh material to be optically transparent to at least comply with bright-field imaging requirements. If immunofluorescence stainings are to be performed directly on the mesh, an additional necessity is that the material is not autofluorescent in the wavelength ranges associated with common fluorescent markers, as this limits the detection ability and quantification of such markers.

- **Medium accessibility** The designed wells or pores in the mesh still facilitate diffusion profiles in the organ-chamber that match the nutritional needs of the embedded tissue. This must hold during the application of continuous flow.
- **Particle transport** Secreted factors must not get trapped in the microwells of the mesh and must be able to diffuse out of the mesh into the common medium stream. In this way they can reach the adjacent organ compartment to exert a downstream effect. This consideration should be taken into account when designing the aspect ratios of the wells.
- **Top surface area** Since flow is required to continuously supply fresh medium to the organ-chambers, the mesh must not block the fluid stream. The effect of the mesh on the flow profile must be minimal in order to ensure controllable conditions in the chip. This can be achieved by keeping the top surface area minimal such that maximal diffusion of medium into the microwells is facilitated.

The mesh was originally developed as a fit-for-purpose strategy to circumvent CMTs flushing problems. However, to maintain cardiac and renal chip conditions comparable, a similar mesh was developed for the KOs. The main identified hurdle related to embedding a KO on chip, was to maintain tissue integrity during the manual transferring process. Therefore, rather than organoid trapping, the main purpose of this mesh was to provide a transferable culture insert that could be used to pre-culture KOs instead of on top of conventional Transwell inserts. After KO maturation on this mesh, the idea is that the complete package of mesh and KO can be transferred directly on-chip, thus omitting the need to manually pick-up organoids, which is often a problematic experimental step. Additional requirements were:

- **Permeability** Since KOs are to be cultured on top of the mesh directly from the start of their formation, the bottom of the mesh must be permeable to medium supplied from underneath. This medium perfusion must be possible in comparable manner to conventional tissue-culture on top of Transwell® membranes.
- **Flat surface** Since the KOs are naturally larger structures than CMTs, the mesh must be designed in the form of a cup with a flat surface that is capable to host a conventionally sized KO of 500k cells, which is likely to fill near the complete space of the mesh under optimal conditions.

4.4.3. MESH CONCEPTUAL PROTOTYPES

MESH DESIGN: CMTs

The actual mesh design was based on the presented list of requirements and existing solutions to trap 3D tissue models. These include the revolutionary SpheroidBrick inlay that was used to embed liver spheroids by Schimek et al. [62] and the more standardized approach found in the Aggrewell 400TM cell culture plates commonly used to generate spheroids of uniform size and shape.

It was chosen to base the conceptual design on a honeycomb-shaped well array fitted to fill the total chamber area, as shown in Figure 4.6a. The honeycomb shape is useful

to minimize the well-spacing and thus prevent **CMTs** of settling on the surface between the wells rather than sinking to the bottom [63]. The initial size of the microwells was chosen to spaciouly accommodate single **CMTs** and therefore had an inscribed circle diameter of $400\ \mu\text{m}$. The well depth was designed to be $400\ \mu\text{m}$ to ensure that the **CMTs** completely fit in the confined space and to prevent **CMTs** flushing. The mesh was further designed like an insertable cup, and thus featured a completely closed off bottom ($50\ \mu\text{m}$ thickness) and an enclosing wall all around the microwell array. This decision was made as it was hypothesized that a cup-like design was desirable to retrieve the tissues for post-experimental analysis. Vertical pillars reaching up to the top of the organ chamber were included in the design to ensure that the mesh was kept in place and to act like a fence against **CMTs** washout. An schematic overview of the final design is presented in Figure 4.6 **A-C**.

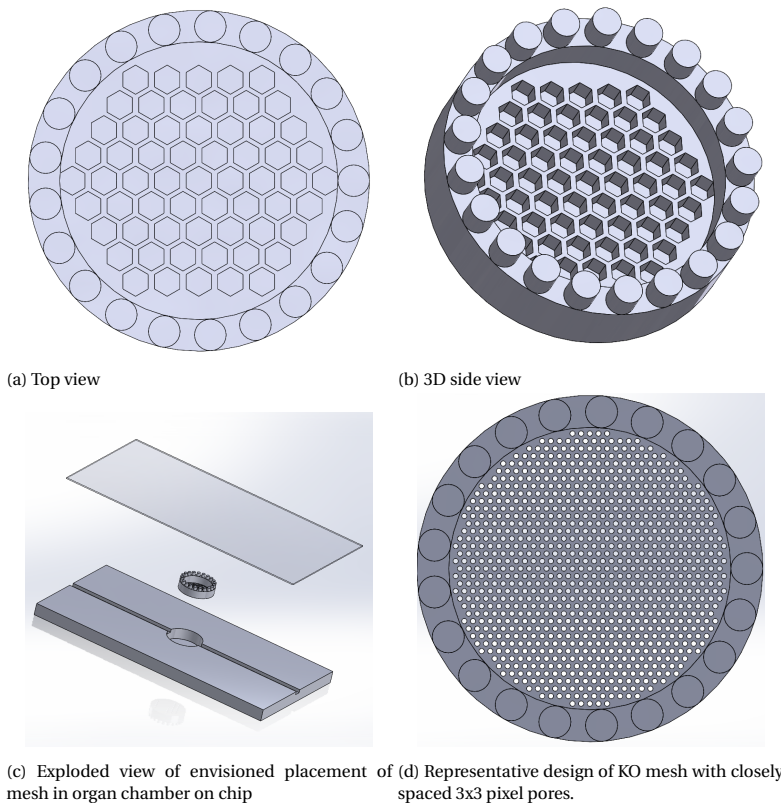


Figure 4.6: **A-C**: Conceptual design for the **CMTs** mesh that features a honeycomb-shaped well array to trap the **CMTs** and the exploded view of its on-chip placement. **D**: One of the conceptual designs for the **KO** mesh.

MESH DESIGN: KOS

To adhere to the permeability requirement of the meshes for **KOs**, the bottom plate was designed to have a pore-like, open structure rather than being completely closed as was

the case in the previous meshes. In this case tissue confinement was not part of the requirements, hence the honeycomb-shaped microwells were omitted in the design. To meet the permeability requirement and to find out which designs were feasible to print with the chosen printing technology, the aspect ratio of the diameter and depth of the pores was manipulated, as will be further commented upon in Section 5.1.4. An overview of the top views of the schematic designs are presented in Appendix C, which illustrates the difference in terms of pore size and inter pore separation distances that were designed for feasibility tests. Figure 4.6d shows a representative design that features **3x3** (**d = 81 μm**) pores with a close pore spacing.

5

FEASIBILITY STUDIES

5.1. BIOLOGICAL AND FUNCTIONAL ASSAYS

5.1.1. MEDIUM

In order to co-culture **CMTs** and **KOs** in a single microfluidic system, a medium had to be found that supplies both tissue types with adequate nutrition. **CMTs** are conventionally cultured and maintained in BPEL medium (Bovine Serum Albumin Polyvinyl alcohol Essential Lipids) supplemented with VEGF (50 ng/ml) and FGF2 (5 ng/ml) [59]. **KOs**, on the other hand, are maintained in animal component-free basal STEMdiff APEL (Albumin Polyvinylalcohol Essential Lipids) medium [58]. The main difference between these two types of medium is the origin of the albumin, which is animal-derived for the **CMTs** and from human origin for the **KOs**. In an effort to identify a suitable common medium for both tissue types, it was initially hypothesized that **KOs** could be differentiated in supplemented BPEL rather than APEL. In this case, BPEL was chosen as the ideal common medium since it is more economical than APEL and considering the large medium volumes required at later stages of the experiments, this would be the preferred choice.

The results presented in Figure 5.1 showed that **KOs** directly grown in BPEL from day 7 on developed fewer renal structures compared to standard APEL conditions. Thus, it was concluded that developing **KOs** directly in BPEL was not optimal. Consequently, it was decided to culture and mature each individual organ-model in their specific medium and only change to the common BPEL medium once the tissues are integrated on-chip.

Since the organ-models are theoretically matured once they are transferred to the chip, it was then hypothesized that at this time point the use of BPEL without any tissue-specific growth factors would be sufficient to supply both tissue types with adequate nutrition. To validate this hypothesis, the morphological structure of **KOs** maintained in BPEL versus APEL in conventional static, well-plate conditions was analysed. To this end, mature **KOs** were changed to unsupplemented BPEL medium and maintained for an additional 72h. Afterwards immunofluorescence stainings were performed as described in

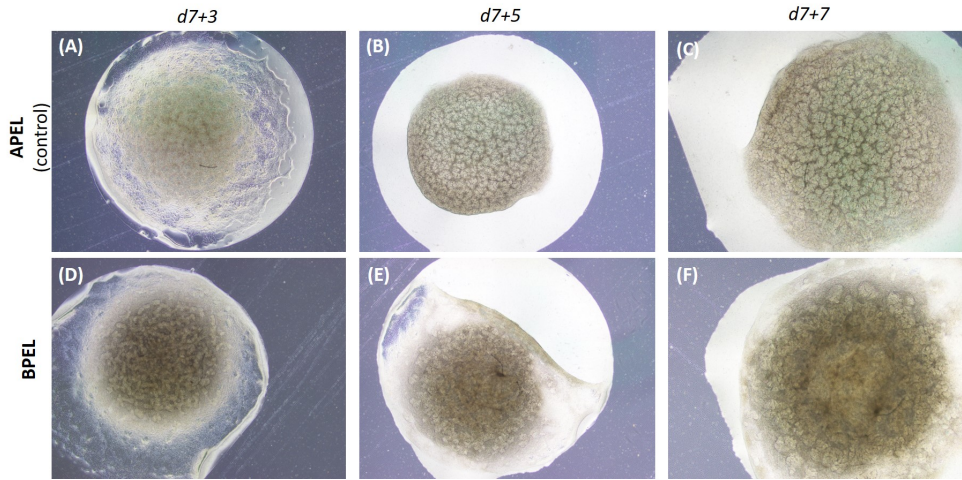


Figure 5.1: Light microscopy images of kidney organoids (500k cells) differentiated in APEL (A-C) vs BPEL (D-F) from day 7 onwards show clear differences in developed intact renal structures.

[64], [65] to look for the presence and integrity of appropriate renal structures (Figure 5.2 A1-B3). LTL marks the proximal tubular structures and NPHS1 marks the podocytes in glomerular structures. Appropriate and morphological similar structures were found for both the control and BPEL culture conditions. Therefore, it was concluded that switching mature *KOs* to BPEL medium does not have any major effect on the structural integrity.

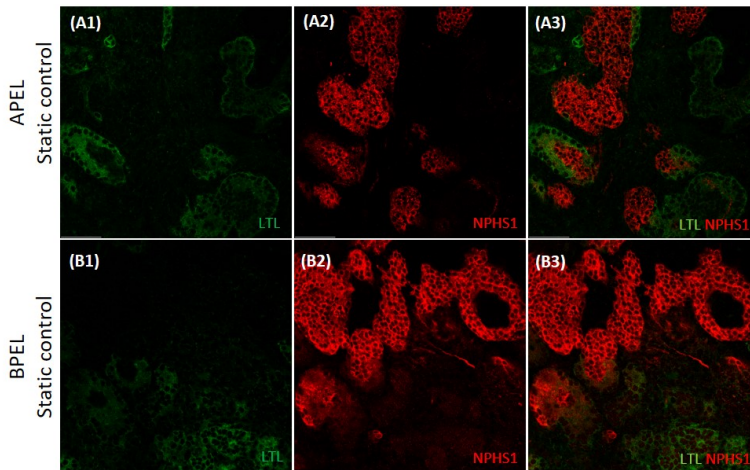


Figure 5.2: Immunofluorescence stainings of *KOs* to evaluate the effect of switching *KOs* from APEL to BPEL medium after maturation. A1-A3: Static control in APEL. B1-B3 Static control in BPEL.

5.1.2. TISSUE VIABILITY AND INTEGRITY IN STATIC CHIP ENVIRONMENT

Thus far, the tissue models used in these studies have mainly been characterized in conventional static culture conditions. However, when performing experiments in microfluidic set-ups the micro-environment is significantly altered and therefore additional characterization and viability studies are required. It is essential to assess the effect of the isolated chip environment on each respective organ-model prior to starting with co-culture experiments or flow experiments. Once control-conditions are well established, can we continue with more advanced experiments varying a single variable at the time. Key to finding conclusive evidence from MOoC experiments is taking a bottom-up, step-wise approach starting with assessing the effect of the chip, flow and co-culture environment on a physiological model.

IMMUNOFLUORESCENCE ANALYSIS

Immunofluorescence stainings were performed on retrieved CMTs and KOs to analyse the structural integrity of tissues after 72h of culture. Static well plate conditions (the control) were compared to static on-chip conditions, keeping all the other parameters equal. No medium changes were performed during the experimental window.

KIDNEY ORGANOID

After 72h of culture, KOs were obtained from the static transwell or retrieved from the chip environment and immunofluorescence stainings were performed as described in [64], [65]. To characterize for renal structures, stainings were performed for LTL (proximal tubule), NPHS1 (glomeruli) and Hoechst (cell nucleus).

Figure 5.3 illustrates representative results from the immunofluorescence analysis performed on KOs maintained in static control conditions and 72h static on-chip conditions (isolated versus co-culture). The results indicate that the renal structures are preserved in the static chip environment, though they look rougher and more cellular debris can be observed. This observation can be attributed to the fact that no medium changes were performed during the 72h experiment and considering the large space that the KOs occupy in the organ-chambers.

CARDIAC MICROTISSUES

After 72h, CMTs were obtained from v-shaped bottom well plates to be used as a control condition and were additionally retrieved from the on-chip static environment. Subsequent to quantitative contraction analysis, as explained in the next paragraph, immunofluorescence stainings were performed on the retrieved CMTs as described in [59] to examine overall morphology and cellular architecture. Results are presented in Figure 5.4. Stainings were for Hoechst (not shown) to visualize the cell nuclei and for cardiac sarcomeric proteins: cardiac troponin I (cTnT) and actinin alpha-2 (ACTN2) present in Z-bands. There was no apparent difference between sarcomere structures of CMTs maintained in static control conditions and CMTs that were transferred to the static chip conditions.

It was thus concluded that the static chip environment does not adversely influence the morphology of the CMTs. This conclusion may be further validated by future work that aims to quantify nuclei density or incorporates live/death stainings to evaluate exact cell viability.

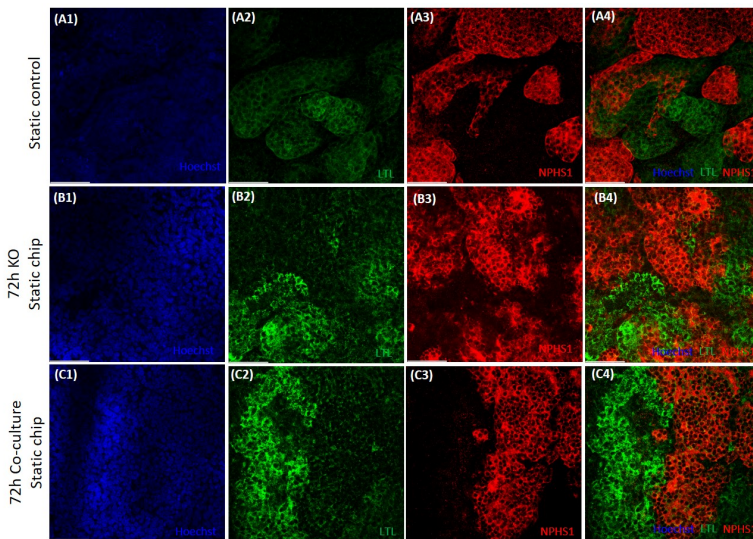


Figure 5.3: Immunofluorescence stainings of KOs to evaluate tissue viability and integrity in static chip environment compared to control conditions. **A1-A4:** Static control in BPEL. **B1-B4** 72h static chip. **C1-C4** 72h static chip co-culture BPEL.

CONTRACTION ANALYSIS

To evaluate the contractile function of retrieved CMTs, CMT contraction was quantified and analysed with the open source MUSCLEMOTION ImageJ macro [66]. CMTs were retrieved from the on-chip environment and paced at a frequency of 1 Hz. Videos of 10 seconds were captured with an acquisition rate of 100 frames per second. The software generates output graphs of the contraction from which relevant parameters can be derived, such as contraction duration, time to peak, relaxation time and contraction amplitude expressed in arbitrary units (a.u.). Figure 5.5 shows a representative CMT and associated contraction profile generated with the MUSCLEMOTION software. Figure 6.5 shows the overall results from the subsequent data analysis of all analysed CMTs. The data presented here was based on CMTs that were kept in static, on-chip culture (isolated or co-culture) for 72h and a control condition. For each condition, five CMTs were analysed and the performed statistical test was the Kruskal-Wallis Test with multiple comparisons post hoc.

As becomes evident from the results, no significant differences were observed in the contraction profiles of retrieved CMTs kept in various conditions. Their respective contraction forces and frequencies seemed unaffected by the static chip environment, which aligns with the conclusions drawn from the immunofluorescence stainings executed on these samples.

5.1.3. TISSUE LOCALIZATION IN CHIP

In the MOoC flow experiments it is of utmost importance that tissue specimens stay in their respective organ chambers and are not flushed out during the assay due to the

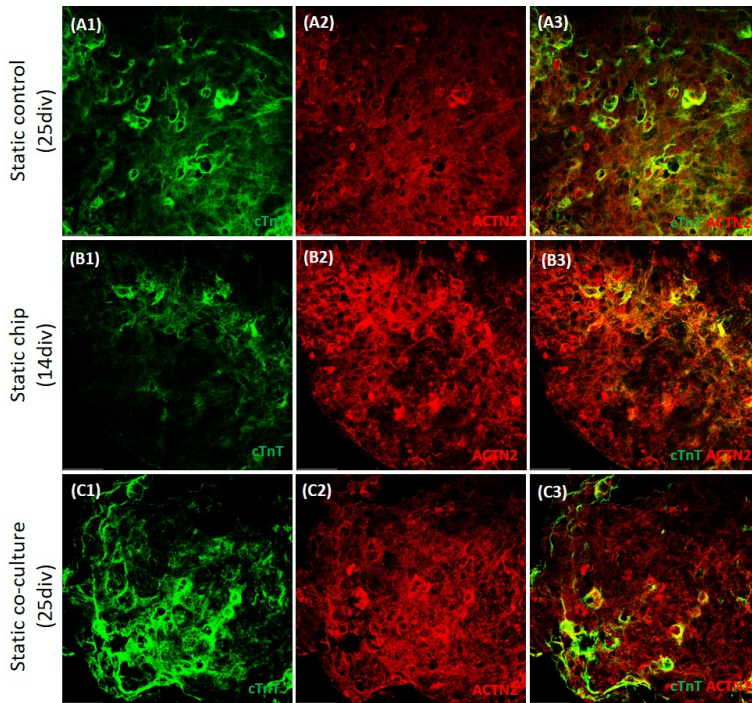
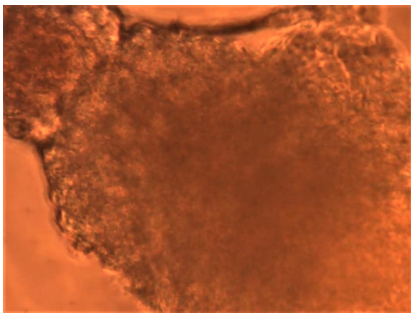
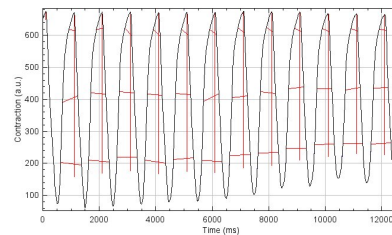


Figure 5.4: Immunofluorescence stainings of **CMTs** to evaluate tissue viability and integrity in static chip environment compared to control conditions. **A1-A3** Static control BPEL (25div). **B1-B3** 72h static chip BPEL (14div). **C1-C3** 72h static chip co-culture BPEL (25div).



(a) 25div CMT image snapshot from acquired video used for the contraction analysis.



(b) MUSCLEMOTION generated time course profile of contraction with contraction force expressed in arbitrary units (a.u.) Peaks correspond to contractions.

Figure 5.5: Representative results of MUSCLEMOTION analysis performed on 25 div **CMTs** subject to pacing at 1Hz.

application of flow or due to rough handling. During initial feasibility experiments it was found that critical step to prevent **CMTs** flushing, is when connecting the tubing to the chip inlet. However, by careful handling and working delicately the issue could be

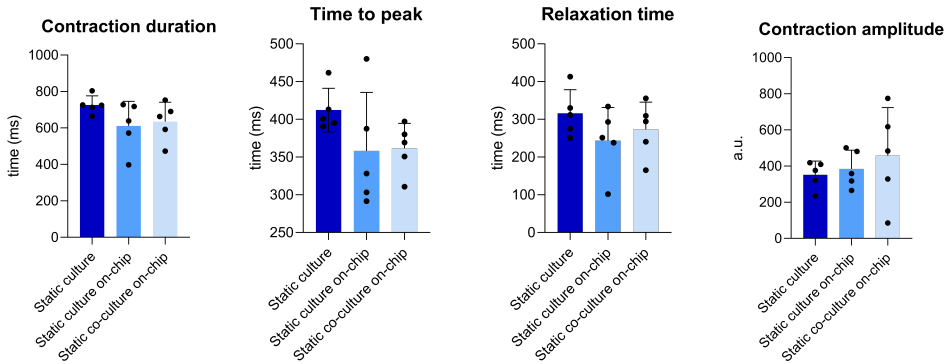


Figure 5.6: Musclemotion results showed no significant differences in contraction duration, time to peak, relaxation time and contraction amplitude when cultured in static conditions or static on-chip conditions. Black dots represent obtained results for single microtissue.

prevented. Since the KO is much larger in size, the flushing issue is not nearly as relevant and indeed did not give rise to any problems

5.1.4. MESH PROTOTYPING

PROTOTYPE MESH FOR CMTs

The first print iteration of the honeycomb mesh described in paragraph 4.4.3 was produced with a digital light processing printer (DLP). This type of printing produces objects in a layer-by-layer fashion via photopolymerization of a liquid resin [67] and is especially suitable to produce micron-scale feature sizes and smooth surfaces. The initial material was Mojin Tech Clear Resin, which is promoted as a material particularly suited for microfluidic applications and optimized for optical transparency and high resolution printing. After printing, a post-processing step is required to remove the uncured monomer. This was done with an isopropyl alcohol (IPA) treatment in all described cases here. It was found that the meshes were printed accurately and maintained their structure throughout the entire process, with few exceptions. The 3D printed results are shown in Figure 5.7.

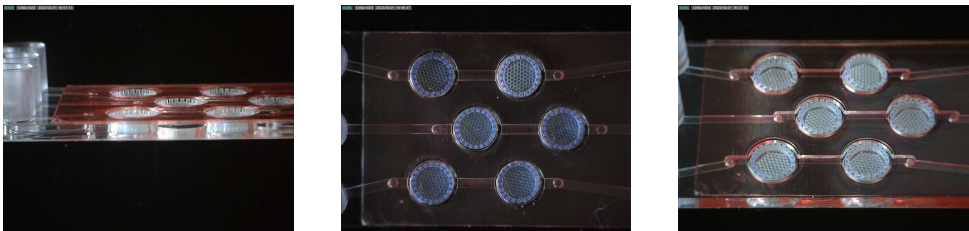


Figure 5.7: First iteration of printed meshes for trapping CMTs fitted inside the Ibidi μ -slide

PROTOTYPE MESH FOR KOs

Various designs were created according to a straight forward scheme presented in Table 5.1. As the scheme illustrates various combinations of pore diameter and pore depth have been tested for printing feasibility. Since the printing resolution in the x-y space is approximately 2 pixels, with one pixel measuring $27 \mu\text{m}$, the minimal spacing between features was always designed to be at least $54 \mu\text{m}$. Furthermore, the layer height resolution is set to $5 \mu\text{m}$, but to ensure stability of the design during removal from the printing bed it was chosen to stick to $50 \mu\text{m}$ as a minimal thickness for the bottom plate of the mesh. Other thicknesses included in the designs were $70 \mu\text{m}$ and $100 \mu\text{m}$ were included. In total this resulted in 15 different mesh designs, each of which has been printed in triplet during the first iteration.

The meshes designed to accommodate the KOs were produced in a similar manner as described for the honeycomb meshes. Again the used material was the Moiin Tech Clear Resin. The main goal of this prototyping iteration was to identify the optimal aspect ratios for the mesh design such that the mesh adheres to the printing limitations and yet allows for maximum permeability such that the growing KOs continuously receive enough medium. The 3D-printed results are shown in Figure 5.8.

Table 5.1: Aspect ratios tested in the design for KO meshes to achieve required permeability. Various pore diameters versus pore depths have been tested. The table reports the printing success.

Pore size (pixels)	Pore depth (= bottom thickness)		
	50 μm	70 μm	100 μm
2x2 (d = 54 μm) <i>Spacing 108 μm</i>	X	X	X
3x3 (d = 81 μm) <i>Spacing 162 μm</i>	X	X	✓
3x3 (d = 81 μm) <i>Spacing 135 μm</i>	X	X	?
4x4 (d = 108 μm) <i>Spacing 270 μm</i>	X	X	✓
4x4 (d = 108 μm) <i>Spacing 189 μm</i>	X	X	?

X = Failed to print due to ruptured membrane or absence of open pore structure; ? = Unclear if printed successfully; ✓ = Successful print used for functional testing.

The results for the printing feasibility have been summarized in Table 5.1. The main conclusions drawn from this first print iteration serve as a starting point to further optimize

the presented design and include the following:

- Pore depths of 50 μm or 75 μm result in a bottom thickness that is too thin to result in intact, reproducible prototypes. Especially the removal from the printing bed becomes problematic with these thicknesses.
- Designs with pores of 2x2 pixels, diameter = 54 μm , result in a membrane-like structure that is only partially open at a pore depth of 100 μm .
- Designs with pores of 3x3 pixels (diameter = 81 μm) and 4x4 pixels (diameter = 108 μm) with a small inter pore spacing, taken to be 2 pixels, were found to most-likely have ruptured membranes. However, the results were inconclusive as the particular designs were hard to identify from the other designs. Another print iteration should be performed to be certain.
- Designs with pores of 3x3 pixels (diameter = 81 μm) and 4x4 pixels (diameter = 108 μm) with a inter pore spacing equal to the pore diameter itself were **successful**.

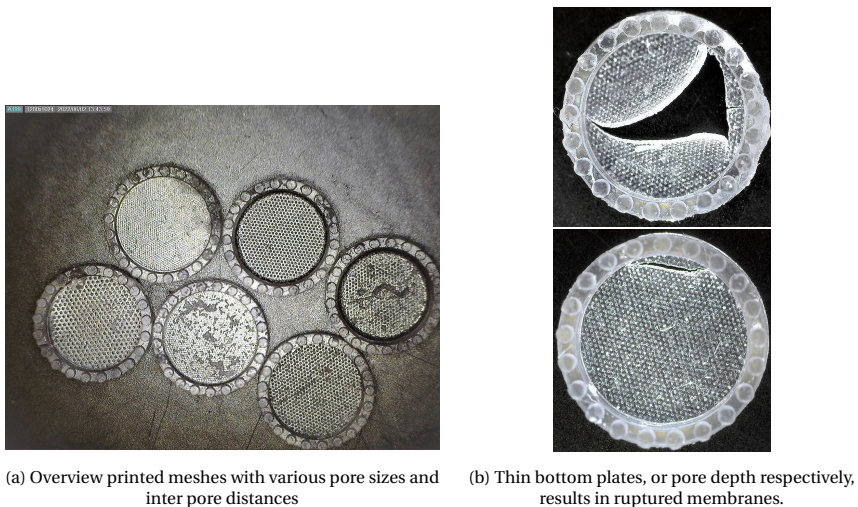


Figure 5.8: Results of 3D-printed KO meshes simulating pore-like membranes

5.1.5. MESH FUNCTIONAL TESTING

PROTOTYPE MESH FOR CMTs

Upon mesh exposure to medium, it was observed that small bubbles form inside the honeycomb microwells, which may induce adverse effects on the embedded tissue. It was hypothesized that this issue could be addressed by improving the wettability of the material. Accordingly, a plasma-treatment was proposed and the results showed significant improvement in terms of medium distribution on top of the mesh, see Figure 5.9. CMTs were deposited on top of the treated meshes and it was observed that the micro-tissues successfully sediment to the bottom of the wells. As becomes evident from the results presented in Figure 5.9, the honeycomb wells with an inner diameter of 400 μm

render enough space for single microtissues.

Besides demonstrating successful trapping of CMTs in the mesh, it was confirmed that CMTs can also be retrieved from the structure for end-point analysis, which is an important requirement. Furthermore, the mesh was found to be transparent enough to monitor microtissues with brightfield microscopy. However, quantitative observation or imaging of the CMTs inside the mesh with inverted microscopy is limited due to the opacity of the mesh.

Further proof-of-principle studies should focus on addressing the influence of the mesh on the flow profile generated in the organ-chambers. A first approach is taken by setting up computational fluid dynamics simulations as explained in Section 5.2.1.

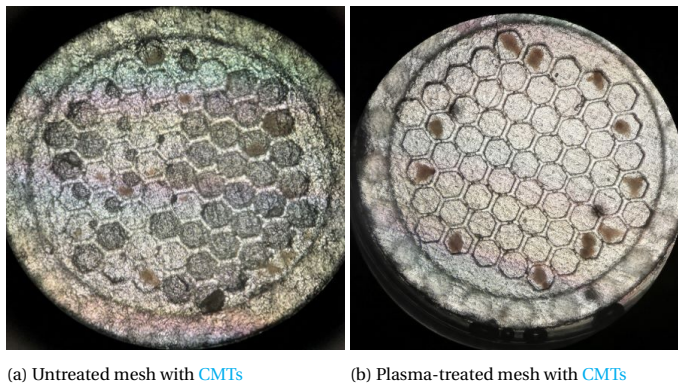


Figure 5.9: Post-processing plasma-treatment of mesh improves the wettability of the material and results in better tissue-sedimentation into the honeycomb wells.

PROTOTYPE MESH FOR KOs

To evaluate the applicability of the meshes developed for the KOs, fresh KOs were deposited on top of the meshes at the time point at which they would normally be pipetted on top of transwell membranes. The remainder of the prescribed, robust protocol for KOs formation was followed as outlined in [58]. In doing so, it was hypothesized that the required air-liquid interface would still be formed and conditions were kept completely equal besides the mesh confinement and different surface material.

The main interest of this first proof-of-concept assay was to assess whether KOs initiated on top of the meshes would give rise to characteristic renal tissue structures. KO development was monitored and compared to control conditions over the subsequent differentiation period. Figure 5.10 shows representative pictures of freshly pipetted KOs on top of the meshes at time point zero.

Unfortunately, it was found that KO development did not occur as intended on the meshes. Instead, structures fell apart and cell viability was greatly affected. Future work is required to further optimize the mesh approach for culturing KOs.

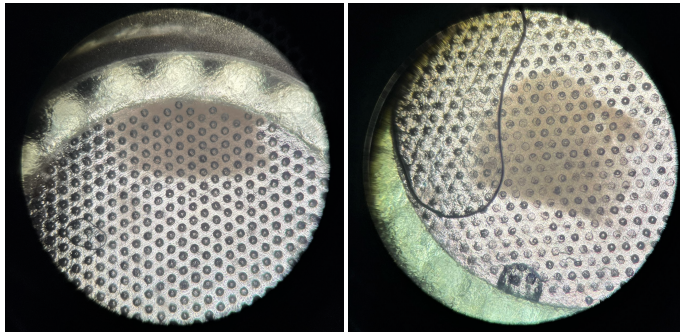


Figure 5.10: Representative pictures of **KOs** pipetted on top of mesh. Images taken at timepoint 0h.

MATERIAL RELATED EFFECT OF MESHES

Since bio-compatibility of the meshes is a high-priority requirement to exclude any type of adverse effect exerted on the functionality and structural integrity of the microtissues, an additional experiment was designed to analyse the potential effect of the meshes on **CMTs**. Two factors were tested:

- The functional effect of the confinement imposed on trapped microtissues by the limited size of the hexagonal shaped microwells.
- The effect of the mesh material on the microtissue functionality.

To perform the experiments, a design iteration was performed on the honeycomb-shaped microwell-arrayed meshes. The prototype design that had previously been proven to be printable and functional in trapping the microtissues, was adapted to fit a 24-well plate, as shown in Figure 5.11. One design featured similar microwells as previously tested and another design merely consisted of a cup with a flat bottom. The mesh was developed in two commercially available printer resins:

- **Moin Tech Clear Resin**
- **FormLabs Clear Resin**

It has been shown previously that post-printing treatment of the printed resins can dramatically improve their biocompatibility [67]. Therefore, various post-processing steps were applied to test which condition best maintains cellular viability: ultraviolet (UV) post-curing (common sterilization method prior to cell culture); autoclaving (another common sterilization method); plasma surface treatment (improves surface wettability) and a combination of autoclaving and plasma surface treatment. Besides, a positive control was included in which **CMTs** were floating in an empty well without any type of mesh present. Mature **CMTs** were pipetted on top of the different pre-conditioned meshes and the inserts were topped of with an excess of medium. Plates were incubated at 37°C and 5% CO_2 .

The experiment was run for 72h, during which the microtissues were optically observed using inverted microscopy at various time points. Beating frequency based on videos

was taken as an experimental end-point to evaluate cytotoxicity of the meshes. This read-out was not further quantified but tissues have been retrieved, fixed and frozen to perform immunofluorescence stainings to quantify the results at later stages. For example by means of a life/death staining. The following observations were made:

Results: Moiin Tech Clear Resin

- When the post-treatment regimen included both a plasma-treatment and autoclaving, CMTs exhibited a similar contraction pattern as found in the control condition.
- UV-post-curing was found to be insufficient to maintain CMTs viability.
- Whereas CMTs were found to be beating in the meshes, they were hard to observe with inverted microscopy technology.

Results: FormLabs Clear Resin

- It is impossible to autoclave the FormLabs Clear Resin material as the heat and pressure exposure causes the meshes to be irreparably damaged.
- CMTs perform better on plasma-treated material than UV-treated material. The observed beating frequency was slightly more rapid and weaker compared to control conditions.
- CMTs placed in the meshes were beating similar as the once in the cups.

Overall, this feasibility experiment showed that CMTs can in fact survive in the meshes when the appropriate post-processing treatment regimen is identified. Based on these preliminary results, CMTs performed best on meshes developed from **Moiin Tech Clear Resin** with a post-treatment of autoclaving followed by a plasma surface treatment. Nevertheless, the material properties of the FormLabs Clear Resin were better suited for microscopic imaging of the seeded CMTs. Further studies should focus on including additional post-processing surface treatments, such as coatings, and aim to identify the most optimal combination. Most importantly, the results must be quantifiable to draw definitive conclusions, which could not be done with the obtained data in this experiment. Even so, the results are promising.

5.2. THEORETICAL PROOF-OF PRINCIPLE STUDIES

5.2.1. COMPUTATIONAL SIMULATIONS OF FLOW DYNAMICS

The fluidic flow profiles in the chambers of the IBIDI μ -Slide III 3D Perfusion chip (4.1) were computed with COMSOL Multiphysics 6.0. This simulation helps to understand the exact flow profile through the complete chambers, the effect of different flow rates and the effect of the mesh on the flow distribution. The simulation can furthermore be used to acquire a basic understanding of the accessibility to fresh medium of the incorporated tissues and to make educated guesses about the final trapped location of the tissues in the chamber.

Comparative 2- and 3D models showed significant differences in the resulting simulated flow, hence it was concluded that the 2D model was an over-simplification of reality.

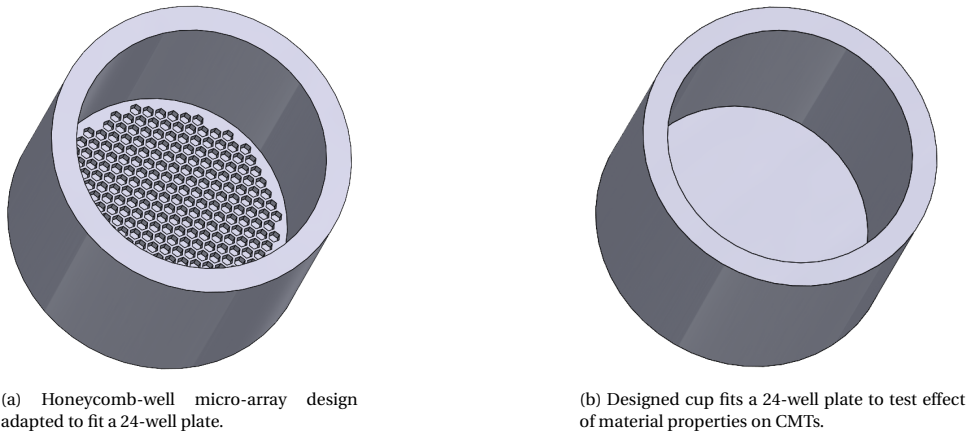


Figure 5.11: The effect of tissue confinement and the potential cytotoxicity of the material on CMT beating patterns was analysed with the help of adjusted designs that fit a 24-well plate.

Therefore, it was chosen to create a **3D** model to account for flow distribution in the complete chamber rather than along a single two-dimensional plane. All presented simulations were executed with this three-dimensional model.

GEOMETRY

The chip geometry was simplified to comprise only a single chamber with a channel that runs on top of the chamber (see Figure 5.12a). The chip dimensions were taken from the instructions file provided by IBIDI. Furthermore, to evaluate the effect of the mesh on the fluid flow in the chip, the 3D CAD model of the mesh created in Solidworks2021 was imported into COMSOL (see Figure 5.12b).

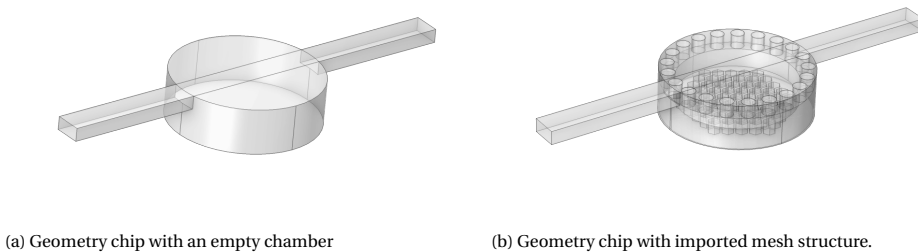


Figure 5.12: Schematic representation of the used geometry in the COMSOL Multiphysics simulations.

ADDITIONAL SIMULATION PARAMETERS FLOW VELOCITY

In these simulations the fluid, representing medium or the 'blood substitute', was approximated to have similar properties as water. The fluid properties (density and dynamic viscosity) from water were used as a reference fluid at a temperature of 310.15 K. This temperature was chosen as it represents the condition under which chip experi-

ments are normally performed. The mesh component was modelled as a solid with the material properties of acrylate, a polymer. For the finite element simulation, a 'physics-controlled' mesh, which is a software default mesh, was chosen and the mesh element size was set to 'fine'.

In order to incorporate the physics, the 'Laminar Flow' interface was used. Since a microfluidic application was modelled, steady state Stokes flow valid for low Reynolds number was assumed. Furthermore the fluid was simulated as a Newtonian fluid and therefore the fluid flow was considered incompressible. Under these conditions, the movement of fluid is governed by the continuity Equation (5.1) and the incompressible Navier-Stokes Equation (5.2) [68], where ' ρ ' is the density of the fluid in $[\text{kg}/\text{m}^3]$, ' \vec{U} ' is the flow velocity vector in $[\text{m}/\text{s}]$, ' p ' is the pressure in $[\text{Pa}]$, ' ∇ ' is the divergence and ' $[\vec{\tau}]$ ' is the shear stress tensor in $[\text{Pa}]$.

$$\nabla \cdot \vec{U} = 0 \quad (5.1)$$

$$\rho \left(\frac{\delta \vec{U}}{\delta t} + \vec{U} \cdot \nabla \vec{U} \right) = -\nabla p + \rho \vec{g} + \nabla \cdot [\vec{\tau}] \quad (5.2)$$

In the laminar flow regime the boundary condition at the wall was set to 'no slip', which implies that the speed of the fluid layer that is in direct contact with the solid boundary is equal to the velocity of this boundary. The flow inlet is modelled with a 'fully developed flow' boundary condition and the inlet flow rate V_0 was set to $100 \mu\text{L}/\text{min}$ or $1.667 \text{e-}9 \text{ m}^3/\text{s}$, which is equal to the flow used during the experiments. In addition, simulations were performed with a flow rate of $300 \mu\text{L}/\text{min}$ or $5.9 \text{e-}9 \text{ m}^3/\text{s}$ to visualize the on-chip effect of increased flow and draw a comparison. Additionally, the pressure at the channel outlet was set to $P = 0 \text{ Pa}$, which implies that there is no backpressure. Since relatively low flow rates are applied and due to the small overall microchannel dimensions, turbulence was excluded from the model.

Equations 5.1 and 5.2 were solved by the computational fluid dynamics simulations to evaluate the velocity fields, shear stresses and the pressure in the microfluidic channel and chamber. To do so, a fully-coupled stationary solver was implemented assuming that the flow profiles did not change over time. The chosen solver was the Iterative GMRES solver. The velocity magnitude results of the flow are plotted in 2D-surface plots with a scaled legend to facilitate theoretical comparisons among various conditions, see Section 6.3.1.

ADDITIONAL SIMULATION PARAMETERS PARTICLE TRACING

Besides simulating the flow velocity profiles it was of interest to visualize the actual spread of particles through the chip chambers and how this is affected by the inclusion of a mesh component in the chip. To this end the 'Particle Tracing for Fluid Flow' interface in COMSOL was used. Particle release and propagation were defined to be Newtonian and release times were explicitly defined. Here, a 'bouncing' wall condition was used.

The particle properties were set in accordance with the reported properties of the 'Blue Florescent Polymer Microspheres' that were used to evaluate the Fluigent set-up as described in 6.3.3: density 1050 kg/m^3 and diameter $0.5 \mu\text{m}$. The particle type was set to 'Solid Particle'. Moreover, a 'Stokes' drag force was implemented to account for the resistance that the particles experience by the fluid medium. Finally, the time dependent solver was used to solve for the particle trajectories over time, using the previously obtained results from the stationary solver for the flow velocity profiles. The applied solver was again the fully-coupled iterative GMRES solver. The results are presented in Section 6.3.2.

5.2.2. SCALING THE CARDIORENAL SYSTEM

Realistic coupled **OoC** systems require accurate scaling of various parameters to achieve a physiologically representative system. In this context it is essential to consider on-chip tissue-to-tissue ratios, volume-to-cell ratios, flow rates and actual tissue functionality. This paragraph serves to explore the applicability of the currently designed set-up in terms of relative scaling ratios.

CELL-TO-CELL SCALING

In this study, the basic organ models to embed comprise **cardiac microtissues (CMTs)** to replicate heart tissue and kidney organoids that resemble functional kidney tissue. **3D** cardiac microtissues were developed by combining three hiPSC-derived cardiac cell types as described in [59]. In short, each CMT is developed from 5×10^3 cells, comprising 15% endothelial cells, 70% cardiomyocytes and 15% cardiac fibroblasts and reaching a mature size of approximately $300 \mu\text{m}$ in diameter. On the other hand, each KO is developed from 500×10^3 hPSCs as described in [58] and has been shown to simultaneously include different renal structures: segmented nephrons connected to collecting ducts, surrounded by renal interstitial cells and an endothelial network. The final size of a mature kidney organoid is approximately 2 mm in diameter. Table 5.2 provides an overview of the tissue characteristics of each organ model to be embedded, which serves as an important limitations when deciding on the particular scaling method.

Table 5.2: Parameters of the organoid models to be embedded in the system.

Tissue type	# Cells/ organoid	Cell types	Approximate diameter
Cardiac Microtis- sues (CMTs)	5000	15% endothelial cells; 70% cadiomyocytes; 15% cardiac fibroblasts	200-300 μm
Kidney Organoids (KOs)	500 000	hPSCs: nephrons; collecting ducts; endothelial cells interstitial cells	3.5 mm; height 500 μm

In Section 2.4, various scaling approaches and their limitations have been explained in more detailed. To date, a scaling approach based on organ mass or volume ratios is among the most rigorous and provides a relatively straightforward method to obtain an initial idea about physiologically relevant relations in any microfluidic system. As a starting point, *in vivo* values for organ mass, specific density and blood flow rates have been gathered from literature to subsequently determine their relative ratios. Even though there is only one reference given for each of the parameters, the representative mean values have been verified with separate references [32], [69]–[71]. The values reported here (Table 5.3) are taken from the International Commission on Radiological Protection (ICRP) Report 23 of the Task Group on Reference Man [72], which was found to be the main reference cited in other reports that provide data on physiological parameters. The data is based on a reference human male adult with a body weight of 70 kg [72].

Table 5.3: Physical parameters used to determine first ball-park estimation of relevant scaling ratios for cardiorenal MOoC-system. Values based on 70 kg reference human [72]

Organ	<i>In vivo</i> organ mass (g)	Specific density (g/cm ³)	Relative Organ Weight (%BW)
Heart	330 ^a	1.03	0.47
Kidneys	310	1.05	0.44
Blood	5500	1.06	7.9

^a Tissue only

Microfluidic systems are defined by their volumes rather than mass, therefore accurate models require that the organ weight data presented in Table 5.3 are converted to units of volume. However, since the specific density of most visceral organs can be approximated to be 1.00, a mass-to-volume conversion may be ignored for the sake of simplification [69]. Furthermore, if we assume a linear relationship between organ mass and cell number, a representative kidney-to-heart-cell ratio can be established which would render an ideal MOoC system. Namely **1:1**.

For the purpose of initial feasibility studies, ten CMTs were coupled to one KO in the co-culture set-up. Considering the number of cells used to constitute a single organoid of each type (see Table 5.2), this implies that in the complete chip we currently find a cell-to-cell ratio of 50 000 : 500 000, or simplified **1:10**. This implies that in the set-up as such there is approximately a 10x difference between the physiological cell-cell ratio and the on-chip achieved ratio, which is deemed acceptable for the first try-outs.

TISSUE-TO-VOLUME SCALING

The total volume used in any MOoC system is first of all limited by the required on-chip volume to completely fill the microfluidic channels and chambers. The total on-chip volume (channel and wells) of a single lane on the IBIDI μ -slide III 3D Perfusion is equal to 250 μ L. If chip experiments are performed under static conditions or if flow is realized by means of a rocker platform, this is the minimal volume of any experiment. Yet, when experiments are to be performed with external pumps to realize either recirculation or single-pass unidirectional flow, this volume most definitely has to be increased. This will further complicate the possibility to achieve relevant volume-to-tissue ratios.

Table 5.4 presents the physiological volumes and relative ratios of the heart, kidney and inter-capillary blood volume *in vivo*, which are to be approximated as best as possible in the microfluidic set-up. Take note, that the presented volumes are based on complete organs. To improve on this first ballpark estimation, functional *in vivo* volumes may be used instead of whole organ volumes by subtracting the blood vessel content [32].

To determine the tissue-to-volume ratios, a volumetric approximation rather than cell-number based calculation should be made. To this end, the tissue volume cultivated in the system was calculated based on the organoid size data presented in Table 5.2. The KO was approximated to have a disc-like shape with a total volume of 4.8 μL (Equation 5.3). The total CMTs volume, based on 10 microtissues, was calculated to be 0.14 μL (Equation 5.4). Furthermore, the total microfluidic medium volume is 250 μL . An overview is provided in Table 5.4.

$$\pi r^2 h = \pi \times 1.75^2 \times 0.5 = 4.8 \text{ mm}^2 = 4.8 \mu\text{L} \quad (5.3)$$

$$\frac{4}{3} \pi r^3 = \frac{4}{3} \pi \times 0.15^3 \times 10 (\text{CMTs}) = 0.14 \text{ mm}^3 = 0.14 \mu\text{L} \quad (5.4)$$

With these volumes, the scaling factor can be determined relative to the *in vivo* counterparts of the KO, CMTs and on-chip media respectively. The systemic tissue-to-media ratio for the on-chip co-culture becomes 1 : 34: 1790 for the CMTs, KO and on-chip medium volume, respectively. When comparing the physiological relative tissue-to-volume ratio to the achieved on-chip relative ratio, it becomes evident that there is still a large discrepancy to be solved as the tissues are currently scaled by a very different factor relative to the human body. In fact, in the current model the relative scaling ratio is determined to be 1:38:112, which implies that the KO is relatively 38x times larger than the heart component and the medium (blood surrogate) volume is even 112 times too large compared to the calculated *in vivo* ratios that should be achieved. This large liquid-to-tissue ratio directly affects the concentration of crosstalk-mediating molecules as they are over-diluted in the system, complicating accurate read-outs as well as tissue interactions on the microscale.

Table 5.4: Overview volumetric data of *in vivo* tissues compared to on-chip tissue and medium volumes [72].

Type	<i>In vivo</i> volume (ml)	Relative <i>in vivo</i> ratio	On-chip volume (μL)	Achieved on-chip relative ratio	Scaling factor compared to <i>in vivo</i>
CMTs	320	1	0.14	1	2 286 000
KO	295	0.9	4.8	34	61 500
Blood	5200	16	250	1 790	20 800

Taken together, the current scaling does not yet comply with the requirements for a physiologically relevant MOoC cardiorenal system. Since the medium volume cannot effectively be lowered than 250 μL on-chip, the solution lies in up-scaling or down-scaling the

size of embedded tissue specimens. With an available organ-chamber volume of 30 μL , relative tissue ratios can theoretically be achieved with the available space.

To establish proper scaling ratios between individual OoC models is challenging as multiple methods have been proposed, but no consensus has yet been reached on the most robust method. Besides, changing the size of current models is difficult, as each organ model has been extensively characterized and is based on optimized robust protocols. Furthermore, the scaling problem becomes increasingly complex as organoids rather than 2D cellular monolayers are used, as the specific volumes and surface areas of those tissue specimens are inherently more difficult to quantify. The scaling assessment presented here is only a first approach to validate the relevancy of the current cardiorenal system and serves as a starting point for further optimization of the system. This will most likely require a more detailed analysis of the embedded tissues and included cell types, taking into account their functionality and metabolic activity, their volume and surfaces. Caution should be taken, as different organs scale differently especially on the microscale, and thus direct scaling based on a single scaling factor may prove to be result in distorted tissue-to-tissue relationships.

FLOW RATE

The flow rate in microfluidic applications is an important determinant of tissue perfusion rates and thus molecules' resident time in organ model [30]. Usually stringent flow rate requirements are in order to prevent tissue exposure to high shear stresses. However, since the presented MOoC model involves organoid models rather than cellular monolayers, shear stress is not the main concern and therefore there is not a straight forward method to determine the ideal flow rate under these circumstances. The prime requirement is that organ cross-talk is facilitated and that nutrition is provided and gas exchange is adequate. It should be further validated whether this is indeed the case, but a flow rate of 100 $\mu\text{L}/\text{min}$ serves as a good starting point, as the simulation results presented in Paragraph 6.3.1 show that the fluid velocity inside the organ-chamber is relatively low. Once data is obtained for the metabolic activity of the CMTs and KOs, the flow rate can be reassessed based on *in vitro* secretome data.

5.2.3. CHAPTER SUMMARY

The feasibility studies presented here serve as an important step towards realizing a complete cardiorenal microfluidic system. It is only upon acquiring a complete understanding of each separate microfluidic component and biological aspect that all components can be combined into a single set-up and evaluated as such. To recap the most important findings of the performed proof-of-concept studies:

- CMTs and KOs are differentiated and matured in their respective tissue-specific media. Upon integration of the organoids on-chip, the economically preferred BPEL medium deprived of any additional tissue specific growth factors is used as the common medium for co-culture over a period of 72h.
- KOs are structurally not affected by the static on-chip environment within a 72h time frame. Further experiments should confirm this observation.

- **CMTs** remain viable and structurally intact over a culture period of 72h in static on-chip conditions. This is confirmed by functional beating analysis. Further experiments should confirm this observation.
- Tissue specimens do not flush out of the on-chip organ chambers due to applied flow. However, careful handling is required during the assembly of the set-up to prevent tissue wash-out.
- Plasma-treated honeycomb micro-well meshes for **CMTs** were printed successfully and were able to effectively trap **CMTs**. The meshes require a post-printing plasma-treatment to increase the wettability.
- Though a viable design was found, KO pore-like meshes have been unsuccessful in providing an alternative route to pre-culture kidney organoids on a specifically designed insert in order to omit the need for manual transfer and thus disturbance of the kidney organoid.
- A first effort at performing cytotoxicity studies, identified the Mojin Tech Clear Resin as the optimal printing material for the meshes if they are autoclaved and exposed to a plasma surface treatment in the post-printing phase.
- Computational Fluid Dynamics simulations were successfully generated to visualize the velocity flow profiles in the IBIDI μ -slide. Subsequently, the simulation was used to identify the flow-related effect of inserting a 3D printed mesh in the on-chip organ chambers.
- The achieved tissue-to-tissue ratios in terms of cell number differ by a factor of ten, which is acceptable for the initial stage of this project.
- The microfluidic tissue-to-volume ratio is not near physiologically relevant and requires optimization efforts to ensure feasibility of the presented system designs.

Despite answering some of the outstanding questions related to the feasibility of a cardiorenal **MOoC** system, some open issues remain to be addressed in follow up studies. Among these are the respective sizes of **KOs** and **CMTs** as they currently scale very differently. Furthermore, it is yet uncertain what the ideal timing of organoid embedding is. To increase the reproducibility of the executed experiments, a specific organoid maturation time point should be selected that is found to result in the best on-chip responses. Besides, efforts must be directed towards in-depth characterization of biological and metabolic tissue properties as this data will serve as the root information to further optimize any presented system.

6

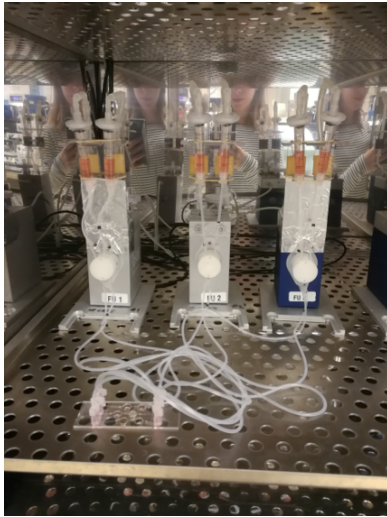
EVALUATION OF THE DESIGN

The performance of the feasibility studies set the stage for evaluating the chosen conceptual microfluidic set-ups as described in 4.2. This chapter presents the practical results obtained with the IBIDI pump system and the Fluigent set-up and furthermore comments on the results obtained with the computational fluid simulations.

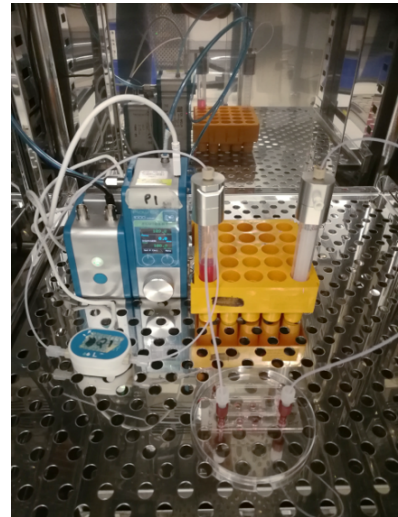
6.1. SYSTEM SET-UP

The conceptual designs presented in Chapter 4 have been realized to first of all test their general functionality and second of all to test their applicability for the purpose of creating an integrated cardiorenal MOoC system. The results may be used to guide decision making with respect to which system to use for follow-up experiments. The following findings are related to the overall use of working with any microfluidic set-up:

- Establishing a well-defined **handling protocol** is key to working with microfluidic systems. Minor manual interventions may have great disruptive effects on the delicate environment and therefore it is important to follow the same steps every time, with minimal user dependency.
- **Pre-warming** the slides, tubing and medium prior to starting an experiment is essential. By placing all these parts in the incubator, the plastic components are degassed which helps to avoid air bubbles as the material can absorb less gas at higher temperatures.
- **Technical issues** related to device set-up and subsequent operation were found to be a major challenge when aiming to ensure reproducibility between experiments. This includes bubble formation, software connection issues and other dysfunctional microfluidic components.



(a) Microfluidic set-up for recirculation with the IBIDI pump system



(b) Microfluidic set-up for flow-controlled single-pass perfusion with the Fluigent system.

Figure 6.1: Evaluated microfluidic circuits for the purpose of this project.

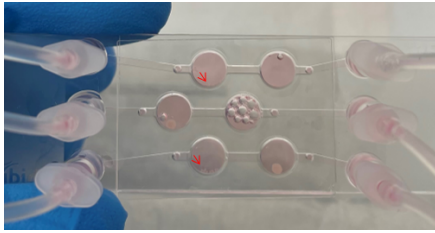
6.1.1. IBIDI SET-UP PERFORMANCE

The IBIDI pump system was used to create the set-up shown in Figure 6.1a. With this circuit it was possible to realize recirculation for at least 72h at a set flow rate of $100 \mu\text{L}/\text{min}$. Three parallel lanes could be perfused simultaneously, which is beneficial as one chip could be used to establish both control conditions for individual organ-models as well as for the co-culture. Following the flow experiment, the embedded tissues were retrieved from the chip and analysed by means of immunofluorescence staining and contraction analysis.

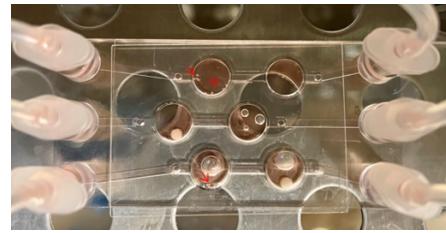
A recurring problem during the assembly of the set-up, and in particular of the microfluidic chip, was the appearance of air bubbles as shown in Figure 6.2. Whereas, it was observed that these bubbles do not negatively impact nor interfere with the tissue models, it was impossible to evaluate their exact effect due to the lack of real-time measurements and real-time tissue monitoring. On top of that, the air bubbles do disrupt the flow velocity profile and increase the chance of blocking the tubing over the time course of an experiment.

On a final note, assembling the complete set-up was found to suffer from inconsistencies due to material wear or manual handling issues. The BLACK perfusion set was autoclaved and re-used during subsequent experiments, but this can only be done a limited number of times before the functionality diminishes. If this system is to be used, it is essential to validate that no micro-particles are released from the material that might possibly adversely affect the tissue. In addition, the reliability of the electrodes that connect the FU's to the pump system was found to be limited, possibly due to the age of the system itself. The technical issues that presented itself during the experiments are wor-

risome as they greatly impacted the success rate of the performed assays and are hard to anticipate beforehand due to their inconsistent nature.



(a) Chip right after assembly (0h)



(b) Chip after 72h culture under flow

Figure 6.2: Air bubbles were encountered upon assembly of the microfluidic chip. Air bubble localization does change over the time course of an experiment. The red arrows indicate the location of the microtissues.

6.1.2. FLUIGENT SET-UP PERFORMANCE

Various set-ups have been created to evaluate the Fluigent system performance. First of all, a single-pass unidirectional circulation was established with components that were readily available in the lab (see Figure 6.1b). Compared to the conceptual unidirectional single-pass set-up presented in Section 4.2.2, a link module was added to allow for easy and direct read-out of flow parameters and a flow sensor of type Large was included in the circuit rather than the proposed S sensor. To validate the concept, the flow rate was set to $10 \mu\text{L}/\text{min}$ and the system was run successfully for a total of 22h, thus requiring a medium reservoir with at least 14 mL of fresh medium. Over this time course no technical issues were encountered.

While the total required volume does result in high liquid-to-tissue ratios and only a single channel could be perfused with the presented set-up, the system was quick and robust to assemble. It was found that the flow-rate control worked accurately, thus keeping the flow conditions relatively stable during the experimental time span. Additionally, this single-pass circulation circuit facilitates easy collection of whole volume medium for downstream analysis. Nevertheless, future experimental iterations should aim at further minimizing the required medium volume. It should also be noted that in this proof-of-principle studies a single channel was perfused, but the ultimate goal is to at least be able to perfuse three channels simultaneously. The next trial must focus on extending the current set-up accordingly. On top of that, maintaining sterility during the assembly of the complete set-up must be optimized as this was not as straightforward compared to the IBIDI set-up.

RECIRCULATION

The recirculation scheme presented in 4.4 has not yet been established and functionally tested in the lab. Unfortunately, technical issues were encountered with the required components, which therefore had to be repaired and replaced. Proof-of-principle tests to validate the feasibility of establishing a recirculation circuit with the Fluigent set-up will be included in future work.

6.1.3. SYSTEM RELATED CONCLUSIONS

Overall, the findings of the experimental evaluation of the two presented microfluidic operation systems can be summarized as presented in Table 6.1. These findings, together with the results obtained from the feasibility studies, form the basis for further decision making with regard to the development of a clinically relevant cardiorenal MOoC system.

Table 6.1: Overview of advantages and disadvantages of evaluated microfluidic systems based on experimental observations.

	IBIDI pump system	Fluigent system
<i>Advantages</i>	<ul style="list-style-type: none"> • Three channels can be perfused in parallel with a single IBIDI pump. • Experiments can be run for at least 72h without the requirement of a medium change. • Set-up optimized for recirculation experiments. • The complete set-up can be assembled under sterile conditions • Uses standardized perfusion sets 	<ul style="list-style-type: none"> • Very versatile system, easy to adapt to make fit-for-purpose. • The system can be operated with very low as well as high flow rates. • Flow rate control based on direct feedback. • Open-source software with friendly user-interface is available to write automation protocols in line with the research question. • Real-time data can be retrieved from software. • Tubing length can be adjusted to ensure that the entire set-up fits in the incubator environment. • Suitable to design single-pass unidirectional circuits. • Has potential to create automatized recirculation set-up with few additional components.
<i>Disadvantages</i>	<ul style="list-style-type: none"> • Not suitable for single-pass experiments. • Only runs with relatively high flow-rates (starting from +/- 100 $\mu\text{L}/\text{min}$). • Lack of modularity complicates system adaptation to specific research needs. • System operation, including pressure control and flow rate calculations, relies on pre-programmed software settings which are impossible to adapt manually. • Very prone to technical issues. 	<ul style="list-style-type: none"> • Perfusing multiple channels simultaneously greatly increases complexity, rendering the system prone to human handling errors. • Sterile assembly is not optimized. • Manual cutting of tubing may lead to variable tubing lengths across experiments. • With the current set-up, a too large volume of medium is required to keep the experiment running for extended periods of time.

6.2. TISSUE CHARACTERIZATION

6.2.1. KIDNEY ORGANOIDS

Immunofluorescence stainings were performed on retrieved KOs to analyse the structural integrity after 72h of isolated culture and co-culture under flow conditions. The experimental procedure was similar as discussed before in Section 5.1.2. A static control condition was included for comparative analysis. Figure 6.3 shows representative results from the immunofluorescence stainings for markers of Hoechst, LTL and NPHS1. The results clearly show that the structural integrity of KOs is better preserved in the on-chip environment if flow is applied compared to the static chip-environment con-

ditions (Figure 5.3). As becomes evident there are no major morphological differences when comparing across the conditions. As such, it is concluded that in the on-chip environment perfusion of medium is required to ensure the viability of the KO as otherwise the tissue suffers from a lack of either adequate oxygenation or nutrition.

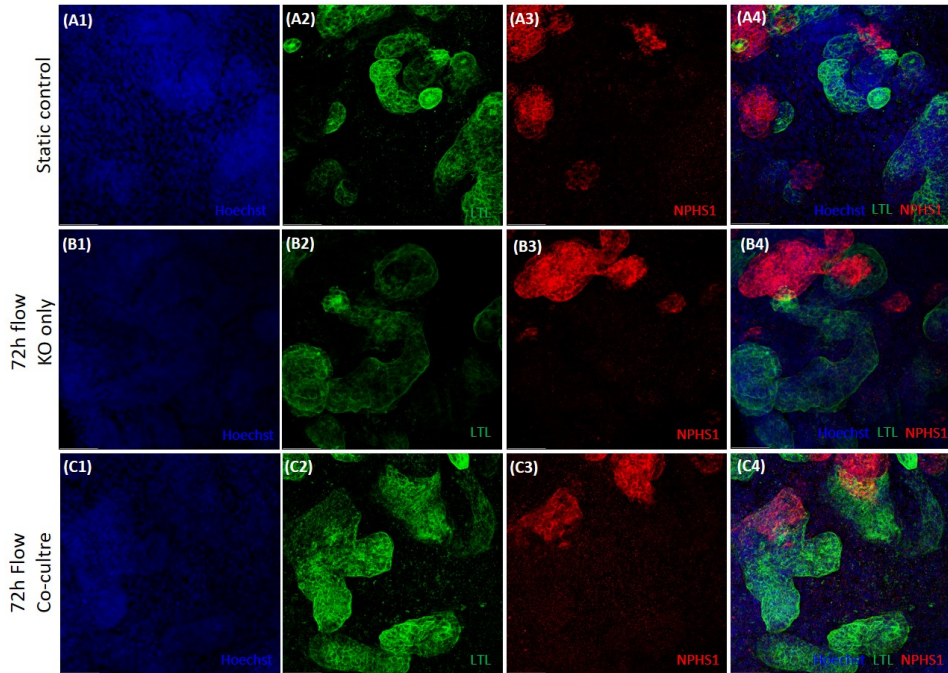


Figure 6.3: Immunofluorescence stainings of KOs after 72h culture under flow compared to control conditions. **A1-A4** Static control conditions. **B1-B4** 72h flow conditions KO only. **C1-C4** 72h flow conditions co-culture.

6.2.2. CARDIAC MICROTISSUES

Likewise, immunofluorescence stainings were performed on **CMTs** retrieved from the chip after 72h of culture under flow. Static control conditions were compared to isolated culture and co-culture of **CMTs** on-chip under a constant perfusion of $100 \mu\text{L}/\text{min}$ for 72h. The results presented in Figure 6.4 for stainings of Hoechst, cTnT, ACTN2, show that cardiac structures are still present after prolonged exposure to flow. Though the microtissues seem to have slightly decreased in size, the structural integrity was evaluated to not be significantly affected. Therefore, it was concluded that the flow does not induce major adverse tissue effects in the **CMTs**. Noteworthy, this conclusion is based solemnly on the observational analysis presented here and should be further validated by more quantitative types of experiments.

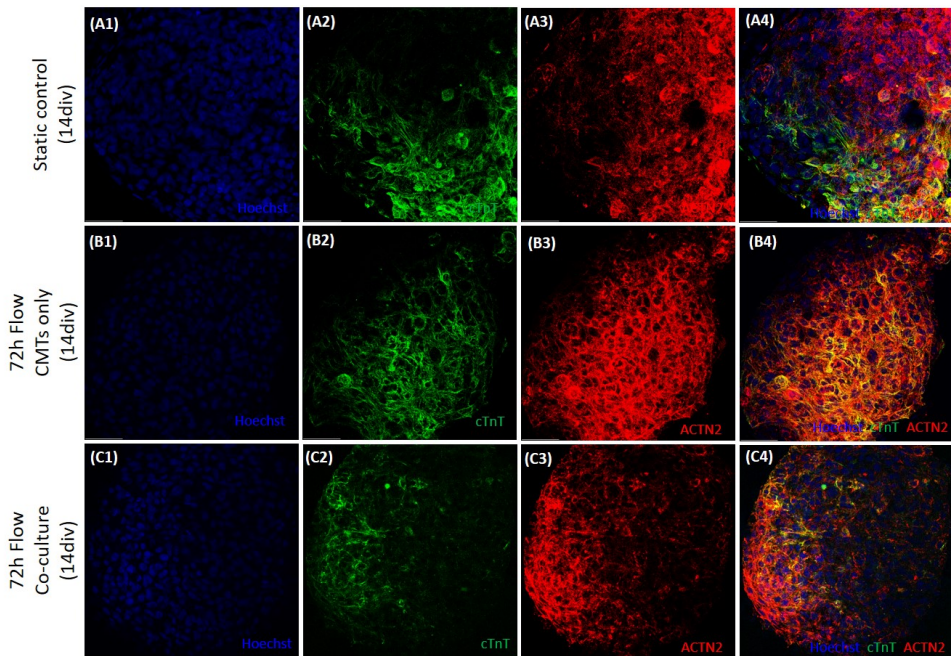


Figure 6.4: Immunofluorescence stainings of CMTs after 72h culture under flow compared to control conditions. A1-A4 Static control conditions (14div). B1-B4 72h flow conditions only CMTs (14div). C1-C4 72h flow conditions co-culture (14div).

6.2.3. MUSCLEMOTION ANALYSIS CMTs

As described previously in Section 5.1.2, MUSCLEMOTION analysis was performed to functionally evaluate the viability of CMTs after 72h of culture while exposed to flow conditions. Ideally, the contraction and beating profiles of CMTs are not significantly altered compared to static conditions due to their introduction into a microfluidic environment. Figure 6.5 shows the results from the performed data analysis on CMTs that were kept in static control conditions, isolated flow conditions and co-culture flow conditions.

Unfortunately, no experiments have yet been successfully performed that include all possible conditions simultaneously: static control, static on-chip, and flow on-chip. This implies that the data presented before related to static tissue characterization in the feasibility studies (Section 5.1.2) was based on a different set of experiments. Due to experimental variability it is therefore hard to draw definitive conclusions, as comparisons between static and flow conditions might be biased. Besides, the number of microtissues used for the analysis was limited as some were lost during the process.

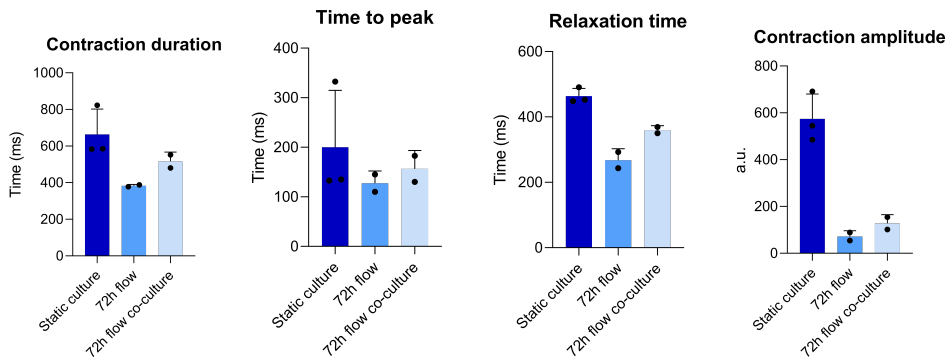


Figure 6.5: Musclemotion results showed no significant differences in contraction duration, time to peak, relaxation time and contraction amplitude when cultured in static conditions or flow conditions for 72h. Black dots represent obtained results for single microtissue.

6.3. RESULTS COMPUTATIONAL SIMULATIONS

6.3.1. VELOCITY PROFILES

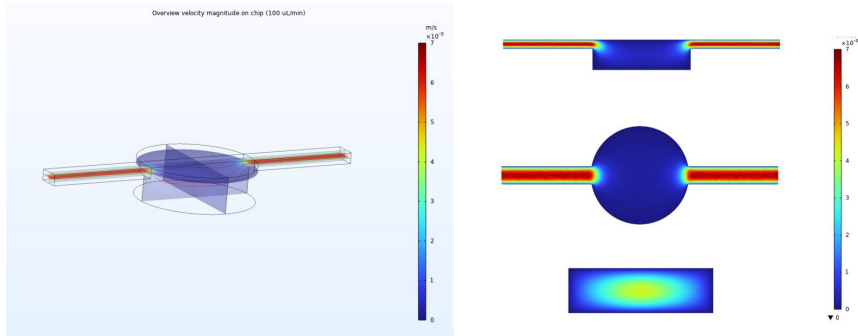
The flow velocity profiles were simulated as described in Section 5.2.1. Representative 2D surface plots have been generated to show the flow velocity at various locations in the chip if a flow of $100 \mu\text{L}/\text{min}$ or $300 \mu\text{L}/\text{min}$ respectively is applied at the chip inlet.

The results (see Figure 6.6) show that the velocity magnitudes of the flow are the highest in the narrow inlet and outlet parts of the chip, but relatively low throughout the chambers itself. Furthermore, the highest velocity values are found in the centre of the chamber and in the middle of the channels, whereas velocities decrease towards zero towards the wall of the device, which is in line with the no-slip boundary condition. Note that the scale of the presented cross-section is up-scaled by a factor ten.

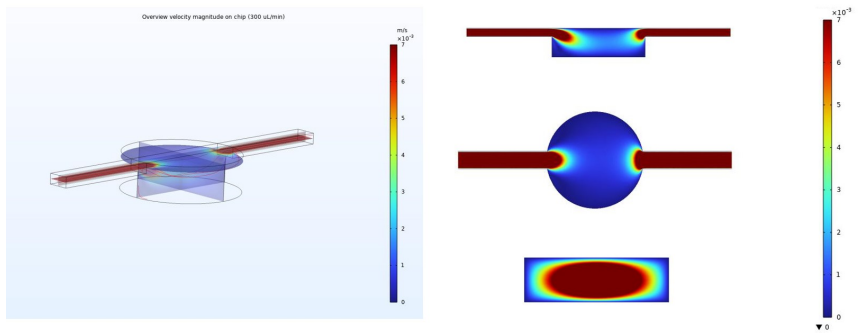
Furthermore, the simulation allowed to quantify the theoretical shear rate and shear stress within the culture chambers and channels. This is relevant to determine the exposure of the tissues to shear stress and thus get an idea about the possible tissue disturbance due to the flow. Seeing that water, a Newtonian fluid, was used as a reference fluid to run simulations, the shear stress ' τ ' is directly proportional to the shear rate ' $\dot{\gamma}$ ' according to Equation 6.1. Here ' μ ' represents the dynamic fluid viscosity.

$$\tau = \mu \dot{\gamma} \quad [\text{Pa}] \quad (6.1)$$

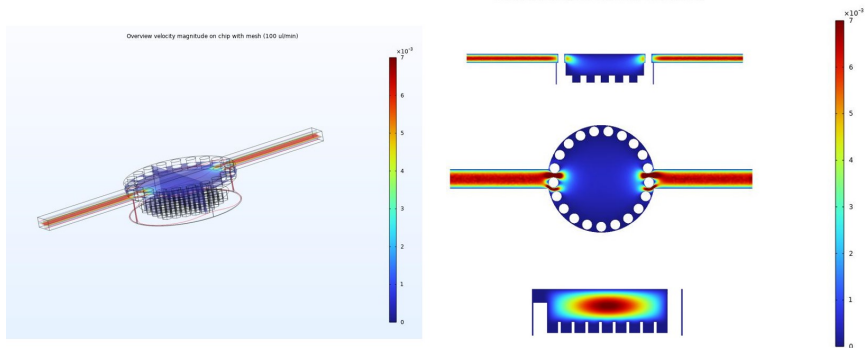
Shear stress profiles were computed for a flow rate of $100 \mu\text{L}/\text{min}$ in the reference simulation and the simulation with a mesh, respectively. Figure 6.7 presents the computed shear stress at the near bottom of the chamber, $h = 0.2 \text{ mm}$, and at the middle of the chamber, $h = 0.85 \text{ mm}$, plotted against the total width of the circular chamber (5.5 mm). Figure 6.7a shows that the shear stress in the middle of the chamber (blue line) is lower than the shear stress on the bottom of the chamber (green line). In addition, in the middle of the chamber the shear stress increases towards the edges, while the opposite is



(a) Simulated velocity magnitude in chip (m/s) at a flow rate of $100 \mu\text{L}/\text{min}$.



(b) Simulated velocity magnitude (m/s) in chip at a flow rate of $300 \mu\text{L}/\text{min}$.



(c) Simulated velocity magnitude (m/s) in chip at a flow rate of $100 \mu\text{L}/\text{min}$ with mesh.

Figure 6.6: Simulation results for velocity magnitude in IBIDI μ -slide Perfusion exposed to various flow rates and with an inserted mesh. Computational Fluid Dynamic Simulations were performed using COMSOL Multiphysics.

true at the bottom of the chamber. Yet, it must be noted that the overall values in the organ-chamber are very low. Importantly, when CMTs are placed in the organ-chamber, they will sink to the bottom of the device due to the gravitational effect and thus be exposed to the shear stress that is found here (presented by green line).

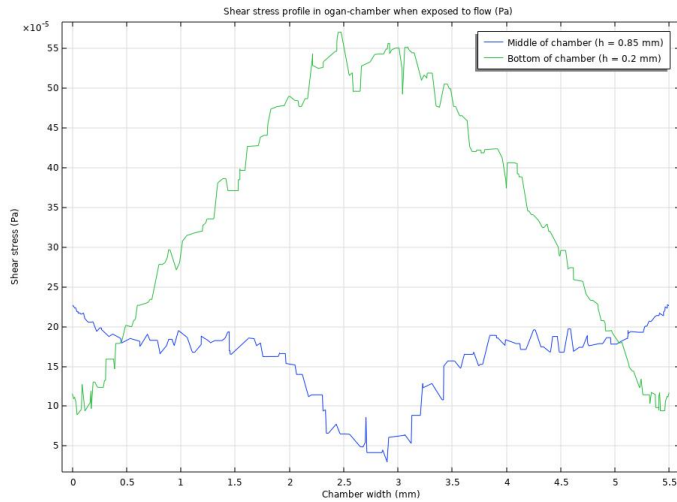
Figure 6.7b shows the shear stress simulation outcome when a honeycomb mesh is included in the organ-chamber as shown before in Figure 5.12b. The mesh reduces the shear stress in the bottom of the chamber (half-way up the micro-wells) to a value that is comparable to the shear stress otherwise present in the middle of the chamber when no mesh is included. Therefore, the mesh seems to be capable to form a shear-stress protected niche for microtissues, which might be beneficial to prevent tissue outflow and to maintain organoid integrity. However, it also has a significant effect on the shear stress profile in the middle of the chamber (blue line), which now is maximal in the middle of the chamber and reduces towards the chamber walls. Compared to Figure 6.7a, the shear stress profile in the middle of the chamber with mesh thus seems to be reversed and shows striking similarities with the shear stress profile found in the bottom of an empty chamber.

Since the shear stress values computed in this simulation are rather low, they are hypothesized not to exert a major effect on tissue specimens. Yet, once flow rates are further increased or other structural components besides this mesh are to be added to the organ-chamber it is good practice to keep the tissue effects of induced shear stress in mind.

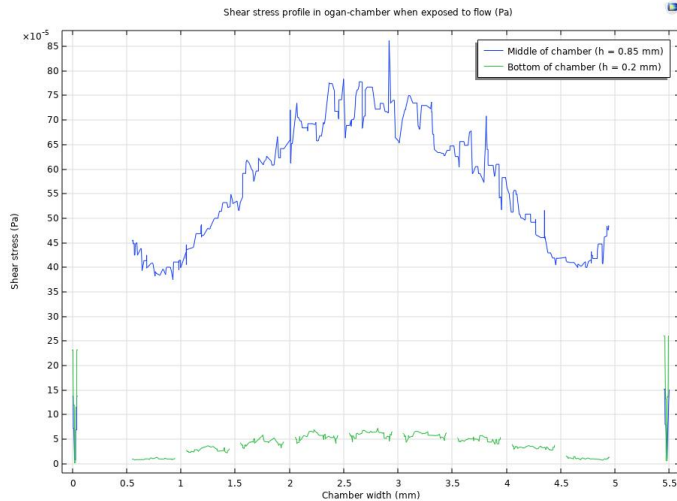
6.3.2. RESULTS PARTICLE TRACE

Particle traces have been computed to visualize the flow and spread of medium in the chip over time at a defined flow rate of $100 \mu\text{L}/\text{min}$. The simulation was run for 15 seconds to limit the computation time. Snapshot figures taken at the end of the simulation are provided in Figure 6.8. The Supplementary Information include videos of the complete particle traces (Videos SII-SI4). Overall the results imply that the flow profiles among the two conditions are rather comparable, and the vertical pillars of the mesh do not seem to interfere adversely with the fluid flow. Inevitably, the mesh does confine the available space inside the organ-chamber as it is designed with a relatively thick wall to ensure stability of the insert. Consequently, the chamber residence time of medium seems to be reduced if a mesh is to be embedded, as well as that the maximum flow rate is slightly increased.

Furthermore, the result show that particles do not readily enter the niches created by the honeycomb structures. From a fluidic perspective, this can be attributed to the fact that the top part of the organ-chamber is perfusion dominated, whereas the bottom part of the chamber is diffusion dominated. In the honeycomb micro-wells, diffusion dominated exchange of fluids would ensure optimal nutrition while protecting the embedded microtissues from exposure to high shear stresses. Theoretically, the created micro-wells could therefore form a well-protected niche compartment to host each CMTs in the system. To validate this hypothesis, more detailed calculations should be made to express



(a) Computed shear stress profile in an empty organ-chamber at different heights.



(b) Computed shear stress profile in an organ-chamber with inserted mesh at different heights.

Figure 6.7: Simulated shear stress profiles to determine the effect of flow rate and the insertion of a mesh on fluid dynamics.

the relative dominance of competing physical phenomena that determine mass transfer and gas exchange in the microenvironment created on-chip [26]. It is critical to ensure that the chosen flow rate ensures sufficient convective delivery of nutrients, biochemical factors and gases, while simultaneously allowing for sufficient organoid-uptake in the niches.

When further optimising the system, a good start would be to calculate the ratio of

the Péclet number (Pe) versus the Damköhler number (Da), which is a way to quantify whether the convective or diffusive regime holds. At the same time also considering the relevant reaction timescales [26].

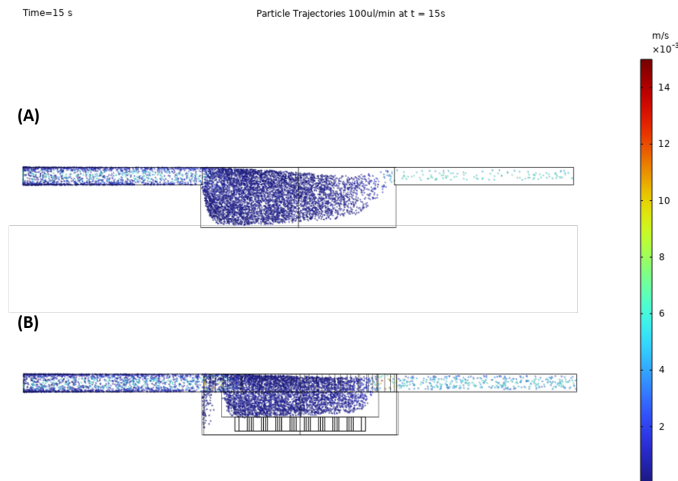


Figure 6.8: Sideview of the results from simulated particle traces at a flow rate of $100 \mu\text{L}/\text{min}$. Figures represent the 15 second time point. The legends indicate the maximum and minimal particle velocities. (A) Spread of particles in an empty organ-chamber. (B) Spread of particles in chip with a honeycomb-array mesh inserted.

6.3.3. *In vitro* FLOW PROFILE VALIDATION

To characterize the on-chip flow profiles *in vitro*, the Fluigent set-up presented in Figure 6.1b was used to perfuse the IBIDI μ -slide III Perfusion slide with a solution of PBS mixed with ThermoScientificTM Fluoro-Max dyed polystyrene microspheres, which are fluorescent at low wavelengths. Movement of the beads throughout the chip was detected by fluorescent microscopic live-imaging. Videos were taken at different points in the chip to assess the flow profile, see Figure 6.9. Subsequently, the flow characterization experiment was repeated with embedded microtissues and with an inserted mesh to visualize their effect on the dynamic flow distribution in the chip. The main goal was to acquire *in vitro* flow data to validate the simulation outcomes.

The main findings were the following:

- The simulation results are comparable to the flow velocity profile found *in vitro*. See Video **SI1 versus SI5** and Figure 6.9.
- The flow rate on top of the chamber appears to be high, whereas in the bottom of the chamber almost no flow was detected.
- **CMTs** were observed to sink to the bottom of the chamber and localize towards the outlet of the chamber where they accumulate together.
- The flow did not have an effect on the microtissues once they had settled, Video **SI6**, but the microscopic effect cannot be determined from this experiment.

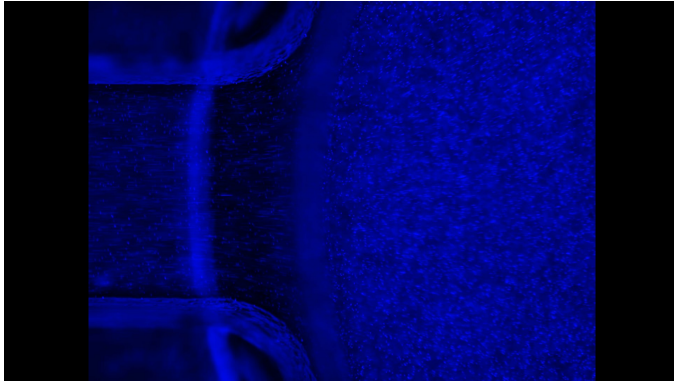


Figure 6.9: Snapshot of *in vitro* flow profile validation with Fluoro-Max dyed polystyrene microspheres at a flow rate of $100 \mu\text{L}/\text{min}$.

Together, this experiment served to evaluate the simulation results as well as provide insights on the actual flow velocity profiles that we are working with. This aids in our understanding of the dynamic effects to be observed during further *in vitro* experiments with viable tissues. These initial results contribute to finding fit-for-purpose solutions to remaining problems.

7

DISCUSSION

The heart and kidneys have been modeled separately *in vitro*, but models are typically too simplistic to capture the dynamic reciprocal cross-talk in the context of disease [13]. Nevertheless, emerging technologies based on converged knowledge from various fields have led to substantial advances in the applicability and feasibility of OoC models to accurately mimic human physiology on the microscale. This has resulted in a tremendous rise in reported MOoC models, which are especially useful for research into the complex biological mechanisms causative of systemic diseases. CRS is one example for which a validated unified organoid system could greatly help in resolving outstanding questions related to the molecular mechanisms and pathways that contribute to disease onset and progression. It is with this ultimate goal of modelling CRS in mind that this project focused on designing and setting up a 'cardio-renal unit' to fluidically connect established organoid models of the heart and kidney *in vitro*.

To achieve a physiologically relevant model, there are many biological and technical challenges to be addressed. Here, the experimental evaluation of proposed microfluidic systems served to refine our understanding of the encountered technological challenges and identify high-priority feasibility studies to be performed. The current experiments were performed as a form of pilot experiments and should be interpreted as such. The results provide a benchmark to further define and refine optimal co-culture conditions in a microfluidic environment and serve to guide decision making at future stages of this overall project.

7.1. EXPERIMENTAL SYSTEM EVALUATION

In this project, multiple microfluidic set-ups have been proposed and tested to establish a first proof-of-principle cardiorenal MOoC model. The tested designs enabled perfused co-culture conditions in a common medium of ten CMTs and one KO for up to 72h with recirculation. On top of that, a microfluidic circuit was built that allowed single-pass perfusion effectively. It was shown that CMTs remain viable and functional in the mi-

crofluidic environment, though their structural integrity and beating frequency was reduced. Furthermore, it was observed that the renal structures of **KOs** was maintained in the static on-chip environment after 72h of culture despite small medium volume availability. This observation must be validated by finding and evaluating relevant biomarkers to quantify (live) **KO** functionality.

Noteworthy, the proof-of-principle experiments reported in this thesis had low statistical power due to low experimental throughput, thus reducing the chance of detecting true effects following co-culture or culture in a microfluidic environment. More experimental iterations have to be performed to convincingly draw conclusions about the effect of on-chip culture and tissue exposure to continuous flow. The results obtained so far from immunofluorescence stainings and contraction analysis give reason to assume that we are going in the right direction. It is concluded that extended co-culture inside the chosen IBIDI μ -slide III 3D Perfusion chip is indeed possible with the evaluated set-ups if further optimization strategies are implemented.

7.1.1. MICROFLUIDIC CHIP SELECTION

Whereas the IBIDI μ -slide III 3D perfusion chip was found as a suitable option, at later stages of this project, the choice of chip must be re-evaluated based on the obtained results from the initial feasibility experiments. The proven potential must at all times outweigh the encountered disadvantages and an eye must be kept on novel products emerging on the market as it is expected that spheroid perfusion systems are likely to become more common.

7.1.2. PRESSURE PUMP SYSTEMS

Referring to the findings of the microfluidic set-up experiments performed with both the IBIDI pump system and Fluigent system, the main take-away was that system design must be focused on simplicity, ease-of-use and versatility. Considering the many aspects related to designing novel **OoC** experiments, as presented in Chapter 2, and the many resulting design choices to be made, it is key to define the main research question and come up with a model as simple as possible without compromising the biological relevance too much. Upon achieving a validated simple model, it can then be extended from there onwards by incorporating additional components into the microfluidic set-ups, such as for instance sensors. Furthermore, keeping the set-up straightforward hopefully alleviates the common occurrence of technical issues, that was found to be the main hurdle during the presented microfluidic experiments.

Commercially available **OoC** systems are now widely spread and designed for a broad range of applications. In spite of that, finding an off-the-shelf solution that directly complies with all the specific research requirements remains difficult. On top of that, the aim of synergistically integrating **OoC** approaches with organoid technology further complicates the choice as most microfluidic chips are not suited for organoid tissue models. Here, it was observed that both tested systems hold potential to establish a functional microfluidic circuit, but require additional design adaptations. Systems that can easily be rendered fit-for-purpose by making adaptations based on minimal interventions are best suited for laboratory applications. In doing so, the power of commercially devel-

oped systems in terms of their reliability and standardization is harnessed, while still offering customization potential to meet research demands.

Based on the system evaluation results, it is recommended to continue this research with the Fluigent system. This recommendation is substantiated by the high associated versatility and automizable, accessible control interface the system offers. The ease-of-use and compatibility of the Fluigent products were found to have more potential compared to the limited versatility of the IBIDI pump system. Moreover, the Fluigent set-up is compatible with any commercial microfluidic chip as tubing and connections can be interchanged with ease, as well as that it might be adapted to integrate two single chips for the different organ models. This would not be possible with the IBIDI system, but might be required if the IBIDI μ -slide turns out to be inadequate after all. Furthermore, the range of technical issues encountered with the Fluigent system was smaller compared to the IBIDI system, which is an additional benefit.

The proof-of-principle studies presented here served as a starting point to determine the ideal microfluidic circuit design, though some key issues still need to be tackled. First of all, in the present set-up high fluid-to-tissue ratios are likely to prevent effective cellular communication, as secreted factors are diluted within the medium volume [35]. There is a need to further reduce the internal volume by eliminating excessive volume in the medium reservoirs and finding the minimal tubing lengths. As became evident from the experimental evaluation, the internal volume is mostly accounted for by the reservoir volumes as the dead tubing volume was comparatively low. That means that in order to further optimize the circulation, proof-of-principle tests should be run to identify the least amount of reservoir medium that still renders the pressure-based circulation functional. Afterwards, further tweaking may be performed by altering the tubing internal diameter or total tubing length.

As an alternative to mechanically reducing the required medium volume, flow rate is another important determinant of total required volume, especially if single-pass flow is applied. The flow rate was mostly set to 100 $\mu\text{L}/\text{min}$ for the purpose of proof-of-principle studies and obtaining comparative results across the IBIDI and Fluigent system. However, this rate was primarily chosen based on the limitations posed by the IBIDI BLACK perfusion set rather than by tissue demands. Ideally, the flow rate is further optimized to ensure adequate perfusion and gas exchange while allowing continuation of the experiment over prolonged time. It is suggested to determine chosen flow rates on metabolic activity data, physiologically relevant residence-times in the organ-chambers or based on simulation results.

7.1.3. BIOLOGICAL EVALUATION

In the initial stages of this project the common medium was defined to be unsupplemented BPEL. Whereas it was superficially validated that changing KOs maintenance medium to this alternative did not have any noticeable consequences, it would be best to perform additional tests. In these feasibility studies, only IF-stainings to visualize the tissue morphology and microscope images were taken as evidence, whereas other more reliable and quantifiable read-outs may better serve the purpose. Therefore it is

recommended that the medium compatibility be tested more extensively by performing life/death stainings, quantifying ATP content and LDH release and obtaining gene expression profiles. The same holds for testing the exact effect of merely the static microfluidic chip environment on tissue integrity.

In this project, the proposed MOoC system is based on the use of iPSCs derived tissues, which inherently offer an unprecedented advantage over conventional cell-line based 2D-cell cultures. In addition, as this disease model is ultimately to be used for elucidating biomarkers and molecular pathways involved in various types of CRS and define novel therapeutic targets, the use of patient-specific biological material is beneficial. Yet, the existing methods to generate both CMTs and KOs require extended differentiation times (up to three weeks), which poses a great limitation to the experimental throughput. Moreover, the established protocol to generate KOs results in rather large organoids that surpass the dimensions of most commercially available OoC devices. Lastly, a common problem with the use of hiPSC derived tissues, is the immature phenotype that can be achieved before tissue degradation is induced. Tissue size and determining the right level of maturity before assembling microfluidic devices requires further addressing in future work.

On a final note, the end-goal of the overall research is to develop a novel cardiorenal disease model. Up until now, the presented biological models were all representative healthy controls, however a method must be identified to create robust disease representations. As concomitant cardiovascular and renal disorders often arise due to deleterious neurohormonal and inflammatory relations, it is ideal to model CRS from a systemic point of view. Tissue fibrosis has been identified as an interesting marker of progressed CRS, since it captures quantifiable changes in tissue morphology compared to healthy controls. Therefore, it may be considered a relevant pathophysiological mechanism underlying CRS and can thus be chosen as a starting point to create CRS disease models. It is envisioned, that future work will see fibrotic tissue models to be embedded in the microfluidic chip environment [18].

7.2. MESHES

To render the chosen microfluidic chip fit-for-purpose, various microwell meshes to insert in the organ-chamber were designed, developed and tested. The main purpose was to ensure robust trapping of CMTs in the organ-chambers and prevent unwanted tissue wash-out during the experimental procedures. The produced inserts required a post-printing plasma-surface treatment to improve the wettability, but were found to be a promising solution.

The produced honeycomb microwell meshes for the CMTs can be customized in size and integrated in other off-the-shelf commercially available microfluidic chips to make them fit-for purpose to use with pre-matured cardiac microtissues. This method serves as a low-cost and high-throughput approach to perform iterative evaluation tests with microfluidic set-ups. First attempts at cytotoxicity studies of the 3D-printed material on tissue viability were promising and CMTs were found to maintain their beating capacity over a 72h culture time. It became evident that the post-printing treatments have a sig-

nificant effect on bio-compatibility. Therefore it is essential to further quantify the exact effect and optimise the post-processing steps accordingly. Ideally, culture of CMTs on top of the microwell meshes does not have any effect on tissue morphology nor should it trap any of the secreted biomolecules. Furthermore, computational dynamics simulations showed that the meshes potentially create micro-niches in which tissue specimens are protected from induced shear stress. Though, caution should be taken that the meshes do interfere with the organ-chamber flow velocity profile possibly complicating adequate nutrition.

In this studies a single design was tested, which was found to be functional. However, design iterations to identify the most optimal mesh architecture may include the following:

- Changing the vertical wall-thickness of the meshes or completely removing the outer wall, such that merely a micro-well featuring surface is created [73].
- Honeycomb wells with included pores on the bottom to facilitate tissue wash out at the end of experiment. This should increase the ease of post-experiment tissue retrieval.
- Increased size of the honeycomb-wells to ensure that CMTs viability is not affected by the restricted space.

Unfortunately, printing results for the KO-meshes were not all successful. To further improve the printing quality of these meshes, layer height print resolution might be decreased as this is expected to result in more accurate prints if small dimensions are included in the design. Furthermore, functional feasibility experiments performed with the KO-meshes showed not enough potential to continue with design iterations at this point of the research as the viability of developing KOs was greatly implicated. As an alternative the manual transfer of the KOs to the organ-chambers should be optimized to minimally disturb the tissue. It is hypothesized that this is practically feasible and will adequately address the encountered problem of tissue rupture.

7.3. COMPUTATIONAL FLUID DYNAMICS SIMULATION

For the purpose of this thesis, the simulations were primarily generated to characterize the flow profiles in the on-chip organ-chambers and to validate the effect of varying flow-rates on the microenvironment dynamics. However, the results of these simulations can be extended to make calculated guesses about the exposure of embedded tissue specimens to circulating biochemical factors. To do so, the generated velocity magnitudes may be integrated over streamlines at the positions in near proximity of the embedded tissues (the so-called contact zone) [31]. As such, the parameters obtained from the computational fluid dynamics can aid in determining optimal flow rates for the particular research purpose. Besides, simulations are effectively quicker to generate results compared to conventional biological experiments and can therefore serve as important starting points to establish suitable experimental conditions prior to starting out in the lab.

7.4. FUTURE WORK

Although the presented microfluidic cardio-renal unit shows potential and some initial design choices have been made during this project, there are many improvements to be made and remaining challenges to be addressed.

Most importantly, a lack of information with respect to biological characterization of the used tissue models was encountered. This complicates optimization of flow parameters and finding accurate scaling ratios *in vitro*. It is therefore recommended that the project first of all continues with a focus on acquiring an in-depth understanding of the physiological tissue biology, after which the proposed microfluidic circuits can be optimized more efficiently. Assays may aim to quantify the metabolic activity of embedded tissue, identify the secreted factors of interest and their timely concentrations and focus on obtaining an accurate RNA and gene expression profile of 'healthy' tissue that should be referred to as the control condition during subsequent experiments. With the validation of these parameters, it becomes feasible to establish disease models and draw conclusions about cause and effect observed in co-culture conditions under flow. The need for well-verified control conditions is extremely high, since MOoC models are known to include a multitude of aspects that can all contribute to confounding effects if not monitored precisely. As a starting point it may be considered to perform glucose consumption and lactate release analysis on retrieved medium samples [74] to quantify metabolic activity and monitor tissue functionality. If these values for metabolic activity are found to reach a steady-state similar to control levels during on-chip co-culture experiments, it may be concluded that cell viability and tissue turnover on-chip is stable. Alternatively, sampled medium supernatants may be used to perform high-performance liquid chromatography (HPLC), liquid chromatography-mass spectrometry (LC-MS) or ELISA analysis to get an idea about the global and specific (protein) secretome.

To this end, it is not straightforward to identify the factors of interest that are both relevant for the heart as well as for the kidney model. Ideally, biomarkers are identified that function across the cardio-renal axis. Based on data reported in the Human Protein Atlas available from www.proteinatlas.org it was found that BMP10 (Bone Morphogenetic Protein 10), NPPA (Natriuretic Peptide A) and NPPB (Natriuretic Peptide B) are all blood-secreted factors by cardiac tissue that function to maintain cardio-renal homeostasis. Alongside, α -Cystatic c was found to be one of the few blood-secreted factors both by the heart and kidneys. Though, it is ideal to initiate biomarker identification by obtaining global mass spectrometry profiles, the above mentioned factors might be of interest to keep an eye out for.

What is more, is that the long term stability and long term on-chip tissue viability is yet to be validated. At present, maximal experimental run-time has been 72h, which is relatively short compared to the *in vitro* organoid maturation time that takes up to three weeks. Since the microfluidic environment is to be used to evaluate bidirectional organ-organ interaction, it is likely that experimental times have to be increased. Systemic disease manifestations generally do not happen overnight, but are more likely to arise with time. This factor must be taken into account when designing future experiments.

Furthermore, although not addressed in the present study, oxygenation of coupled or-

gan models may prove a crucial consideration in coupled organ models [27]. It must be validated that oxygen is not absorbed by the microfluidic components, thus depriving tissue specimens from appropriate oxygen tension. One way to do this, is by modelling and measuring oxygen levels directly in chip through the embedding of oxygen sensors. Selective oxygenation of medium reservoirs or ensuring that the microfluidic chip materials are gas-permeable may also contribute to maintaining physiologically relevant oxygen gradients.

When a functional physiologically healthy cardiorenal MOoC is established, including accurate flow rate, minimized internal volume, correctly scaled organoids and total experimental run-time, the proposed microfluidic perfusion set-ups can be re-evaluated. The conceptual perfusion system must be characterized based on the feasibility to measure required outputs, most likely secreted biomarkers, and adapted accordingly. To truly arrive at a physiological model that includes all the desired functionalities to recapitulate a systemic disease as CRS, it is anticipated that additional biological components must be integrated into the technology. MOoC platforms should ideally include representatives for the immune system, metabolism, microbiome and complete vasculature to account for those essential interactions during disease development. These systems impact the health and functionality of all organ systems in the body and are therefore essential to capture a true systemic dimension on the microscale [26]. It would, however, come at the cost of greatly increasing the complexity and controllability of experiments.

From a microfluidic system perspective, future work is required to further optimize the set-ups and validate whether the presented systems indeed comply with the presented requirements if more complex circulations are to be realized. This holds especially for the Fluigent system. Whereas the system has great potential and showed few technical issues, it has only been applied and validated during the perfusion of a single channel. Only if this circuit can indeed be extended to perfuse a total of three channels, it will become a feasible and competitive system compared to the IBIDI system.

8

CONCLUSION

The presented work is the first step towards developing an integrated MOoC cardiorenal model to study the reciprocal crosstalk between the two organs. To date no such system has been reported. Therefore this project set out to first-of-all establish the design criteria and thereafter conceptualize various possible microfluidic set-ups. Two commercially available pressure-based systems were evaluated on the basis of their experimental performance and to what extent they complied with the list of requirements. Inevitably, there is not one conceptual design that meets all requirements and rather a decision should eventually be made based on available information and feasibility. It is concluded that the commercial system that is the easiest to adapt and customizable to the particular needs of any experiment is advantageous. In this study two microfluidic operation systems have been evaluated: the IBIDI pump system and the Fluigent system. The Fluigent based set-up was found to render the highest modularity, robustness of use and controllability and is thus recommended as the system of choice for further studies.

The main take-away from the presented research is that in order to develop a suitable microfluidic set-up, emphasis must be placed on the adaptability of the system to realize various circulation circuits, while ensuring minimal occurrence of technical issues. Fit-for-purpose design with minimally invasive alterations to adapt commercially available systems paves the way towards robust, reliable and most importantly feasible microfluidic experiments. On top of that, it was shown that computational fluid dynamics simulations as well as 3D-printing technology may be exploited to characterize and optimize the commercial microfluidic set-up.

All together, MOoC design is not straightforward and conclusively requires a step-wise bottom-up approach in order to realize disease-models. Meanwhile, establishing well-defined control conditions in which every variable is extensively characterized is key to ultimately determine causative disease-related effects.

BIBLIOGRAPHY

- [1] M. Sarraf, A. Masoumi, and R. W. Schrier, “Cardiorenal Syndrome in Acute Decompensated Heart Failure,” *Clinical Journal of the American Society of Nephrology*, vol. 4, no. 12, pp. 2013–2026, Dec. 2009, ISSN: 1555-9041. DOI: [10 . 2215 / CJN . 03150509](https://doi.org/10.2215/CJN.03150509). [Online]. Available: <https://cjasn.asnjournals.org/content/4/12/2013%20https://cjasn.asnjournals.org/content/4/12/2013.abstract>.
- [2] C. Ronco, P. McCullough, S. D. Anker, *et al.*, “Cardio-renal syndromes : report from the consensus conference of the Acute Dialysis Quality Initiative,” vol. 31, pp. 703–711, 2010. DOI: [10.1093/eurheartj/ehp507](https://doi.org/10.1093/eurheartj/ehp507).
- [3] F. Savira, R. Magaye, D. Liew, *et al.*, “Cardiorenal syndrome: Multi-organ dysfunction involving the heart, kidney and vasculature,” *British Journal of Pharmacology*, vol. 177, no. 13, pp. 2906–2922, Jul. 2020, ISSN: 1476-5381. DOI: [10 . 1111 / BPH . 15065](https://doi.org/10.1111/BPH.15065). [Online]. Available: <https://onlinelibrary-wiley-com.tudelft.idm.oclc.org/doi/full/10.1111/bph.15065%20https://onlinelibrary-wiley-com.tudelft.idm.oclc.org/doi/abs/10.1111/bph.15065%20https://bpspubs-onlinelibrary-wiley-com.tudelft.idm.oclc.org/doi/10.1111/bph.15065>.
- [4] G. Gembillo, L. Visconti, M. A. Giusti, *et al.*, “Cardiorenal Syndrome: New Pathways and Novel Biomarkers,” *Biomolecules 2021, Vol. 11, Page 1581*, vol. 11, no. 11, p. 1581, Oct. 2021, ISSN: 2218273X. DOI: [10 . 3390 / BIOM11111581](https://doi.org/10.3390/Biom11111581). [Online]. Available: <https://www.mdpi.com/2218-273X/11/11/1581/htm%20https://www.mdpi.com/2218-273X/11/11/1581>.
- [5] K. Hebert, A. Dias, M. C. Delgado, *et al.*, “Epidemiology and survival of the five stages of chronic kidney disease in a systolic heart failure population,” *European Journal of Heart Failure*, vol. 12, no. 8, pp. 861–865, Aug. 2010, ISSN: 1388-9842. DOI: [10 . 1093 / EURJHF / HFQ077](https://doi.org/10.1093/EURJHF/HFQ077). [Online]. Available: <https://miami.pure.elsevier.com/en/publications/epidemiology-and-survival-of-the-five-stages-of-chronic-kidney-di>.
- [6] D. E. Forman, J. Butler, Y. Wang, *et al.*, “Incidence, predictors at admission, and impact of worsening renal function among patients hospitalized with heart failure,” *Journal of the American College of Cardiology*, vol. 43, no. 1, pp. 61–67, Jan. 2004, ISSN: 0735-1097. DOI: [10 . 1016 / J . JACC . 2003 . 07 . 031](https://doi.org/10.1016/J.JACC.2003.07.031). [Online]. Available: <https://pubmed-ncbi-nlm-nih-gov.tudelft.idm.oclc.org/14715185/>.
- [7] J. Jankowski, J. Floege, D. Fliser, M. Böhm, and N. Marx, “Cardiovascular Disease in Chronic Kidney Disease,” *Circulation*, vol. 143, pp. 1157–1172, Mar. 2021, ISSN: 15244539. DOI: [10 . 1161 / CIRCULATIONAHA . 120 . 050686](https://doi.org/10.1161/CIRCULATIONAHA.120.050686). [Online]. Available: <https://www.ahajournals.org/doi/abs/10.1161/CIRCULATIONAHA.120.050686>.
- [8] S. Thompson, M. James, N. Wiebe, *et al.*, “Cause of Death in Patients with Reduced Kidney Function,” *Journal of the American Society of Nephrology : JASN*, vol. 26, no. 10, pp. 2504–2511, Oct. 2015, ISSN: 1533-3450. DOI: [10 . 1681 / ASN . 2014070714](https://doi.org/10.1681/ASN.2014070714). [Online]. Available: <https://pubmed-ncbi-nlm-nih-gov.tudelft.idm.oclc.org/25733525/>.

- [9] L. G. Bongartz, M. J. Cramer, P. A. Doevendans, J. A. Joles, and B. Braam, "The severe cardiorenal syndrome: 'Guyton revisited'," *European heart journal*, vol. 26, no. 1, pp. 11–17, Jan. 2005, ISSN: 0195-668X. DOI: [10.1093/EURHEARTJ/EHI020](https://doi.org/10.1093/EURHEARTJ/EHI020). [Online]. Available: <https://pubmed-ncbi-nlm-nih-gov.tudelft.idm.oclc.org/15615794/>.
- [10] J. Rangaswami, V. Bhalla, J. E. Blair, *et al.*, "Cardiorenal Syndrome: Classification, Pathophysiology, Diagnosis, and Treatment Strategies: A Scientific Statement From the American Heart Association," *Circulation*, vol. 139, no. 16, E840–E878, Apr. 2019, ISSN: 15244539. DOI: [10.1161/CIR.0000000000000664](https://doi.org/10.1161/CIR.0000000000000664). [Online]. Available: <https://www.ahajournals.org/doi/abs/10.1161/CIR.0000000000000664>.
- [11] Bright, "Cases and observations illustrative of renal disease, accompanied with the secretion of albuminous urine," *Med Chir Rev.*, vol. 25, no. 49, pp. 23–35, Jul. 1836. [Online]. Available: <https://www-ncbi-nlm-nih-gov.tudelft.idm.oclc.org/pmc/articles/PMC5093576/>.
- [12] H. Yogasundaram, M. C. Chappell, B. Braam, and G. Y. Oudit, "Cardiorenal Syndrome and Heart Failure—Challenges and Opportunities," *Canadian Journal of Cardiology*, vol. 35, no. 9, pp. 1208–1219, Sep. 2019, ISSN: 0828-282X. DOI: [10.1016/J.CJCA.2019.04.002](https://doi.org/10.1016/J.CJCA.2019.04.002).
- [13] B. Gabbin, V. Meraviglia, C. L. Mummery, *et al.*, "Toward Human Models of Cardiorenal Syndrome in vitro," *Frontiers in Cardiovascular Medicine*, vol. 0, p. 1390, May 2022, ISSN: 2297-055X. DOI: [10.3389/FCVM.2022.889553](https://doi.org/10.3389/FCVM.2022.889553). [Online]. Available: <https://www.frontiersin.org/articles/10.3389/fcvm.2022.889553/full>.
- [14] Y. Funahashi, S. Chowdhury, M. B. Eiwaz, and M. P. Hutchens, "Acute Cardiorenal Syndrome: Models and Heart-Kidney Connectors," *Nephron*, vol. 144, no. 12, pp. 629–633, Dec. 2020, ISSN: 1660-8151. DOI: [10.1159/000509353](https://doi.org/10.1159/000509353). [Online]. Available: <https://www.karger.com/Article/FullText/509353%20https://www.karger.com/Article/Abstract/509353>.
- [15] S. Liu, A. R. Kompa, S. Kumfu, *et al.*, "Subtotal nephrectomy accelerates pathological cardiac remodeling post-myocardial infarction: implications for cardiorenal syndrome," *International journal of cardiology*, vol. 168, no. 3, pp. 1866–1880, Oct. 2013, ISSN: 1874-1754. DOI: [10.1016/J.IJCARD.2012.12.065](https://doi.org/10.1016/J.IJCARD.2012.12.065). [Online]. Available: <https://pubmed-ncbi-nlm-nih-gov.tudelft.idm.oclc.org/23347614/>.
- [16] S. Chua, F. Y. Lee, H. J. Chiang, *et al.*, "The cardioprotective effect of melatonin and exendin-4 treatment in a rat model of cardiorenal syndrome," *Journal of pineal research*, vol. 61, no. 4, pp. 438–456, Nov. 2016, ISSN: 1600-079X. DOI: [10.1111/JPI.12357](https://doi.org/10.1111/JPI.12357). [Online]. Available: <https://pubmed-ncbi-nlm-nih-gov.tudelft.idm.oclc.org/27465663/>.
- [17] T. W. Secomb, "Hemodynamics," *Comprehensive Physiology*, vol. 6, no. 2, p. 975, Apr. 2016, ISSN: 20404603. DOI: [10.1002/CPHY.C150038](https://doi.org/10.1002/CPHY.C150038). [Online]. Available: [/pmc/articles/PMC4958049/](https://pubmed-ncbi-nlm-nih-gov.tudelft.idm.oclc.org/pmc/articles/PMC4958049/) [?report=abstract%20https://www-ncbi-nlm-nih-gov.tudelft.idm.oclc.org/pmc/articles/PMC4958049/](https://pubmed-ncbi-nlm-nih-gov.tudelft.idm.oclc.org/pmc/articles/PMC4958049/?report=abstract%20https://www-ncbi-nlm-nih-gov.tudelft.idm.oclc.org/pmc/articles/PMC4958049/).
- [18] F. Zannad and P. Rossignol, "Cardiorenal Syndrome Revisited," *Circulation*, vol. 138, pp. 929–944, 2018. DOI: [10.1161/CIRCULATIONAHA.117.028814](https://doi.org/10.1161/CIRCULATIONAHA.117.028814). [Online]. Available: <http://ahajournals.org>.

- [19] M. Trapecar, "Multiorgan microphysiological systems as tools to interrogate interorgan crosstalk and complex diseases," *FEBS Letters*, Dec. 2021, ISSN: 1873-3468. DOI: [10.1002/1873-3468.14260](https://doi.org/10.1002/1873-3468.14260). [Online]. Available: <https://onlinelibrary-wiley-com.tudelft.idm.oclc.org/doi/full/10.1002/1873-3468.14260><https://onlinelibrary-wiley-com.tudelft.idm.oclc.org/doi/abs/10.1002/1873-3468.14260><https://febs-onlinelibrary-wiley-com.tudelft.idm.oclc.org/doi/10.1002/1873-3468.14260>.
- [20] M. Malik, Y. Yang, P. Fathi, G. J. Mahler, and M. B. Esch, "Critical Considerations for the Design of Multi-Organ Microphysiological Systems (MPS)," *Frontiers in Cell and Developmental Biology*, vol. 9, Sep. 2021, ISSN: 2296634X. DOI: [10.3389/fcell.2021.721338](https://doi.org/10.3389/fcell.2021.721338). [Online]. Available: [/pmc/articles/PMC8459628/%20/pmc/articles/PMC8459628/?report=abstract%20https://www.ncbi.nlm.nih.gov/pmc/articles/PMC8459628/](https://pubmed.ncbi.nlm.nih.gov/35459628/).
- [21] S. Jalili-Firoozinezhad, C. C. Miranda, and J. M. Cabral, "Modeling the Human Body on Microfluidic Chips," *Trends in Biotechnology*, vol. 39, no. 8, pp. 838–852, Aug. 2021, ISSN: 0167-7799. DOI: [10.1016/J.TIBTECH.2021.01.004](https://doi.org/10.1016/j.tibtech.2021.01.004).
- [22] L. A. Low, C. Mummery, B. R. Berridge, C. P. Austin, and D. A. Tagle, "Organs-on-chips: into the next decade," *Nature Reviews Drug Discovery* 2020 20:5, vol. 20, no. 5, pp. 345–361, Sep. 2020, ISSN: 1474-1784. DOI: [10.1038/S41573-020-0079-3](https://doi.org/10.1038/S41573-020-0079-3). [Online]. Available: <https://www-nature-com.tudelft.idm.oclc.org/articles/s41573-020-0079-3>.
- [23] F. Zheng, Y. Xiao, H. Liu, Y. Fan, and M. Dao, "Patient-Specific Organoid and Organ-on-a-Chip: 3D Cell-Culture Meets 3D Printing and Numerical Simulation," *Advanced Biology*, vol. 5, no. 6, p. 2000024, Jun. 2021, ISSN: 2701-0198. DOI: [10.1002/ADBI.202000024](https://doi.org/10.1002/adbi.202000024). [Online]. Available: <https://onlinelibrary-wiley-com.tudelft.idm.oclc.org/doi/full/10.1002/adbi.202000024><https://onlinelibrary-wiley-com.tudelft.idm.oclc.org/doi/abs/10.1002/adbi.202000024><https://onlinelibrary-wiley-com.tudelft.idm.oclc.org/doi/10.1002/adbi.202000024>.
- [24] N. Picollet-d, A. Zuchowska, I. Lemeunier, and S. L. Gac, "Multiorgan-on-a-Chip : A Systemic Approach To Model and Decipher Inter-Organ Communication," *Trends in Biotechnology*, vol. 39, no. 8, pp. 788–810, 2021, ISSN: 0167-7799. DOI: [10.1016/j.tibtech.2020.11.014](https://doi.org/10.1016/j.tibtech.2020.11.014). [Online]. Available: <https://doi.org/10.1016/j.tibtech.2020.11.014>.
- [25] T. Takebe, B. Zhang, and M. Radisic, "Synergistic Engineering: Organoids Meet Organ-on-a-Chip," *Cell Stem Cell*, vol. 21, no. 3, pp. 297–300, Sep. 2017, ISSN: 1934-5909. DOI: [10.1016/J.STEM.2017.08.016](https://doi.org/10.1016/j.stem.2017.08.016).
- [26] C. M. Leung, P. de Haan, K. Ronaldson-Bouchard, *et al.*, "A guide to the organ-on-a-chip," *Nature Reviews Methods Primers* 2022 2:1, vol. 2, no. 1, pp. 1–29, May 2022, ISSN: 2662-8449. DOI: [10.1038/S43586-022-00118-6](https://doi.org/10.1038/S43586-022-00118-6). [Online]. Available: <https://www-nature-com.tudelft.idm.oclc.org/articles/s43586-022-00118-6>.
- [27] L. Vernetti, A. Gough, N. Baetz, *et al.*, "Functional Coupling of Human Microphysiology Systems: Intestine, Liver, Kidney Proximal Tubule, Blood-Brain Barrier and Skeletal Muscle," *Scientific Reports* 2017 7:1, vol. 7, no. 1, pp. 1–15, Feb. 2017, ISSN: 2045-2322. DOI: [10.1038/srep42296](https://doi.org/10.1038/srep42296). [Online]. Available: <https://www.nature.com/articles/srep42296>.

- [28] A. Herland, B. M. Maoz, S. S. F. Jeanty, *et al.*, “Robotic fluidic coupling and interrogation of multiple vascularized organ chips,” *Nature Biomedical Engineering*, vol. 4, no. April, 2020, ISSN: 2157-846X. DOI: [10.1038/s41551-019-0497-x](https://doi.org/10.1038/s41551-019-0497-x). [Online]. Available: <http://dx.doi.org/10.1038/s41551-019-0497-x>.
- [29] B. J. van Meer, H. de Vries, K. S. Firth, *et al.*, “Small molecule absorption by PDMS in the context of drug response bioassays,” *Biochemical and Biophysical Research Communications*, vol. 482, no. 2, pp. 323–328, Jan. 2017, ISSN: 0006-291X. DOI: [10.1016/J.BBRC.2016.11.062](https://doi.org/10.1016/j.bbrc.2016.11.062).
- [30] J. H. Sung, Y. Wang, and M. L. Shuler, “Strategies for using mathematical modeling approaches to design and interpret multi-organ microphysiological systems (MPS),” *APL Bioengineering*, vol. 3, no. 2, p. 021 501, Jun. 2019, ISSN: 24732877. DOI: [10.1063/1.5097675](https://doi.org/10.1063/1.5097675). [Online]. Available: <https://aip-scitation-org.tudelft.idm.oclc.org/doi/abs/10.1063/1.5097675>.
- [31] J. Hübner, M. Raschke, I. Rüttschle, *et al.*, “Simultaneous evaluation of anti-EGFR-induced tumour and adverse skin effects in a microfluidic human 3D co-culture model,” *Scientific Reports*, vol. 8, no. 1, Dec. 2018, ISSN: 20452322. DOI: [10.1038/S41598-018-33462-3](https://doi.org/10.1038/S41598-018-33462-3).
- [32] L. Chen, Y. Yang, H. Ueno, and M. B. Esch, “Body-in-a-Cube: a microphysiological system for multi-tissue co-culture with near-physiological amounts of blood surrogate,” *Microphysiological Systems*, vol. 4, no. 12, pp. 1–1, 2020. DOI: [10.21037/mps-19-8](https://doi.org/10.21037/mps-19-8).
- [33] S. Bauer, C. Wennberg Huldt, K. P. Kanebratt, *et al.*, “Functional coupling of human pancreatic islets and liver spheroids on-a-chip: Towards a novel human ex vivo type 2 diabetes model,” *Scientific Reports 2018 7:1*, vol. 7, no. 1, pp. 1–11, Nov. 2017, ISSN: 2045-2322. DOI: [10.1038/s41598-017-14815-w](https://doi.org/10.1038/s41598-017-14815-w). [Online]. Available: <https://www.nature.com/articles/s41598-017-14815-w>.
- [34] N. Ucciferri, T. Sbrana, and A. Ahluwalia, “Allometric Scaling and Cell Ratios in Multi-Organ in vitro Models of Human Metabolism,” *Frontiers in Bioengineering and Biotechnology*, vol. 2, no. DEC, 2014, ISSN: 22964185. DOI: [10.3389/FBIOE.2014.00074](https://doi.org/10.3389/FBIOE.2014.00074). [Online]. Available: [/pmc/articles/PMC4269269/%20/pmc/articles/PMC4269269/?report=abstract%20https://www.ncbi.nlm.nih.gov/pmc/articles/PMC4269269/](https://pubmed.ncbi.nlm.nih.gov/pmc/articles/PMC4269269/).
- [35] J. P. Wikswo, E. L. Curtis, Z. E. Eagleton, *et al.*, “Scaling and systems biology for integrating multiple organs-on-a-chip,” *Lab on a chip*, vol. 13, no. 18, pp. 3496–3511, Sep. 2013, ISSN: 1473-0189. DOI: [10.1039/C3LC50243K](https://doi.org/10.1039/C3LC50243K). [Online]. Available: [https://pubmed-ncbi-nlm-nih-gov.tudelft.idm.oclc.org/23828456/](https://pubmed.ncbi.nlm.nih.gov/tudelft.idm.oclc.org/23828456/).
- [36] D. Park, J. Lee, J. J. Chung, Y. Jung, and S. H. Kim, “Integrating Organs-on-Chips: Multiplexing, Scaling, Vascularization, and Innervation,” *Trends in Biotechnology*, vol. 38, no. 1, 2020. DOI: [10.1016/j.tibtech.2019.06.006](https://doi.org/10.1016/j.tibtech.2019.06.006). [Online]. Available: <https://doi.org/10.1016/j.tibtech.2019.06.006>.
- [37] G. B. West and J. H. Brown, “The origin of allometric scaling laws in biology from genomes to ecosystems: towards a quantitative unifying theory of biological structure and organization,” *Journal of Experimental Biology*, vol. 208, no. 9, pp. 1575–1592, May 2005, ISSN: 0022-0949. DOI: [10.1242/JEB.01589](https://doi.org/10.1242/JEB.01589). [Online]. Available: <https://journals.biologists.com/jeb/article/208/9/1575/9371/The-origin-of-allometric-scaling-laws-in-biology>.

- [38] C. Moraes, J. M. Labuz, B. M. Leung, M. Inoue, T. H. Chun, and S. Takayama, "On being the right size: Scaling effects in designing a human-on-a-chip," *Integrative Biology (United Kingdom)*, vol. 5, no. 9, pp. 1149–1161, 2013, ISSN: 17579694. DOI: [10.1039/c3ib40040a](https://doi.org/10.1039/c3ib40040a).
- [39] G. B. West, J. H. Brown, and B. J. Enquist, "A general model for the origin of allometric scaling laws in biology," *Science*, vol. 276, no. 5309, pp. 122–126, Apr. 1997, ISSN: 00368075. DOI: [10.1126/SCIENCE.276.5309.122](https://doi.org/10.1126/SCIENCE.276.5309.122)/ASSET/C437345F-C208-4FBB-993E-E8995AE77F9D/ASSETS/GRAPHIC/122-IMG022.GIF. [Online]. Available: <https://www-science-org.tudelft.idm.oclc.org/doi/abs/10.1126/science.276.5309.122>.
- [40] S. L. Lindstedt and I. W. A. Calder, "Body Size, Physiological Time, and Longevity of Homeothermic Animals," <https://doi-org.tudelft.idm.oclc.org/10.1086/412080>, vol. 56, no. 1, pp. 1–16, Oct. 2015, ISSN: 0033-5770. DOI: [10.1086/412080](https://doi.org/10.1086/412080). [Online]. Available: <https://www-journals-uchicago-edu.tudelft.idm.oclc.org/doi/abs/10.1086/412080>.
- [41] B. M. Maoz, A. Herland, E. A. Fitzgerald, *et al.*, "A linked organ-on-chip model of the human neurovascular unit reveals the metabolic coupling of endothelial and neuronal cells," *Nature biotechnology*, vol. 36, no. 9, pp. 865–877, Oct. 2018, ISSN: 1546-1696. DOI: [10.1038/NBT.4226](https://doi.org/10.1038/NBT.4226). [Online]. Available: <https://pubmed-ncbi-nlm-nih-gov.tudelft.idm.oclc.org/30125269/>.
- [42] I. Wagner, E. M. Materne, S. Brincker, *et al.*, "A dynamic multi-organ-chip for long-term cultivation and substance testing proven by 3D human liver and skin tissue co-culture," *Lab on a Chip*, vol. 13, no. 18, pp. 3538–3547, 2013, ISSN: 14730189. DOI: [10.1039/c3lc50234a](https://doi.org/10.1039/c3lc50234a).
- [43] M. B. Esch, H. Ueno, D. R. Applegate, and M. L. Shuler, "Modular, pumpless body-on-a-chip platform for the co-culture of GI tract epithelium and 3D primary liver tissue," *Lab on a Chip*, vol. 16, no. 14, pp. 2719–2729, Jul. 2016, ISSN: 1473-0189. DOI: [10.1039/C6LC00461J](https://doi.org/10.1039/C6LC00461J). [Online]. Available: <https://pubs-rsc-org.tudelft.idm.oclc.org/en/content/articlehtml/2016/lc/c6lc00461j><https://pubs-rsc-org.tudelft.idm.oclc.org/en/content/articlelanding/2016/lc/c6lc00461j>.
- [44] A. Tajeddin and N. Mustafaoglu, "Design and Fabrication of Organ-on-Chips : Promises and Challenges," *Micromachines*, vol. 12, no. 1443, pp. 1–33, 2021.
- [45] J. Kong, Y. Luo, D. Jin, *et al.*, "A novel microfluidic model can mimic organ-specific metastasis of circulating tumor cells," *Oncotarget*, vol. 7, no. 48, pp. 78 421–78 432, 2016, ISSN: 1949-2553. DOI: [10.18632/ONCOTARGET.9382](https://doi.org/10.18632/ONCOTARGET.9382). [Online]. Available: <https://pubmed.ncbi.nlm.nih.gov/27191997/>.
- [46] J. Theobald, M. A. Abu el Maaty, N. Kusterer, *et al.*, "In vitro metabolic activation of vitamin D3 by using a multi-compartment microfluidic liver-kidney organ on chip platform," *Scientific Reports 2019 9:1*, vol. 9, no. 1, pp. 1–11, Mar. 2019, ISSN: 2045-2322. DOI: [10.1038/S41598-019-40851-9](https://doi.org/10.1038/S41598-019-40851-9). [Online]. Available: <https://www-nature-com.tudelft.idm.oclc.org/articles/s41598-019-40851-9>.

- [47] A. Chramiec, D. Teles, K. Yeager, *et al.*, “Lab on a Chip Devices and applications at the micro-and nanoscale Integrated human organ-on-a-chip model for predictive studies of anti-tumor drug efficacy and cardiac safety Lab on a Chip Integrated human organ-on-a-chip model for predictive studies of a,” vol. 20, p. 4357, 2020, ISSN: 1473-0197. DOI: [10.1039/d01c00424c](https://doi.org/10.1039/d01c00424c).
- [48] Y. S. Zhang, J. Aleman, S. R. Shin, *et al.*, “Multisensor-integrated organs-on-chips platform for automated and continual in situ monitoring of organoid behaviors,” *Proceedings of the National Academy of Sciences of the United States of America*, vol. 114, no. 12, E2293–E2302, Mar. 2017, ISSN: 10916490. DOI: [10.1073/PNAS.1612906114/-/DCSUPPLEMENTAL](https://doi.org/10.1073/PNAS.1612906114/-/DCSUPPLEMENTAL). [Online]. Available: <https://www-pnas-org.tudelft.idm.oclc.org/content/114/12/E2293%20https://www-pnas-org.tudelft.idm.oclc.org/content/114/12/E2293.abstract>.
- [49] A. Skardal, M. Devarasetty, S. Forsythe, A. Atala, and S. Soker, “A reductionist metastasis-on-a-chip platform for in vitro tumor progression modeling and drug screening,” *Biotechnology and bioengineering*, vol. 113, no. 9, pp. 2020–2032, Sep. 2016, ISSN: 1097-0290. DOI: [10.1002/BIT.25950](https://doi.org/10.1002/BIT.25950). [Online]. Available: <https://pubmed.ncbi.nlm.nih.gov/26888480/>.
- [50] A. Skardal, S. V. Murphy, M. Devarasetty, *et al.*, “Multi-tissue interactions in an integrated three-tissue organ-on-a-chip platform,” *Scientific Reports 2017 7:1*, vol. 7, no. 1, pp. 1–16, Aug. 2017, ISSN: 2045-2322. DOI: [10.1038/s41598-017-08879-x](https://doi.org/10.1038/s41598-017-08879-x). [Online]. Available: <https://www.nature.com/articles/s41598-017-08879-x>.
- [51] M. H. Wu, S. B. Huang, Z. Cui, Z. Cui, and G. B. Lee, “A high throughput perfusion-based microbioreactor platform integrated with pneumatic micropumps for three-dimensional cell culture,” *Biomedical microdevices*, vol. 10, no. 2, pp. 309–319, Apr. 2008, ISSN: 1387-2176. DOI: [10.1007/S10544-007-9138-3](https://doi.org/10.1007/S10544-007-9138-3). [Online]. Available: <https://pubmed.ncbi.nlm.nih.gov/18026840/>.
- [52] Y. Baert, I. Ruetschle, W. Cools, *et al.*, “A multi-organ-chip co-culture of liver and testis equivalents: A first step toward a systemic male reprotoxicity model,” *Human Reproduction*, vol. 35, no. 5, pp. 1029–1044, 2020, ISSN: 14602350. DOI: [10.1093/humrep/deaa057](https://doi.org/10.1093/humrep/deaa057).
- [53] T. Satoh, S. Sugiura, K. Shin, *et al.*, “A multi-throughput multi-organ-on-a-chip system on a plate formatted pneumatic pressure-driven medium circulation platform,” *Lab on a Chip*, vol. 18, no. 1, pp. 115–125, Dec. 2017, ISSN: 1473-0189. DOI: [10.1039/C7LC00952F](https://doi.org/10.1039/C7LC00952F). [Online]. Available: <https://pubs.rsc.org/en/content/articlehtml/2018/1c/c71c00952f%20https://pubs.rsc.org/en/content/articlelanding/2018/1c/c71c00952f>.
- [54] C. D. Edington, W. L. K. Chen, E. Geishecker, *et al.*, “Interconnected Microphysiological Systems for Quantitative Biology and Pharmacology Studies,” *Scientific Reports 2018 8:1*, vol. 8, no. 1, pp. 1–18, Mar. 2018, ISSN: 2045-2322. DOI: [10.1038/s41598-018-22749-0](https://doi.org/10.1038/s41598-018-22749-0). [Online]. Available: <https://www.nature.com/articles/s41598-018-22749-0>.
- [55] K. Shinha, W. Nihei, H. Nakamura, *et al.*, “A Kinetic Pump Integrated Microfluidic Plate (KIM-Plate) with High Usability for Cell Culture-Based Multiorgan Microphysiological Systems,” *Micromachines*, vol. 12, no. 9, Aug. 2021, ISSN: 2072-666X. DOI: [10.3390/MI12091007](https://doi.org/10.3390/MI12091007). [Online]. Available: <https://pubmed-ncbi-nlm-nih-gov.tudelft.idm.oclc.org/34577652/>.

- [56] J. Aleman and A. Skardal, "A multi-site metastasis-on-a-chip microphysiological system for assessing metastatic preference of cancer cells," *Biotechnology and Bioengineering*, vol. 116, no. 4, pp. 936–944, Apr. 2019, ISSN: 1097-0290. DOI: [10.1002/BIT.26871](https://doi.org/10.1002/BIT.26871). [Online]. Available: <https://onlinelibrary.wiley.com/doi/full/10.1002/bit.26871><https://onlinelibrary.wiley.com/doi/abs/10.1002/bit.26871><https://onlinelibrary.wiley.com/doi/10.1002/bit.26871>.
- [57] C. Zhang, Z. Zhao, N. A. Abdul Rahim, D. Van Noort, and H. Yu, "Towards a human-on-chip: Culturing multiple cell types on a chip with compartmentalized microenvironments," *Lab on a Chip*, vol. 9, no. 22, pp. 3185–3192, Nov. 2009, ISSN: 14730189. DOI: [10.1039/B915147H](https://doi.org/10.1039/B915147H). [Online]. Available: <https://pubs-rsc-org.tudelft.idm.oclc.org/en/content/articlehtml/2009/1c/b915147h><https://pubs-rsc-org.tudelft.idm.oclc.org/en/content/articlelanding/2009/1c/b915147h>.
- [58] C. W. V. D. Berg, L. Ritsma, M. C. Avramut, *et al.*, "Renal Subcapsular Transplantation of PSC-Derived Kidney Organoids Induces Neo-vasculogenesis and Significant Glomerular and Tubular Maturation In Vivo," *Stem Cell reports*, vol. 10, pp. 751–765, 2018. DOI: [10.1016/j.stemcr.2018.01.041](https://doi.org/10.1016/j.stemcr.2018.01.041).
- [59] E. Giacomelli, V. Meraviglia, G. Camprostrini, V. V. Orlova, M. Bellin, and C. L. Mummery, "Article Human-iPSC-Derived Cardiac Stromal Cells Enhance Maturation in 3D Cardiac Microtissues and Reveal Non-cardiomyocyte Contributions to Heart Disease II Human-iPSC-Derived Cardiac Stromal Cells Enhance Maturation in 3D Cardiac Microtissues and Reveal," pp. 862–879, 2020. DOI: [10.1016/j.stem.2020.05.004](https://doi.org/10.1016/j.stem.2020.05.004).
- [60] ibidi GmbH, "Instruction Manual ibidi Pump System Version 2.6," Tech. Rep., 2022, pp. 1–72.
- [61] IBIDI, *Instructions: μ -Slide III 3D Perfusion*, 2021. [Online]. Available: https://ibidi.com/img/cms/products/labware/channel_slides/S_8037X_III_3D_Perfusion/IN_8037X_III_3D_Perfusion.pdf.
- [62] K. Schimek, S. Frentzel, K. Luettich, *et al.*, "Human multi-organ chip co-culture of bronchial lung culture and liver spheroids for substance exposure studies," *Scientific Reports 2020 10:1*, vol. 10, no. 1, pp. 1–13, May 2020, ISSN: 2045-2322. DOI: [10.1038/S41598-020-64219-6](https://doi.org/10.1038/S41598-020-64219-6). [Online]. Available: <https://www-nature-com.tudelft.idm.oclc.org/articles/s41598-020-64219-6>.
- [63] A. Ali Manzoor, L. Romita, and D. Kun Hwang, "A review on microwell and microfluidic geometric array fabrication techniques and its potential applications in cellular studies," *Can. J. Chem. Eng.*, vol. 99, pp. 61–96, 2021. DOI: [10.1002/cjce.23875](https://doi.org/10.1002/cjce.23875).
- [64] M. Takasato, P. X. Er, H. S. Chiu, *et al.*, "Kidney organoids from human iPSCs contain multiple lineages and model human nephrogenesis," *Nature*, vol. 526, p. 565, 2015. DOI: [10.1038/nature15695](https://doi.org/10.1038/nature15695).
- [65] M. Takasato, P. X. Er, H. S. Chiu, and M. H. Little, "Generation of kidney organoids from human pluripotent stem cells," *Nature Publishing Group*, vol. 11, no. 9, pp. 1681–1692, 2016, ISSN: 1754-2189. DOI: [10.1038/nprot.2016.098](https://doi.org/10.1038/nprot.2016.098). [Online]. Available: <http://dx.doi.org/10.1038/nprot.2016.098>.
- [66] L. Sala, B. J. V. Meer, L. G. J. Tertoolen, *et al.*, "New Methods in Cardiovascular Biology A Versatile Open Software Tool to Quantify Cardiomyocyte and," pp. 5–16, 2018. DOI: [10.1161/CIRCRESAHA.117.312067](https://doi.org/10.1161/CIRCRESAHA.117.312067).

- [67] C. Hart, C. M. Didier, F. Sommerhage, and S. Rajaraman, "Biocompatibility of Blank, Post-Processed and Coated 3D Printed Resin Structures with Electrogenic Cells," *Biosensors*, vol. 10, no. 11, pp. 1–14, 2020, ISSN: 20796374. DOI: [10.3390/bios10110152](https://doi.org/10.3390/bios10110152).
- [68] H. Bruus, "Acoustofluidics 1: Governing equations in microfluidics," *Lab on a Chip*, vol. 11, no. 22, pp. 3742–3751, Oct. 2011, ISSN: 14730189. DOI: [10.1039/C1LC20658C](https://doi.org/10.1039/C1LC20658C). [Online]. Available: <https://pubs.rsc.org/en/content/articlehtml/2011/lc/c1lc20658c> <https://pubs.rsc.org/en/content/articlelanding/2011/lc/c1lc20658c>.
- [69] R. P. Brown, M. D. Delp, S. L. Lindstedt, L. R. Rhomberg, and R. P. Beliles, "Physiological parameter values for physiologically based pharmacokinetic models," *Toxicology and industrial health*, vol. 13, no. 4, pp. 407–484, 1997, ISSN: 0748-2337. DOI: [10.1177/074823379701300401](https://doi.org/10.1177/074823379701300401). [Online]. Available: <https://pubmed-ncbi-nlm-nih-gov.tudelft.idm.oclc.org/9249929/>.
- [70] B. Davies and T. Morris, "Physiological parameters in laboratory animals and humans," *Pharmaceutical research*, vol. 10, no. 7, pp. 1093–1095, 1993, ISSN: 0724-8741. DOI: [10.1023/A:1018943613122](https://doi.org/10.1023/A:1018943613122). [Online]. Available: <https://pubmed-ncbi-nlm-nih-gov.tudelft.idm.oclc.org/8378254/>.
- [71] B. C. Allen, C. E. Hack, and H. J. Clewell, "Use of Markov Chain Monte Carlo analysis with a physiologically-based pharmacokinetic model of methylmercury to estimate exposures in US women of childbearing age," *Risk analysis: an official publication of the Society for Risk Analysis*, vol. 27, no. 4, pp. 947–959, Aug. 2007, ISSN: 0272-4332. DOI: [10.1111/J.1539-6924.2007.00934.X](https://doi.org/10.1111/J.1539-6924.2007.00934.X). [Online]. Available: <https://pubmed-ncbi-nlm-nih-gov.tudelft.idm.oclc.org/17958503/>.
- [72] S. W. Snyder, J. M. Cook, R. L. Karhausen, E. S. Nasset, G. Parry Howells, and I. H. Tipton, "Report of the task group on reference man ICRP Publication 23," *Annals of the ICRP*, vol. 3, no. 1-4, p. 3, 1979, ISSN: 01466453. DOI: [10.1016/0146-6453\(79\)90123-4](https://doi.org/10.1016/0146-6453(79)90123-4).
- [73] M. Shinohara, H. Kimura, K. Montagne, K. Komori, T. Fujii, and Y. Sakai, "Combination of microwell structures and direct oxygenation enables efficient and size-regulated aggregate formation of an insulin-secreting pancreatic β -cell line," *Biotechnology Progress*, vol. 30, no. 1, pp. 178–187, 2014, ISSN: 87567938. DOI: [10.1002/btpr.1837](https://doi.org/10.1002/btpr.1837).
- [74] E. M. Materne, A. P. Ramme, A. P. Terrasso, *et al.*, "A multi-organ chip co-culture of neurospheres and liver equivalents for long-term substance testing," *Journal of Biotechnology*, vol. 205, pp. 36–46, 2015, ISSN: 18734863. DOI: [10.1016/j.jbiotec.2015.02.002](https://doi.org/10.1016/j.jbiotec.2015.02.002). [Online]. Available: <http://dx.doi.org/10.1016/j.jbiotec.2015.02.002>.

A

DESIGN REQUIREMENTS

Table A.1: Design requirements for a cardiorenal MOoC set-up, organized in accordance with the theoretical framework.

Demand or Wish	Topic	Requirement
1. Cell sources and culture method		
D	Cell culture conditions	Chip maintenance must be possible at 37°C and 5% CO ₂ for an extended period of time.
D/W	3D hiPSC tissue constructs	Compatible with 3D hiPSC cardiac microtissues and kidney organoids developed in accordance with existing validated protocols.
2. Microfluidic platform configuration		
D	Separate culture chambers	Two separate organ chambers are available in the system to prevent direct cellular contact of the two modelled organ types.
D	Open-culture system	The microfluidic chip features accessible, open culture chambers that can be sealed after tissue transfer.
W	Double-chamber chip	Two microfluidic chambers integrated on a single chip to reduce required connecting components.
3. Cellular environment		
D	Scaffold free	Tissue embedding onto the chip does not require any scaffold material.
W	Culture inserts	Existing culture inserts may be used to pre-culture organoids under controlled conditions and simplify their transfer to the chip, thus minimizing tissue disturbance.
4. Material		
D	Bio-compatible	All the materials used in the microfluidic set-up are bio-compatible with the tissue constructs and do not release toxic particles over time.
D	Non-absorbing material	Secreted factors and other biomolecules are not absorbed by either the chip or tubing material.
D	Air-permeable coverslip	Culture chambers are closed by an air-permeable coverslip to ensure adequate oxygenation.

D	Sterility	All microfluidic components must be able to be sterilized prior to starting an experiment ensuring that sterilization does not adversely affect the material properties. It must be possible to connect the pump under sterile conditions.
W	Re-usable chips	Due to high costs associated with microfluidic chips it is desirable that chips are not made for single experiments.
W	Re-usable tubing	Perfusion sets and other connecting components can be cleaned and re-used for subsequent experiments.
5. Organ model scaling		
D	Scalable tissues	The incorporated tissue constructs must be able to be scaled to accurate dimensions to achieve near physiological ratios in terms of volume-to-cells and organ-to-organ.
D/W	Chamber size	On-chip culture chamber sizes must accommodate the organoids while maintaining the total internal volume as low as possible.
6. Coupling of organ models		
D	Single-pass system	A series-connection is established between adjacent organ chambers to ensure a single medium pass per circulation.
W	Modularity	To generate a versatile system that can potentially be extended, the used components must be replaceable and compatible with products from various companies.
7. Fluid circulation		
D	Automated flow control	The medium circulation, unidirectional or recirculation, must be computer controlled.
D	Types of flow	The system is able to generate uni-directional, bi-directional and recirculatory flow with the need of minimal adaptations to the set-up to switch between the three types.
W	Pressure pump operated	The flow is generated by a pressure pump as this method is reliable and offers an easy user-interface.
W	Multiple chips in parallel	Multiple chips can be connected to the set-up in parallel to increase the experimental throughput. This implies that a single pressure controller must have multiple output ports.
8. Flow rates		
D	Refreshment of medium to support cell-culture	Flow functions to continuously refresh medium to support cell-culture and facilitate dynamic exchange of secreted factors.
W	Flow rate control per organ chamber	Since multiple organ models are to be embedded, chamber-related control over the flow rate would be ideal.
9. Common media		
D	Common media formulation	A single medium is used throughout the complete set-up, which fulfils the nutritional requirements of both organoid types.
D	Low internal volume	The total volume used in the final set-up must be kept minimal to achieve physiologically relevant volume-to-cell ratios.
10. Analysis		
D	Material retrieval	Cellular material must be accessible for post-experimental analysis and thus it must be possible to collect the material from the chip.
D	Sampling	Since secreted factors are the main experimental target, the system must allow for an effective sampling method of low volumes at various time points during the experiment.
D	Live imaging	Imaging tissues directly inside the chip can be used as a tool to evaluate tissue integrity and viability during an experiment.
D	Chamber access	Access to the tissue constructs at any time provides the possibility to directly manipulate the tissue and observe the secondary effects.
W	Real time monitoring of flow	The control unit can export data of flow-related parameters directly to ensure the experiment is running correctly.

W**Integrated sensors**

Automated sensors can be connected to the system to directly provide continuous, *in situ* data on chip conditions and tissue status.



B

CHOICE OF MICROFLUIDIC SYSTEM

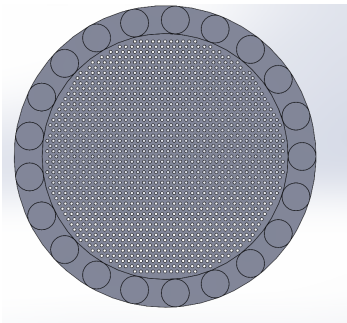
Table B.1: Design requirements evaluated for various commercially available systems to aid in decision making during the conceptual phase.

Demand or Wish	Requirement	Microfluidic system and connected chip		
		TissUse Starter: Chip2	HUMIMIC Humimic	IBIDI Perfusion System: Ibidi μ -slide III
1. Cell sources and culture method				
D	Cell culture conditions	✓		✓
D/W	3D hiPSC tissue constructs	✓		✓
2. Microfluidic platform configuration				
D	Separate culture chambers	✓		✓
D	Open-culture system	✓	✓	✓
		Screw-type lids	Polymer coverslip	Polymer coverslip
W	Double-chamber chip	✓	✓	✓
		Available in 96-well or 24-well format	One-size	One-size
3. Cellular environment				
D	Scaffold free	✓	?	?
W	Culture inserts	✓	X	X
4. Material				
D	Bio-compatible	✓	✓	✓
D	Non-absorbing material	✓	X	X
		PEEK;Polycarbonate	Polymer N.S	Polymer N.S.
D	Air-permeable coverslip	X	✓	✓
		Not available for this chip	Gas-permeable coverslip	Gas permeable coverslip
D	Sterility	✓	✓	?
W	Re-usable chips	X	X	X
W	Re-usable tubing	✓	?	?

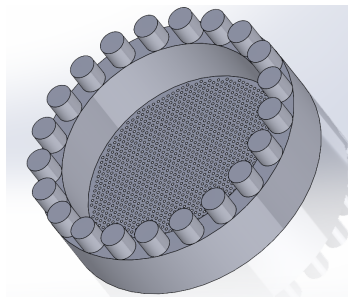
			Perfusion set can be autoclaved multiple times, but wears down	Tubing relatively inexpensive to replace
5. Organ model scaling				
D	Scalable tissues	✓	✓	✓
D/W	Chamber size	✓ Relatively large volume	? Relatively large volume	? ?
6. Coupling of organ models				
D	Single-pass system	✓	✓	✓
W	Modularity	X	X	✓
7. Fluid circulation				
D	Automated flow control	✓	✓	✓
D	Types of flow	X Only recirculation and bi-directional	✓ Only recirculation and bi-directional	? Recirculation possible with adjustments
W	Pressure pump operated	✓ On-chip micropump, similar performance	✓	✓
W	Multiple chips in parallel	✓ 1 controller = 4 chips	X 1 controller = 1 controller	? MFSC TM controller = 2 chips
8. Flow rates				
D	Refreshment of medium to support cell-culture	✓	✓	✓
W	Flow rate control per organ chamber	X	X	X
9. Common media				
D	Common media formulation	✓	✓	✓
D	Low internal volume	✓	? ?	? ?
10. Analysis				
D	Material retrieval	✓	✓	✓
D	Sampling	✓ From chambers	X Closed-system	? From collecting reservoir in uni-directional set-up
D	Live imaging	✓	✓ Only inverted microscopy	✓ Only inverted microscopy
D	Chamber access	✓	X	X
W	Real time monitoring of flow	✓	X	✓
W	Integrated sensors	X	X	✓

C

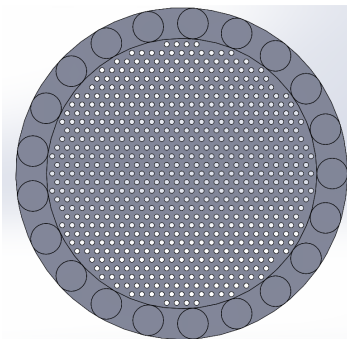
SCHEMATIC OVERVIEW KO-MESH DESIGNS



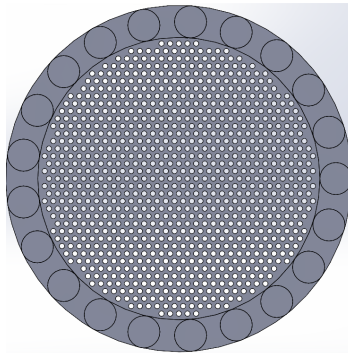
(a) 2x2 pixels ($d = 54 \mu\text{m}$)



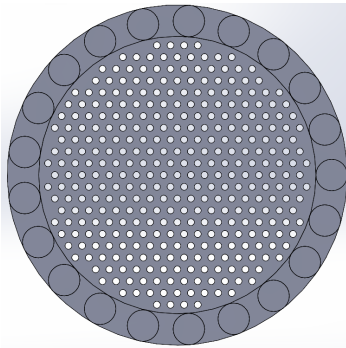
(b) 2x2 pixels ($d = 54 \mu\text{m}$): 3D representation



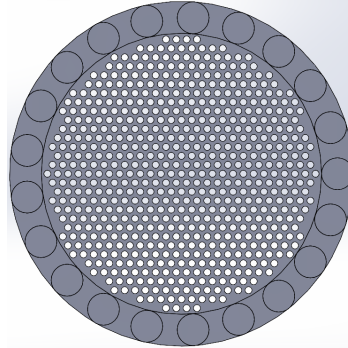
(c) 3x3 ($d = 81 \mu\text{m}$)



(d) 3x3 ($d = 81 \mu\text{m}$): close pore spacing



(e) **4x4 (d = 108 μm)**



(f) **4x4 (d = 108 μm): close pore spacing**

Figure C.1: Schematic overview of tested KO-mesh designs with various pore diameters and inter pore spacing distances.

